

**Experimental and Numerical Studies of Friction Stir Welded  
Joints of Aluminium-alloy (AA5052-H32) Plates**

**THESIS**

Submitted in partial fulfilment of the  
requirements for the degree of  
**DOCTOR OF PHILOSOPHY**

by

**BARLA MADHAVI**  
(ID No.: 2010PHXF0028H)

Under the Supervision of  
**Dr. Jeevan Jaidi, Associate Professor**



**BITS Pilani**  
Pilani | Dubai | Goa | Hyderabad

**BIRLA INSTITUTE OF TECHNOLOGY AND SCIENCE, PILANI**  
**HYDERABAD CAMPUS**

**December 2017**

**BIRLA INSTITUTE OF TECHNOLOGY AND SCIENCE, PILANI  
HYDERABAD CAMPUS**

**CERTIFICATE**

This is to certify that the thesis entitled “**Experimental and Numerical Studies of Friction Stir Welded Joints of Aluminium-alloy (AA5052-H32) Plates**” and submitted by **Barla Madhavi**, ID No - **2010PHXF0028H** for award of Ph.D. of the Institute embodies original work done by her under my supervision.

(Signature of the Supervisor)

Name in capital letters: **Dr. Jeevan Jaidi (IISc, Bangalore)**

Designation: **Associate Professor  
Mechanical Engineering Department  
BITS-Pilani, Hyderabad Campus**

Date:

*Dedicated to my beloved Father, Late. Shri Barla Nageswara Rao*

## ACKNOWLEDGEMENTS

I start this by thanking the **Almighty** for giving me strength and patience. I would like to express my love and gratitude to my parents for their prayers, understanding and never-ending support during the most difficult period in my life so far.

Great appreciation goes to my Doctoral Thesis Supervisor, **Prof. Jeevan Jaidi** for his valuable pieces of advice, expert guidance, patience, encouragement and support given to me throughout the Ph.D programme.

I would like to thank my Doctoral Advisory Committee (DAC) members, **Prof. S. P. Regalla** and **Prof. A. K. Gupta** for their valuable suggestions and support given to me.

I would like to thank the administration of BITS-Pilani, Hyderabad Campus, Prof A.K. Gupta Head of Mechanical Engineering Department, Prof. G. Sundar, Director, BITS-Pilani, Hyderabad Campus and Prof. Souvik Bhattachary, Vice-chancellor, BITS-Pilani, University for providing me the opportunity to carry out this research work and submit my Ph.D thesis.

I would like to acknowledge the Department of Metallurgy and Materials at Defence Metallurgical Research Laboratories (DMRL), Hyderabad for permitting me to carry out the necessary experiments. I sincerely thank **Dr. G. Madhusudhan Reddy**, Scientist - H (DMRL) for his valuable suggestions given to me during the experiments.

I would like to acknowledge BITS-Pilani, Hyderabad Campus and the Department of Mechanical Engineering for granting me to pursue Ph.D Scholarship in this premier institution. The assistance provided by the technicians, **Mr. P. Sreedhar** of Central Workshop and **Mr. Ch. Srinivasa Rao** of Materials Testing Laboratory is greatly appreciated.

I would also like to thank whole heartedly my colleagues in the Department of Mechanical Engineering, Prof. Y. V. D. Rao, Dr. Hussaini, Dr. Nitin Kotkunde, Dr. Amrita and my best friends Dr. Purnima, Mrs. Subha who were such a pleasant company in the very difficult

times. Also, I would like to thank Mr. Anvesh Krishna,(B.Tech student of Department of Mechanical Engineering), who helped me in the initial stages of simulation works. I would like to thank Mr. Sravan Kumar (Doctoral Scholar) of Department of Mechanical Engineering, who helped me in configuring my thesis in a well-organized manner. Last but not the least I would like to thank Mr. Akhil Bharadwaj, Junior Research Fellow and my brother, Sisters, brother-in-laws for their kind support at all times.

Finally, I whole heartedly feel indebted forever to my mother, Barla Lakshmi Aruna Devi, husband, Chukka Vijay Shekar and my son Chukka Sai Rithwik simply because without whose support it would have been impossible to see a light at the end of the PhD tunnel for all their sacrifices, understanding and active co-operation throughout the course of my doctoral thesis enabling me to spend my time efficiently during the slog end.

***(Barla Madhavi)***

## ABSTRACT

The manufacturing industry has shown considerable interest in Friction Stir Welding (FSW) technology in the past two decades. But the detailed understanding of different physical phenomena involved is incomplete. Particularly, the complete understanding of plasticized material flow around the rotating tool is crucial for optimizing the FSW process parameters (tool rotational speed - RS, traverse speed - TS, tool tilt angle -  $\alpha$ , tool-pin height - TPH, axial force - P) and design of tool geometry. Therefore, a detailed experimental and numerical simulation study on the effect of FSW process parameters on the material flow and the resulting mechanical properties of the weldment would contribute to improving the joint quality and increasing the productivity.

A thorough experimental works have been carried out to study the effects of FSW process parameters (TS, RS and TPH) on the nugget geometry(shape and size) and final mechanical properties of aluminium-alloy (AA5052-H32) plates. Butt welding of 4 mm thick plates were done with D2 tool-steel having 6.0 mm pin diameter, 16.0 mm shoulder diameter with 2° inward taper on the tool shoulder. Several initial trial welds were produced with different combinations of process parameters ensuring negligible material outflow and to narrow down the range of process parameters for the selected workpiece thickness. Subsequently, the effects of TS (28-56 mm/min), RS (355-710 rpm) and TPH (2.5-3.5 mm) on mechanical properties such as hardness, tensile strength and percentage (%) elongation were studied for which proper welds with and with out defect welds were observed. The observations from the mechanical testing and optical microscopic studies revealed significant variations in the final mechanical properties across the nugget geometry in contrast to that of the base metal (BM) values. Also, almost minimum to no defects were observed at TPH value equal to 3.0 mm, as compared to 2.5 mm and 3.5 mm, respectively, for the selected 4 mm thick workpieces. Therefore, an optimum value of TPH equal to 3.0 mm was fixed and then the effects of RS and TS were further studied experimentally on the thermal cycles, peak temperatures, grain size and hardness variation across the weldment zones. Also, experiments were done to study the effect of FSW process parameters on strain-hardening behaviour of aluminium-alloy plates using the concepts of hardening capacity ( $H_C$ ) and strain-hardening exponent (n). During this process lüder bands are observed due to severe plastic deformation of the material and as such AA5052-H32 is a Al-Mg alloy which resulted in the formation of

luder bands and are varied with respect to TPH. Also, it was found that by increasing tool rotation speed (RS) and decreasing traverse speed (TS), FSW nuggets showed higher values of  $H_C$  and lower values of  $n$ .

In order to quantify the heat input effects and hence the values of RS, TS and TPH on the resulting microstructures and average hardness, temperatures were measured at selected locations within the workpieces during the FSW process. Furthermore, the thermo-mechanical effects due to the tool's rotation were studied by examining the grain size variation across the nugget geometry for different values of RS and TS. Finally, the peak temperatures and average grain sizes were correlated qualitatively to the resulting hardness within the FSW nugget zones. It was observed that the peak temperatures are higher in the advancing side (AS) than the retreating side (RS) and the resulting hardness values are lower in AS than the RS. This is attributed to the increased grain size which lowered the hardness. Further, the Taguchi technique was used to verify the optimum values of process parameters as well the most sensitive parameter based on the predicted mechanical properties. The signal-to-noise ratio as well as the analysis of variance (ANOVA) data was used to study the influence of FSW process parameters on the weld-joint strength. The results clearly indicated that the tool rotational speed (RS) is the most significant and sensitive process parameter in deciding the tensile strength of the nugget.

Further, a three-dimensional, transient, and non-linear thermo-mechanical model was developed using APDL (ANSYS v14.5) to study the effects of FSW process parameters (RS and TS) on the peak temperatures, thermal cycles and for the thermally induced residual stresses within the nugget and its surrounding regions. As an initial step, the thermo-mechanical model developed by Zhu and Chao (2004) for FSW of 304L stainless steel was verified. Subsequently, the model was used for a parametric study on the effect of various process parameters and clamping location on temperature distribution, peak temperatures, and residual stress within the nugget and the surrounding workpieces. It was found that the peak temperatures primarily depend on tool rotational speed (RS), while the final residual stresses depend on traverse speed (TS). Also, experiments were conducted on the welded plates to predict the residual stresses using XRD technique and the results showed increasing tensile residual stresses with increasing TS.

The overall observations from the present detailed experimental as well as numerical simulations are briefly given below; (i) the nugget geometry (shape and size) is significantly influenced by both RS and TS (ii) the mean hardness across the nugget cross-section increased with increase in RS and decreased with increase in TS value, both on advancing and retreating sides (iii) the tensile strength decreased marginally with increase in RS as well as TS values respectively (iv) the optimal values of process parameters for a given 4 mm thick plates of AA5052-H32 found to be TS = 40 mm/min, RS = 500 rpm and TPH = 3.0 mm, and (v) the thermal tensile stresses are lowered either by increasing TS and/or decreasing RS or combination of both.



# CONTENTS

<b>ACKNOWLEDGEMENTS</b> .....	iv
<b>ABSTRACT</b> .....	vi
<b>CONTENTS</b> .....	ix
<b>LIST OF FIGURES</b> .....	xiii
<b>LIST OF TABLES</b> .....	xvii
<b>NOMENCLATURE</b> .....	xix
<b>CHAPTER 1: Introduction</b> .....	1
1.1 Background of the Welding Technologies.....	1
1.2 Advantages of Friction Stir Welding Process .....	4
1.3 Research Objectives.....	5
1.4 Methodology.....	6
1.5 Organization of the Thesis.....	8
<b>CHAPTER 2: Literature Review</b> .....	9
2.1 Effect of Friction Stir Welding Process Parameters .....	9
2.1.1 Nugget geometry and mechanical properties.....	9
2.1.2 Strain-hardening behaviour, toughness and fractography.....	16
2.2 Effect of Tool-pin Geometry .....	18
2.3 Optimization Techniques.....	20
2.4 Thermal History and Residual Stresses.....	24
2.5 Research Gaps in Friction Stir Welding Process.....	29
<b>CHAPTER 3: Experimental investigations of FSW Process Parameters</b> .....	32
3.1 Friction Stir Welding Process.....	32
3.2 Workpiece Material Specifications of AA5052-H32.....	33
3.3 Preparation of Workpieces and Backing Plate.....	35
3.4 Tool Specifications and Design.....	35

3.5 Advantages of D2 Tool-steel.....	37
3.5.1 Straight cylindrical pin.....	38
3.5.2 Conventional milling machine .....	39
3.5.3 Thermocouples.....	41
3.5.4 Data logger.....	42
3.5.5 Mold preparation.....	42
3.5.6 Polishing and etching.....	43
3.5.7 Zone formation in FSW joint.....	43
3.6 Results and Discussion.....	45
3.6.1 Effect of process parameters vs. nugget geometry.....	45
3.7 Tensile Tests on UTM.....	48
3.7.1 Electric Discharge Machine .....	48
3.7.2 ASTM standards.....	48
3.7.3 Effect of process parameters vs. mechanical properties.....	50
3.7.4 Lüder bands, Strain hardening and toughness.....	53
3.7.5 Toughness.....	57
3.7.6 Fractography.....	58
3.7.7 Summary of $H_c$ , $n$ and Toughness.....	62
3.8 Effect of Process Parameters vs. Thermal Cycles.....	62
3.9 Grain Size and Hardness in FSW nugget.....	67
3.9.1 Grain size.....	67
3.9.2 Hardness variations in FSW joint.....	73
3.10 Residual Stress Measurement using XRD.....	77
3.11 Conclusions.....	78
<b>CHAPTER 4: Optimization of FSW Process Parameters.....</b>	<b>79</b>
4.1 Introduction to Taguchi Method.....	79

4.2 Taguchi’s Method of Design of Experiments .....	80
4.2.1 The Smaller-the-Better (STB).....	80
4.2.2 The Larger-the-Better (LTB).....	81
4.2.3 The Nominal-the-Better (NTB).....	81
4.3 Design of Experiments .....	83
4.3.1 Taguchi method for FSW process.....	83
4.3.2 Selection of Orthogonal Array (OA).....	87
4.4 Results and Discussion.....	88
4.4.1 Analysis of data.....	88
4.4.2 Signal to Noise ratio.....	90
4.4.3 Main effect plot.....	92
4.4.4 Interaction plot.....	93
4.4.5 Result evaluation.....	94
4.4.6 Mathematical modeling.....	97
4.4.7 Confirmation run.....	100
4.5 Conclusions.....	101
<b>CHAPTER 5: Finite Element Modeling and Simulations.....</b>	<b>102</b>
5.1 Thermal and Residual Stresses.....	102
5.1.1 Introduction to ANSYS V14.5.....	104
5.1.2 FSW process modelling using APDL.....	105
5.1.3 FSW computational analysis.....	106
5.1.4 Mathematical modelling.....	108
5.1.5 Computational analysis type.....	108
5.1.6 Thermal histories during FSW process.....	110
5.1.7 Thermal stresses in FSW.....	114
5.1.8 Conclusions.....	119

5.2 Residual Stresses.....	120
5.2.1 Residual stresses in FSW.....	120
5.2.2 Methods to measure residual stresses.....	121
5.2.3 Measurement of residual stresses in welded plates.....	122
5.2.4 Residual stress distribution in nugget.....	124
5.2.5 Uncoupled formulation.....	125
5.2.6 Predicting residual stresses in FSW.....	125
5.3 Conclusions.....	135
<b>CHAPTER 6: Conclusions and Future Work.....</b>	<b>136</b>
6.1 Nugget Mechanical Properties of AA5052-H32.....	136
6.2 Heat and Material Flow in FSW Joints.....	137
6.3 Grain Sizes and Hardness in FSW Joint.....	137
6.4 Taguchi's Orthogonal Array.....	138
6.5 Thermal and Residual Stresses.....	138
6.6 Future Works.....	140
<b>REFERENCES.....</b>	<b>141</b>
<b>LIST OF PUBLICATIONS.....</b>	<b>153</b>
<b>BRIEF BIOGRAPHY OF THE SUPERVISOR.....</b>	<b>154</b>
<b>BRIEF BIOGRAPHY OF THE STUDENT.....</b>	<b>155</b>

## LIST OF FIGURES

Figure (1.1) Schematic of FSW process (Davies, 2005).....	5
Figure (1.2) Methodology used for FSW process.....	7
Figure (3.1) Friction Stir Welding stages.....	32
Figure (3.2) FSW welds with range of parameters.....	33
Figure (3.3) AA5052-H32 workpieces with TC locations.....	34
Figure (3.4) Backing plate with grooves for thermocouple seating.....	35
Figure (3.5) Tool geometry with shoulder surface profile used in FSW process.....	37
Figure (3.6) Tools used with different profiles for FSW welds.....	38
Figure (3.7) Fixture set-up on the bed of Conventional Milling machine.....	39
Figure (3.8) Tool profiles used for FSW welds (a) tapered (b) threaded (c) cylindrical.....	40
Figure (3.9) FSW process on Conventional Milling machine.....	40
Figure (3.10) (a) TCs at different positions (b) K-type Thermocouples.....	41
Figure (3.11) Data logger with 8 channels and display.....	42
Figure (3.12) Molded test specimens.....	42
Figure (3.13) Polishing disc.....	43
Figure (3.14) Trinocular Stereoscope.....	43
Figure (3.15) Different zones in FSW joint for RS=500 rpm, TS=40 mm/min, and TPH=3 mm .....	43
Figure (3.16) Weld nugget geometry for different RS, rpm (a=355; b=500; c=710) TS, mm/min (i=28; ii=40; iii=56) .....	46
Figure (3.17) Electric Discharge Machine used for tensile specimen.....	48
Figure (3.18) American Society for Testing and Materials (ASTM) E-8.....	48
Figure (3.19) Tensile test samples prepared.....	49
Figure (3.20) Universal Testing Machine .....	49
Figure (3.21) Effect of TS on load vs. displacement of FSW joints at different values of	51

TPH, mm; (a) 2.5 (b) 3.0 (c) 3.5. Rotational speed, RS=500 rpm.....	
Figure (3.22) Post UTM test specimen of FSW joints for different values of TS, mm/min (28; 40; 56); (a) TPH=3.0mm (b) TPH=3.5mm.....	51
Figure (3.23) Mechanical properties of the FSW joints with different TS (mm.min)..	52
Figure (3.24) Stress-strain curves at different RS (rpm) and TS = 40 mm/min.....	54
Figure (3.25) Schematic of transition temperature in metals.....	58
Figure (3.26) shows the stress - strain curve for high and low toughness materials.....	58
Figure (3.27) SEM micrograph of tensile fracture surface at 500 rpm, TS = 40 mm/min and TPH=3.0mm.....	59
Figure (3.28) SEM micrograph of tensile fracture surface at 355 rpm, TS = 40 mm/min and TPH =3.0mm.....	60
Figure(3.29) Fracture surface of FSW nugget at 710 rpm, 40mm/min , and TPH =3.0 mm.....	61
Figure (3.30) Thermal cycles at selected locations in AS and RS for different traverse speeds, (TS) and same RS and TPH.....	65
Figure (3.31) Peak temperatures across nugget cross-section and at various depths (y=1.5, 2.5mm) from top surface for RS=355 rpm, TS; (a) 28 (b) 40 and (c) 56 mm/min.....	66
Figure (3.32) Peak temperatures across nugget cross-section and at various depths (y=1.5, 2.5mm) from top surface for RS=500 rpm, and TS= (a) 28 (b) 40 and (c) 56 mm/min.....	66
Figure (3.33) Grain size variation in different zones at TS=56 mm/min, TPH =3.0 mm and RS=500 rpm; (a) SZ (b) TMAZ (c) HAZ (d) BM.....	68
Figure (3.34) Elongated base metal grains.....	69
Figure (3.35) Grains at 710 rpm and 40 mm/min of FSW joints; (a) SZ (b) TMAZ (c) TMAZ/HAZ.....	70
Figure (3.36) Average Grain Diameter at 500 rpm and 40mm/min at depth ,z =5, 6, 7 mm on AS and RS.....	71
Figure (3.37) Grain size variation in different zones at TS = 56 mm/min and RS=355rpm; (a) SZ (b) TMAZ (c) HAZ (d) BM.....	73
Figure (3.38) Grain sizes at selected location (y=2.5 mm, z=5 mm) in AS and RS; (a, b) at TS=40 mm/min, (c, d) at TS 56 mm/min.....	73
Figure (3.39) Hardness variation across nugget cross-section and at various depths from	74

top surface; (a) 1 mm (b) 2 mm (c) 3 mm. Rotational speed, RS=500 rpm.....	
Figure (3.40) Mean hardness variation across nugget cross-section and at various depths from top surface.....	75
Figure (3.41) Grain sizes at selected location (y=3 mm, z=6 mm) in AS and RS; (a, b) at TS=28 mm/min, (c,d) at TS=56 mm/min.....	76
Figure (3.42) Measured residual stress on top surface of the plate at 355 rpm and TPH =3.0mm.....	78
Figure (4.1) Defects in FSW joints at (a) RS=355 rpm (b) RS=710 rpm at TS =28 mm/min and TPH =2.5 mm.....	84
Figure (4.2) Main effects plot for (a) means, (b) S/N ratio on UTS.....	92
Figure (4.3) Main effects plots for (a) means, (b) S/N ratio for temperature.....	92
Figure (4.4) Main affects plots for (a) means, (b) S/N ratio for hardness.....	93
Figure (4.5) Interaction plots for means (a)UTS, (b) temperature.....	93
Figure (4.6) Different residual plots for testing the adequacy of proposed model (a) UTS, (b)Temperature, and (c) Hardness .....	99
Figure (4.7) Percentage contributions of process parameters in model(a) UTS, (b) HV, and (c) Temperature.....	100
Figure (5.1) Schematic of Friction Stir Welding Process.....	103
Figure (5.2) (a) Schematic representation of BC's; (b) Modeled 3D mesh in ANSYS program.....	107
Figure (5.3) Figure (5.3) Thermal cycles at a point (depth, z=1.5 mm and width, y=5 mm) within the 4 mm thick plates; (a) 355 rpm, (b) 710 rpm, (c) both RS values.....	112
Figure (5.4) Predicted temperature distribution for RS=500 rpm and TS=40 mm/min; (a) top view (b) cross-sectional view.....	113
Figure (5.5) Temperature and stress-strain variations during FSW process.....	114
Figure (5.6) Stress variation at peak temperatures (start of heating period) on plate top surface for different RS, rpm; (a) longitudinal stress, $S_x$ (b) transverse stress, $S_y$ .....	116
Figure (5.7) Stress variation at transition point (during cooling period) on plate top surface for different RS, rpm; (a) longitudinal stress, $S_x$ (b) transverse stress, $S_y$ .....	117

Figure (5.8) Stress variation at transition point (end of cooling period) on plate top surface for different RS, rpm; (a) longitudinal stress, $S_x$ (b) transverse stress, $S_y$ .....	117
Figure(5.9) Predicted temperature distribution for RS=355 rpm and TS=40 mm/min; (a) top view (b) cross-sectional view.....	119
Figure (5.10) Schematic of types of stresses.....	121
Figure (5.11) (a) Longitudinal and (b) transversal residual stress (a)Longitudinal $\sigma_y$ and (b) transversal $\sigma_x$ residual stress in a welded zone.....	122
Figure (5.12) Finite element mesh used in numerical study.....	128
Figure (5.13) Finite element mesh constrained.....	129
Figure (5.14) Heat generation model of Friction Stir Welding.....	130
Figure (5.15) Stress distribution and close-up cross-sectional views of the residual stress field in x, y and z directions.....	133
Figure (5.16) Longitudinal residual stress at RS=355 rpm, TS=28 mm/min and TPH=3.0 mm.....	133
Figure(5.17) Longitudinal residual stress at RS=355 rpm, TS=56 mm/min and TPH=3.0 mm.....	134
Figure (5.18) Temperature and residual stress distribution at RS=500 rpm; TS=40, mm/min; TPH=3 mm.....	135



## LIST OF TABLES

Table (2.1) Gap areas in FSW process.....	31
Table (3.1) Chemical composition and mechanical properties of AA5052-H32.....	34
Table (3.2) Chemical composition and hardened tool material (AISI D2 Steel) in wt %	36
Table (3.3) Physical and mechanical properties of tool material (AISI D2 Steel).....	37
Table (3.4) Tool geometry and FSW process parameters used.....	38
Table (3.5) Width and depth of the nugget for different FSW parameters.....	46
Table (3.6) Macrographs with defects at different RS and TS values.....	47
Table (3.7) Mechanical properties of the joint at TPH=3.0 mm.....	50
Table (3.8) Strain-hardening exponent, hardening capacity and toughness values at TPH=3 mm.....	57
Table (3.9) Peak temperatures at width, z=6 mm and different traverse speeds, (mm/min), at fixed RS = 500 rpm.....	64
Table (3.10) Average grain diameter ( in $\mu\text{m}$ ) in FSW joints.....	72
Table (3.11) Mean hardness at TS = 40 mm/min.....	75
Table (3.12) Residual stresses on the top surface of the plate.....	77
Table (4.1) Process parameters with their range and three levels.....	85
Table (4.2) Experimental layout - L27 orthogonal array.....	86
Table (4.3) Process parameters - L27 orthogonal array.....	87
Table (4.4) Response table for Means and S/N ratio-UTS.....	88
Table (4.5) Response table for Means and S/N ratio-Temperature.....	89
Table (4.6) Response table for Means and S/N ratio-Hardness.....	89
Table (4.7) Response table for S/N ratio-UTS,TEMP, and HV.....	91
Table (4.8) ANOVA for tensile strength (Means).....	95
Table (4.9) ANOVA for S/N ration of UTS.....	96
Table (4.10) Estimated model coefficients for Means (UTS).....	97
Table (4.11) Coefficients of model for Means.....	98

Table (4.12) Optimal values from Taguchi method.....	100
Table (5.1) Temperature dependent material properties.....	107
Table (5.2) Average peak temperatures at TS=40 mm/min and different RS (rpm).....	111
Table (5.3) Comparison of longitudinal residual stress results from FE simulations.....	131
Table (5.4) Comparison of transverse residual stress results from FE simulations.....	132
Table (5.5) Residual stresses at RS=500 rpm, TS= 40 mm/min, and TPH=3mm.....	134

## NOMENCLATURE

$\nu$	Poisson's ratio
$\mu$	Coefficient of friction
AGD	Average grain diameter
AS	Advancing Side
ASTM	American Society for Testing and Materials
BM	Base metal
DF	Degree of freedom
DOE	Design of experiments
$d_{pin}$	Diameter of pin
E	Elastic modulus
EDM	Electric discharge machine
FEM	Finite element methods
FSW	Friction-stir welding
HAZ	Heat-affected zone
HCHCr	High carbon and high chromium
$h_{pin}$	Height of tool-pin
LTB	Larger the better
NTB	Nominal the better
MS	Mean of squares
P	Axial load
PWHT	Post weld heat treatment
$Q_p$	Heat of tool-pin
$Q_s$	Heat of tool-shoulder
$R_p$	Radius of tool-pin
RS	Rotational speed
RS	Retreating side
$R_s$	Radius of tool-shoulder
R-sq	Regression squared
R-sq(adj)	Adjusted regression
s	Standard deviation
S/N	Signal to noise ratio
SEM	Scanning electron microscope
SS	Sum of squares
STB	Smaller the better
SZ	Stir-zone
TMAZ	Thermo-mechanically affected zone
TPH	Tool-pin height
TS	Traverse speed
UTM	Universal testing machine
WNZ	Weld nugget zone

# CHAPTER 1

## Introduction

### 1.1 Background of Welding Technologies

Welding is a precise, reliable and cost effective technique used for joining of ferrous and non-ferrous metals. It is widely used because of the high strength of the welded joint when compared to other joining methods like riveting, fastening, adhesive bonding. Welding is an indispensable joining technology (for both fabrication and repair works) used in manufacturing industries, such as automotive, aerospace, ship building, power generation, petroleum production and refining, construction and farm equipment, electronics, and medical devices. Also, welding is used to join beams in constructing buildings, bridges and pipelines. Modern structural concepts demand reduction in the weight and cost of materials. In this regard, welding processes have proven to be efficient and cost effective (Davies, 2005).

Conventional fusion welding processes such as Gas Tungsten Arc Welding (GTAW), Gas Metal Arc Welding (GMAW), Laser Welding (LW), etc., are used because of high joint-strength as compared to non-fusion welding processes. During fusion welding process, heating, melting, solidification, and various solid-state transformations take place and these processes influence the microstructures and mechanical properties of the weldment (fusion and heat-affected zones). Also, considerable residual stresses and strains develop during and after welding, which affects the welded joint strength. A development in joining technologies could assist in the introduction of more aluminium based alloys into the automotive industry. Traditionally, joining in automotive structures has been carried out by mechanical fastening (riveting) and to a lesser extent by fusion welding (electric arc). Mechanical fastening has several advantages, which includes the ease of automation, versatility, high speed, low cost, and low energy consumption while maintaining good joint quality possible. However, the process can become relatively difficult when applied to internal joints. In addition, rivets seem to be a prime target for crevice corrosion, despite the use of protective coatings (Miller *et al.*, 2000).

On the other hand, fusion welding of aluminium-alloys (AA) can be quite problematic in contrast to that of steels. For example, fusion welding of AA requires more heat input per unit length of the weld due to high thermal conductivity as well as the use of inert shielding gases, as in metal inert gas (MIG) welding process. Due to the high affinity of aluminium for

oxygen, the shielding gas is a necessity. Regardless of the alloy type (e.g. heat treatable or non-heat treatable), or the starting temper (aged, work hardened, annealed), the chosen welding technique should have a relatively localized thermal field because temperatures as low as 150-250°C can result in a heat-affected zone (HAZ), which can weaken the joint. Temperatures around 550°C and higher can cause various defects, such as mechanical distortion, porosity, solidification cracks, and liquation cracking (Barnes and Pashby, 2000). The non-uniform heating and cooling during the welding process gives rise to considerable inhomogeneity with respect to strength and ductility across the weldment. The base metal (BM) composition plays a significant role in the final microstructures within the weldment. Also, the effect of alloying elements would be different for different heat inputs. Therefore, the selection of the right set of process parameters (for example, current, voltage and welding speed in fusion welding processes) is the key to achieving a good quality weld-joint.

Today, the focus on research in welding industry is the weldability and weld-joint quality, of materials which are light and possess high strength to weight ratio, such as aluminium-alloys (AA2219, AA5052, AA6083, AA7075, etc). The automotive industry demands the introduction of newer economic and efficient joining techniques, as well as new aluminium-alloy sheets with improved weldability, formability, mechanical, and corrosion resistant properties. With the large differences between steel and aluminium in strength, physical and chemical properties, the introduction of alternative joining becomes crucial and necessary (Nandan *et al.*, 2006). Non-heat treatable and work hardenable Al-Mg (AA5xxx) alloys together with the heat treatable Al-Mg-Si (AA6xxx) alloys are the two classes that are used by the most automotive manufacturers. Currently, AA6xxx series alloys (e.g. AA6016 and AA6111 alloys) are the most widely used class in automotive body panels. However, this class is relatively expensive compared to the AA5xxx series, but its alloys are preferred due to better formability and strength improvements. The AA5xxx series alloys are characterized by good formability, weldability, corrosion resistance, and mechanical properties (Davies, 2005).

AA5xxx series alloys are now explored in automotive industry for improving fuel efficiency and passenger's safety. There is very little information available in the literature on the selection of welding processes and optimum process parameters for different workpiece thicknesses and different grades of these alloys. Therefore, experimental and numerical investigations on the weldability and weld quality of AA5xxx series using conventional and hybrid welding processes have become essential to decide upon the potential for replacement of conventional steels by these aluminium-alloys. The development of process maps (process

parameters vs. final mechanical properties for a given welding technology) is essential for making quality welds. There is an urgency and reliance on mechanized, automated and robotic welding systems due to severe shortage of skilled workforce in the manufacturing sector. This implies a large scope for business in integration, automation and robotisation of welding systems thereby reducing the product development cycle time (Miller et al., 2000; Barnes and Pashby, 2000).

Moreover, the joint surface has to be meticulously cleaned, mechanically and chemically, to remove any hydrocarbon compounds like lubricants, since they can lead to porosity. Recently, alternative fusion and solid-state joining techniques have been suggested and investigated, which includes resistance spot welding (RSW), laser beam welding (LBW), and diffusion bonding (DB). Yet, these techniques are still associated with technical concerns (e.g. electrode wear in RSW, LBW efficiency with highly reflective surfaces, and the surface preparation in DB), as well as their economic limitations due to the high capital investment (Barnes and Pashby, 2000). Recently, the Friction Stir Welding (FSW) technique has been applied successfully to cryogenic tanks, marine structures, train panels, air frames, and even automotive Body in White (BIW). Due to rapid success of FSW technique, its commercialization has started long before establishing a fundamental understanding of the overall process. Research on FSW is expected to encourage further spread of this technique into the transportation industry, notably by studying the influence of the process parameters on weldment properties. This influence can only be established by linking the material features to the micro and macro-properties as well as the mechanical properties, which is the current topic of study.

Materials are explored for automotive applications due to their high strength to weight ratio. In these materials, alloying elements are used to achieve desired mechanical properties. FSW can produce defect free and high-quality welds with respect to different materials, which otherwise may not be possible to weld with other conventional fusion welding technologies. Tool steels are used in FSW of aluminium alloys and is generally considered to be a non-consumable one (Nandan et al., 2006).

## 1.2 Advantages of Friction Stir Welding Process

The key advantages of the Friction Stir Welding (FSW) process are listed below.

- It results in significant microstructural evolution within and around the nugget zone. This leads to substantial changes in weld-joint mechanical properties.
- Thermal and residual stresses are low due to low temperatures as well as slow heating and cooling rates involved.
- Joining of similar and dissimilar light-metals such as aluminium-alloys, composites and high strength materials are possible.
- Full penetration in a single-pass weld, fewer number of defects, no consumables, etc., are the few additional advantages.
- Lastly, consistency weld quality together with high productivity is achievable.

However, the FSW process has few disadvantages, such as exit hole left at the end of the weld, sensitive to joint tolerances, tool material limitations, etc.

Friction stir welding (FSW) technique was invented and patented by W. M. Thomas *et al.*, (1991) of the Welding Institute in Cambridge, United Kingdom. In FSW, a cylindrical and shouldered tool with a profiled probe is rotated and plunged slowly into the joint (a line between two workpiece materials), which are to be butted together. The workpieces are rigidly clamped onto a backing plate in a manner that prevents the abutting joint faces from being forced apart. Frictional heat is generated between the tool shoulder and the workpieces, as shown in Figure (1.1). In FSW process, the movement of tool generates the heat required to soften the material and cause the material to flow. The tool rotation results in stirring and mixing of material around the tool-pin. Also, the rotation of tool causes the flow of stirred material from frontend (advancing side) to rearend (retreating side) of the tool-pin. Finally, it leaves a solid-state without melting the material, i.e., the maximum temperatures involved are below the melting temperature of the workpieces to be joined and hence the name, solid-state joining process.

The applications of FSW process in various industries led to the drastic demand for the joining of both similar and dissimilar materials. The industries which utilize the FSW process are; aerospace, defense, railway, land transportation, ship building, and construction. These industries need lightweight and strong metals such as aluminum-alloys. Therefore, this

dissertation examines the process parameters associated with the FSW with respect to mechanistic process characterization, and considerations necessary for implementation of the optimized process parameters to achieve defect free and quality welds of 4 mm thick AA5052-H32 plates.

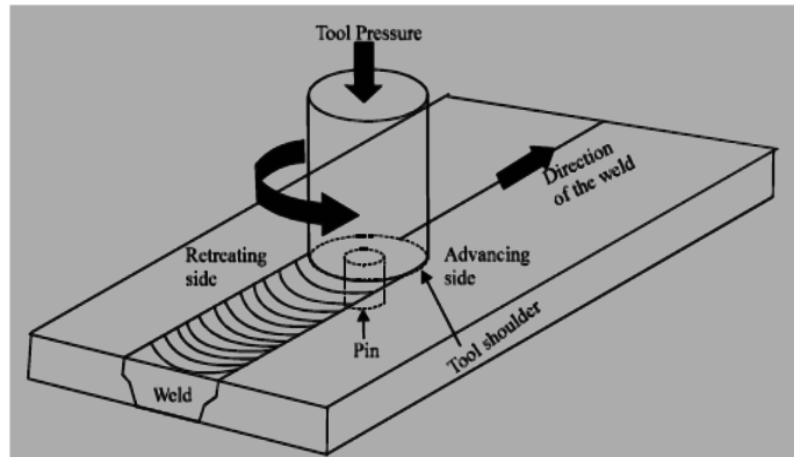


Figure (1.1) Schematic of FSW process (Davies, 2005).

### 1.3 Research Objectives

The aim of the proposed research work is to thoroughly understand the different phenomena (thermal, mechanical and metallurgical) taking place during welding of AA5052-H32 plates using Friction Stir Welding (FSW) technique. The present research work mainly focuses on the following five objectives:

- The First objective is to study the FSW joint quality of AA5052-H32 plates by measuring the weldment properties.
  - Mechanical properties, namely yield strength, tensile strength, % elongation, and hardness of joints.
- The second objective is to study the effects of process parameters and tool's geometry on the resulting mechanical properties of FSW weldments.
  - Process parameters – tool's rotational speed (RS) and traverse speed (TS), also referred to as welding speed.
  - Tool geometry - tool-pin height (TPH) and shape (cylindrical or tapered).
- The third objective is to numerically study the heat and material flow effects on the resulting microstructures and properties of the FSW weldments.
  - Grain size and hardness variation across the nugget cross-section.



- The fourth objective is to optimize the parameters (RS, TS and TPH).
  - Taguchi’s Orthogonal Array method.
  - Validation of optimized values with experimental results.
- The fifth and final objective is to study the different phenomena taking place during FSW process using Finite Element Method (FEM) based software called, ANSYS.
  - Thermal and mechanical phenomena
    - Temperature distribution
    - Thermal stresses
    - Residual stresses

The purpose of numerical study is to understand thoroughly the role of different phenomena taking place simultaneously during the welding process, so that a quantitative data on the resulting microstructures and mechanical properties can be obtained through off-line numerical simulations. Therefore, an integrated thermo-mechanical model will be developed, tested against the experimental data, and finally used to study the effect of process parameters on the resulting weldment. These include, weldment geometry (size and shape), the thermal residuals (stress-strains) in the welded joint, the microstructures, and average mechanical properties within the weldment.

## **1.4 Methodology**

To accomplish the above research objectives set forth for this overall study, a methodology was devised and followed. The methodology is an experimental and numerical approach for the optimization of FSW process parameters. The first task was to sketch a design of experiments (DOE) after considering the various published papers as discussed in the literature review (Chapter 2). The second step was to develop a model using the data generated by the DOE. An optimization technique (Taguchi’s-orthogonal array-OA) was developed to relate process parameters with responses, i.e., RS, TS and TPH. The performance of the developed surrogate model was estimated using statistical measures called ANOVA. The predicted results are verified with the experimental results and a confirmation test was carried to analyze the effect of process parameters on the mechanical properties.

In the next step, a thermo-mechanical model was used to simulate the FSW process. The thermo-mechanical model was developed using commercial finite element analysis

software, called ANSYS V14.5 (APDL), to perform parametric studies and to investigate the effects of various process parameters on temperature distribution, and thermal and residual stresses in the workpiece. Finally, the optimal results were validated by simulations using ANSYS. Figure (1.2) presents the overall methodology of FSW process used in the present study.

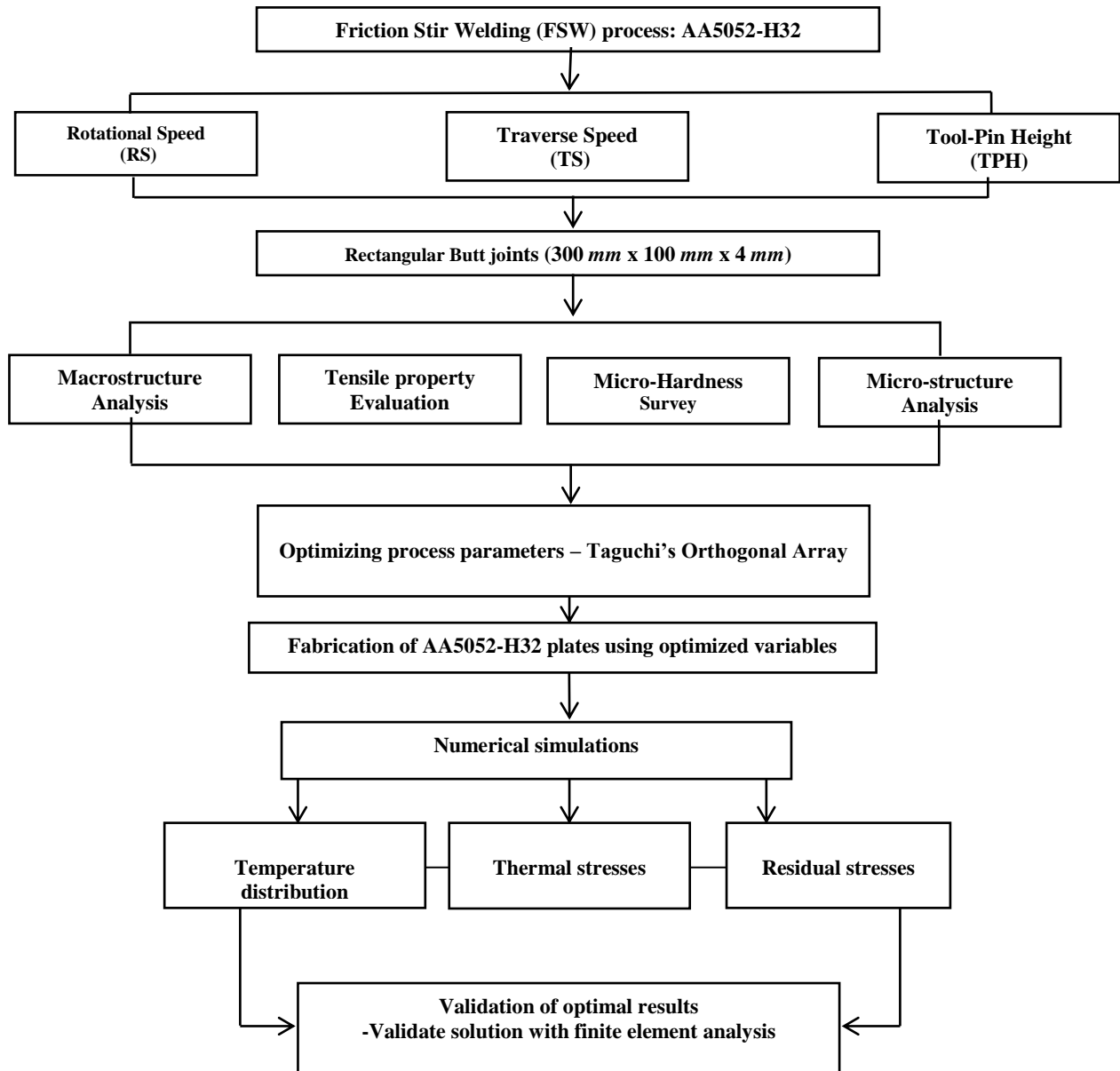


Figure (1.2) Methodology used for FSW Process.

## 1.5 Organization of the Thesis

The following paragraphs briefly explain about the thesis layout in terms of individual chapters.

Chapter 1 presents the rationale and structure of the thesis. The chapter highlights the FSW process along with a brief introduction on welding technologies, including the FSW process, and its merits and applications. The objectives of the proposed research have been described. Finally the organization and the methodology adopted in the thesis have been highlighted.

Chapter 2 presents the detailed literature review on the FSW process and the influences of the parameters, such as the tool's rotational speed (RS), traverse speed (TS) and tool-pin height (TPH) on the resulting mechanical properties of the aluminium-alloy welded joints.

Chapter 3 presents the complete *experimental* investigations carried out to join aluminium- alloy (AA5052-H32) using FSW process and the effects of process and geometry parameters, on the final mechanical properties (tensile strength, hardness, ductility, etc.) as well as the macro and micro-structures of the welded joint.

Chapter 4 briefly explains how the Taguchi's Orthogonal Array (OA) technique was used in the optimization of the process and tool geometry parameters, which results in defect free welded joints. Apart from the process parameters (RS and TS), the tool geometry, tool-pin height (TPH) and shape, also plays an important role in the joint efficiency.

Chapter 5 focuses on the Finite Element (FE) model of FSW process carried out to investigate the thermal history and influence of process parameters on the distribution of heat in different zones of weldment. Also, this chapter gives the detailed analysis from the investigations of FE model on thermal and residual stresses.

Chapter 6 presents on the overall summary and conclusions from the current research study on FSW process and the scope for future works.

## **CHAPTER 2**

### **Literature Review**

This chapter has been divided into four sections. The first section reviews the experimental studies on the Friction Stir Welding (FSW) process parameters such as rotational speed (RS) and traverse speed (TS) as well as their influences on the mechanical properties of different aluminium-alloys. The second section reviews the works related to tool-pin geometry and its effect on strain-hardening exponent, toughness and micro-structure. The third section gives details on the optimization techniques used in the FSW process, and the final section reviews the works on thermo-mechanical modeling studies of the FSW process.

#### **2.1 Effects of FSW Process Parameters**

##### **2.1.1 Nugget geometry and mechanical properties**

In order to produce quality welds by Friction Stir Welding (FSW) technique, it is important to understand the role of process parameters and their effects on the macro- and micro-structures and the final mechanical properties of the weld nugget. In the FSW process, the key parameters include tool rotational speed (RS), traverse speed (TS), axial load (P), tool-pin height (TPH).

The two tool speeds, RS and TS considered in FSW process have significant importance and must be carefully selected to ensure a good weld quality. The relationship between the tool speeds and the net heat input during welding is complex, but in general, it can be said that increasing the RS and/or decreasing the TS will result in more heat input per unit length and hence a hotter weld. In order to produce a successful and defect-free weld, it is necessary that the material surrounding the tool becomes hot enough to enable the sufficient plastic flow required and reduce the forces acting on the tool. If the material is too cold then voids or other flaws may appear in the stir-zone and in extreme cases the tool may even break.

These competing demands led to the requirement of developing a process window and selecting a range of process parameters that produces a good quality weld. This in turn, is judged in terms of the welded joint mechanical properties like yield strength, tensile strength, % elongation, and hardness.

The tool rotational speed (RS) plays an important role in the amount of total heat input supplied during the process. However, this phenomenon is mostly analyzed qualitatively, and the conclusions have been made based on the weld defects observed. The optimum range of RS values is an important parameter required to achieve a high quality weld, since the variation of this parameter will affect the thermo-mechanical conditions which effect the micro-structural changes in the workpieces. This optimum range is affected by various parameters such as the thickness of workpiece, type of metal alloy, geometry of the tool, and welding speed. Studies on similar and dissimilar welds of aluminium-alloy plates by FSW technique and the effects of process parameters on the nugget properties were done by different researchers and their findings are briefly discussed below.

Adamowski et al., (2007) identified and analyzed the mechanical properties like tensile strength and fracture in AA6082-T6 and found that the tensile strength is directly proportional to traverse speed (TS). Softening of the material was observed in the weld region and mostly evident in the heat-affected zone (HAZ) on the advancing side of the welds and corresponded to the failure location in tensile tests. The reason for this phenomenon is due to the kinetic and thermal asymmetry of the FSW process.

Apart from the tensile strength, the ductility of the material influences the formability of the welded joints. Hamilton et al., (2008) studied with respect to AA7136-T76511 and found that the % elongation significantly reduced (50-75%) from its base metal value. Also, the fracture of tensile specimens occurred on retreating side of the weld along the interface between heat-affected zone (HAZ) and thermo-mechanically-affected zone (TMAZ), irrespective of rotational speed. Huang et al., (2012) identified an interface behaviour for filling friction stir weld joining of AA2219 and enhanced mechanical properties in the range of 200-900 rpm for RS and in the range of 100-400 mm/min for TS. No defects were found after tensile tests. The average ultimate tensile strength and elongation were 172 MPa and 11.2%, which are equal to 90% and 82% of the base metal, respectively and without defects.

In dissimilar welding of aluminum-alloys using FSW technique, the following are the few observations made by different researchers. The fractures of the aluminium-alloys were studied by Sevansson et al., (2000) for AA5083 and AA6082. They observed that in AA5083 fracture occurred near the center of the weld, while in AA6082 fracture occurred in HAZ. Also, the tensile strength of AA6082 was lower than the base metal (BM). Hardness was found to be nearly same along the cross-section in AA5083 and minimum in AA6082. Sound welds were obtained and the results were compared with AA7075. Debroy et al., (2010)

analyzed the effects of loading conditions on the failure modes of dissimilar aluminium-alloy joints by FSW process and found that the failure occurred at a much lower load during tensile loading than during shear loading. Also, the authors presented experimental data on load carrying capacities and fatigue of dissimilar aluminium-alloy FSW welds.

Rodrigues *et al.*, (2010) showed that establishing suitable axial-load values depends strongly on base material characteristics. Bozkurt and Duman (2011) studied the mechanical property variations in AA3003-H24 and 2124/Sic/25p-t4 alloy joints at rotational speed of 900 *rpm* and traverse speed of 125 *mm/min*. It was found that the maximum tensile strength is about 182 MPa. And, the hardness across the weld nugget varies and a minimum value occurred on retreating side of the HAZ. Chi *et al.*, (2012) studied the mechanical properties and material mixing patterns of friction-stir spot weld (FSSW) joints of dissimilar aluminum-alloys (5052-H32 and 6061-T6). The parameters such as the axial force and torque were measured as a function of the tool displacement. The experimental results illustrated different process parameter histories, material mixing in the stir-zone (SZ) and material properties, including microhardness distributions and are strongly affected due to stress concentrations induced by the hook near the SZ.

Madhusudhan *et al.*, (2013) studied about joining of dissimilar aluminum-alloys (AA6262-T6 and AA7075-T6) by varying the weld process parameters (tool rotational speed, weld speed and axial force) with cylindrical tool-pin profile. They concluded that better mechanical properties (hardness and tensile strength) are obtained with the FSW plate welded with 1200 *rpm*, 36 *mm/min* and 9kN axial force as compared with other range of values.

Coming to the effect of process parameters on microstructural and other mechanical properties of friction stir welded aluminium-alloys, the hardness and grain sizes observations by different researchers are given below. Hassan *et al.*, (2003) investigated the effect of welding parameters on the structure and properties of the nugget zone in AA7010. It was found that there is an optimum rotational speed, for a given traverse speed, that gives the highest strength and ductility for the nugget zone. As the traverse speed is increased, it is necessary to increase the rotational speed to maintain this optimum condition. For a given traverse speed, there is a significant variation in grain size and hardness from the top to the bottom of the welds.

Basil et al., (2005) used friction stir processing (FSP) on aluminum-alloy (AA5052) and showed that the grain structures are very fine and homogeneous. The hardness of FS processed area increased with the decrease in RS, and the increase of TS resulted in the hardness profiles higher at the bottom and lower at the edge of the processed zone. Based on microstructural results, they developed a correlation between the resulting grain sizes and the Zener-Holloman parameter. Smaller grain sizes were found at lower rotational speeds, and less effect of traverse speed on the grain sizes are identified. Raghu Babu et al., (2008) investigated the effect of process parameters on mechanical and microstructural properties of aluminium-alloy (AA6082-T6). They identified that the tensile strength of the joint is lower than that of the base metal. Decrease in hardness in the weld region and tunnel defect were observed at the intersection of SZ and thermo-mechanically affected zone (TMAZ) due to high rotational speed and traverse speed. Also, the welded samples did not fail in bend test. Cam et al., (2009) studied on the microstructural and mechanical characterization of friction stir butt joints of 63%Cu - 37%Zn brass plate and investigated the joint performance by conducting optical microscopy micro-hardness measurements and mechanical testing by both tensile and bend tests. The effect of process parameters on the joint performance was studied and found that 1600 rpm and 225 mm/min gave 2.8 mm penetration for 3 mm thick workpieces with 4 mm tool root diameter, and the 3 mm tip diameter.

Govind et al., (2010) compared the hardness, yield strength, ultimate tensile strength, and % elongation with Metal Matrix Nano Composites (MMNC). They found that the joint strength increased to 88% compared to fusion welded joints and fine grain structures were observed. Varun kumar et al., (2012) carried out the experiments with and without silicon carbide powder and analyzed the effect of RS in the range of 600-1200 rpm and TS in the range of 36-72 mm/min. The optimal values were found at 1200 rpm, 72 mm/min and axial load of 8 kN. Also, it was found that maximum hardness occurred at the centre of the weld as compared to other zones of weld joint and is attributed to intensive stirring process.

Razal et al., (2013) investigated on the magnesium alloy (AZ61A) with five different rotational speeds to fabricate the alloy joints. Tensile properties of the joints were evaluated and correlated with the microstructures observed in the stir-zone (SZ). The formations of very fine grains in the SZ were observed, which create superior tensile properties for the joints. The yield strength (YS) and tensile strength (UTS) of all the joints were found to be less than that of the base material, irrespective of the RS and TS values used.

Therefore, from the above reviews, it can be concluded that the rotational speed alone will not yield or impart strength to the FSW joints, but also the other process parameters like traverse speed, axial load also influences the weldability and joint quality of the plates.

Material stirring and heat generation in friction stir welding processes induces significant microstructure and material properties alterations. The RS and TS values for a given alloy are determined by the necessity of producing a defect free solid weld. If the energy input per unit length travelled is too high, melting occurs in the workpiece. If the energy input per unit length travelled is too low, incomplete fusion occurs. In both cases, the FSW process is a failure case. Therefore, limiting the parameter selection to a specific range of rotational speeds and traverse speeds is an important stage.

In precipitation strengthened aluminum-alloys such as AA6061, the energy input into the weld nugget raises the temperature high enough to dissolve strengthening precipitates. Regardless of the material, the resulting microstructures are different in three distinct zones that result from the FSW process. They are stir-zone, SZ (lies at the center of the weld along the weld centerline), thermomechanically-affected zone, TMAZ (bordered on either side of SZ) and heat-affected zone, HAZ (surrounding the outside edges of the TMAZ).

In particular, the experimental research works revealed several aspects of different phenomena affecting the mechanical properties and are briefly discussed below.

*Stir-Zone (SZ)*: This zone is also known as Dynamically Recrystallized Zone (DXZ). The DXZ is defined as the area that has direct interaction with the tool probe and is also referred to as the weld nugget. Dynamic recrystallization is the process by which extreme strains and elevated temperature cause recrystallization of material in the weld nugget as the tool passes through it, resulting in a dispersion of fine, equiaxed grains in this area. The DXZ is relatively small, and is characterized by a shape loosely resembling the FSW tool used. The zone is characteristic of all friction stir welds, and has several qualities that are significantly different from the surrounding microstructural zones. In DXZ, the dynamically recrystallized grains are sometimes an order of magnitude smaller than the grains of the base material (Mishra and Ma, 2005). Another notable characteristic of the DXZ is the occurrence of the phenomenon known as “onion rings”. Onion rings are features of the microstructure depicted in Chapter 3, where shell extrusions in the DXZ create a visible circular geometry that has a cross-sectional view that is similar to a sliced onion.



*Thermo-Mechanically Affected Zone (TMAZ):* The TMAZ is a zone entirely unique to FSW and is characterized by severe plastic deformation of grains of the base material as well as exposure to elevated temperature from proximity to the DXZ. The grains in this zone are plastically deformed from shear induced by the tool rotation. The degree of plastic deformation in the TMAZ varies by proximity to the weld and depth in the joint. Grains have a higher degree of plastic deformation closer to the weld and nearer to the tool shoulder, tapering to grains that are less deformed further from the weld centerline (Mishra and Ma, 2005). Mishra and Ma (2005) reported and discussed the results provided by a numerical and experimental investigation on AA2024-T3 butt joint made by FSW process using an unthreaded conical tool. In particular, attention was focused on the influence of RS and TS on joint quality, microstructure and mechanical properties, adopting a full factorial design of experiments

*Heat-affected Zone (HAZ):* The HAZ is characterized by a microstructure that is not plastically deformed but is still affected by the thermal energy of the FSW process. The welding parameters may vary significantly depending on the nature and intent of the process, resulting in a significant variation in corresponding HAZ width and depth. The boundary between the unaffected base material and the HAZ is difficult to distinguish because the variation in properties between these is very small. The works on friction stir welding of AA6061 alloy and optimizing the process parameters to obtain a defect free weld are studied by Khumbhar et al., (2008), who analyzed the microstructural changes associated with the mechanical properties of the joint. Kumar and Kailash (2008) reported that grain sizes increased with increasing axial load. It was reported that high density secondary particles exhibited large resistance to recrystallization in SZ. Fujimoto et al., (2008) studied about the joint hardness distribution controlled by the density of the precipitates between the two sheets of AA6061 alloy in the SZ and observed a fine grain structure without any inclusions or precipitates due to intense plastic strain lead to dynamic recrystallization.

Bahemmat et al., (2009) observed that the hardness in SZ decreased with increasing tool rotational speed. However, the grains in SZ are larger with tapered tool-pin than the four-flute tool-pin. The fine and equiaxed grains in SZ were observed by other research groups and attributed to recrystallization phenomenon at higher RS (600-1000 rpm). Good surface appearance was observed at these rotational speeds. At higher rotational speed, plastic deformation is more pronounced due to increased heat generation, leading to material outflow and hence tunnel defects.

Xu et al., (2009) studied the dynamic recrystallization effects on grain sizes and found that the grain sizes decreased from top to bottom in SZ. Further, the authors observed that the formation of onion ring structures in SZ and its size increased with increasing RS. It was also reported that in SZ the grain sizes decreased with increasing RS.

Yong-Jai et al., (2009) investigated the grain sizes and insoluble particle densities in SZ and found that the density of secondary particles decreased due to recrystallization phenomena.

An empirical model was developed by Rajakumar et al., (2012) to predict the average grain size, hardness, and tensile strength by incorporating the tool-pin geometry and FSW process parameters.

Koilraj et al., (2012) published a comprehensive review report on mechanisms responsible for the formation of welds, microstructural refinements and the effect of process parameters on final mechanical properties of friction-stir welded joints.

Shen et al., (2012) studied that grain size in the recrystallization area is affected by RS and TS in AZ31B magnesium-alloy joints. Also, micro-hardness profiles showed W-shape with a peak in the SZ and minimum value between the TMAZ and the HAZ. An increase in the tool-pin diameter led to the coarsening of  $\alpha$ -Mg grains in all three zones (SZ, TMAZ and HAZ) because of more heat generation. This led to the decrease in the microhardness values across the weld cross-section. Carlone et al., (2013) observed that the higher rotational speed allowed adequate flow conditions and material deposition, resulting into the absence of defects. At lower rotational speed several defects (channel and kissing bond defects) have been detected in the advancing side of the SZ.

The final mechanical properties depend on the process parameters (RS and TS) and tool geometry (TPH). The tool geometry plays an important role to allow the severely plasticized material to move forward from AS to RS within a finite width for a required thickness of the workpiece without defects. The extruded material from bottom surface of the workpiece to the top surface will flow from the gap provided by the concavity (not more than 2°) of the tool shoulder and tool-pin height (minimum) gap provided leading to fine grain size in the nugget zone and solid transformation in TMAZ and HAZ which will result in high tensile strength and can initiate crack if sufficient amount of material is not filled and lead to defects. It further leads to increase in the zone size in width and depth direction of HAZ as the tool traverses. Increase in the size of HAZ results in crack propagation in AS and is clearly visible from the fracture of the tensile specimens.

This further enabled us to find the optimum process parameters and form DOE to perform further experiments. The increase and decrease in width and depth direction for

different values of RS, TS and TPH of different zones are calculated and observed the effect of weld joint quality in terms of tensile strength, ductility, hardness etc. This is not studied by any researcher on AA5052- H32 and created gap areas which lead to one of the objective of my research. The increase in the size of HAZ lead to the fatigue crack propagation resulting in smaller cracks in the weldment. This further rises to the compressive residual stresses. So the HAZ zone should be decreased and it is possible through optimum process parameters only.

Many researchers tried to decrease the size of the HAZ through post welding heat treatment (PWHT) which reduces likelihood for fatigue to initiate the crack in the central portion of the weld track and also change the mechanical properties of the weldment when compared with base metal properties.

Strong joints with lower process forces can be obtained by the optimum tool-pin height by checking the macrographs width and depth of zones. Fixed TPH has an observable impact on the microstructure and resulting properties of the weld by suppressing the weld porosity and worm hole defects.

The effects of process parameters (RS and TS) on the microstructure and hardness of various zones of FS welded aluminum plates, are analyzed. Apart from RS and TS, tool geometry had an effect on the weld nugget, and the SZ had very fine grains due to its higher temperature and severe plastic deformation. Madhavi et al., (2014) observed that by moving away from the weld center and towards HAZ, the grain sizes increased. At a distance of 4 mm from the weld center, many of the prior grains of the parent material started to appear which was corresponding to the HAZ, and the hardness dropped here as the precipitates were coarsened.

### **2.1.2 Strain-hardening behaviour, toughness and fractography**

Along with the microstructures and mechanical properties, strain-hardening behaviour of the FSW joints plays an important role in the material load bearing properties. Strain-hardening is one of the most common methods practiced to enhance the strength of the materials by inducing plastic deformations. Strain-hardening behaviour is greatly influenced by grain size and dislocation density. Therefore, it plays an important role in determining the mechanical properties in FSW joints due to severe plastic deformation. During this process lüder bands are observed due to plastic deformation of the material. Deformation is non homogeneous at small plastic strains and concentrated in discrete bands in regions of stress concentration (that

yield first) which are undesirable and studied with FSW process parameters which is the significant gap area.

Afrin et al., (2007) reported that the flow stress in FSW samples are less compared to the base alloy using two modified equations of hardening capacity and strain-hardening exponent, where the elastic deformation stage was excluded. Chowdhury et al., (2010) observed that hardening capacity ( $H_c$ ) of the double-sided arc welded samples are twice that of the base metal, with the hardening capacity of FSW samples lying in between them. Lakshminarayanan et al., (2010) concluded that the microstructural configuration influences the stress-strain behaviour of the material by work hardening due to the plastic deformation. Chen Xu (2010) confirmed through SEM results that a remarkable influence comes from the precipitates and second phases, which led to the formation of dimples and ductile fracture. Ceeri et al., (2011) worked on double-lap Friction Stir Welded joints of 2024-T3 and AA7075-T6 followed by post-weld heat treatment and found that tensile properties vary with and without post-weld heat treatments. However, the strain-hardening coefficient decreased with post-weld heat treatment. Feng et al., (2011) showed that the yield strength, ultimate tensile strength, ductility, joint efficiency, and net flow stress after yielding increased with increasing the traverse speed. Khodaverdizadeh et al., (2012) found that decreasing traverse speed and increasing tool rotational speed resulted in reduction of dislocation density and grain growth in SZ and HAZ, which lead to increased hardening capacity and decreased strain-hardening exponent. Dawood et al., (2014) found that reduction in surface roughness reduces friction and narrows down the HAZ at the weld root. Ahmed et al., (2014) found onion ring patterns in SZ, which appears like lamellar structures. Also, the fatigue test revealed step formation in the FSW joint of AA5052-7075. Liang et al., (2016) worked on the strain-hardening behaviour of TZAV-30 alloy with various heat treatments and observed that strain-hardening exponent is approximately 0.061 for WA (water quenching + air cooling) specimen, 0.068 for FC (furnace cooling), 0.121 for AC (air cooling) and 0.412 for WQ (water quenching). Mansoor et al., (2016) found that the morphology of the Si phase was altered to acicular structure due to the modification process. In comparison, the un-modified alloy contained Si phase in needle-like structure. The effect of modifier improved the mechanical properties (yield strength by 50%, tensile strength by 56% and elongation by 200%). Dorbane et al., (2016) identified that at temperature lower or equal to 200°C, the main crack initiation and fracture occurred in AA6061-T6, and ductility decreased.

It can be found from open literature that studies are reported on the strain-hardening behaviour of Al-alloys, but not with the FSW joints of AA5052-H32. So, with increasing RS

or decreasing TS, the FSW nuggets revealed higher hardening capacity and lower strain-hardening exponent in contrast to the base metal (BM). The tool rotational speed (RS) has significant effects on stress-strain curve and hence the ductility and toughness. FSW joints of AA5052-H32 plates (150 mm x 100 mm x 4 mm) were made for different process parameters and the results are discussed in Chapter 3.

## **2.2 Effect of Tool-Pin Geometry**

Besides the effect of FSW process parameters (RS and TS) on weldability and weld quality, the influence of tool geometry (size and shape) has been studied by few researchers and is discussed below.

Elangovan et al., (2008) conducted experiments to know the influence of tool-pin profile and welding speed (traverse speed, TS) on the formation of friction stir processing (FSP) zone in AA2219. The study revealed that out of straight cylindrical, tapered cylindrical, threaded cylindrical, square and triangular tool pin profiles; square tool pin profile gives the highest tensile strength and yield strength value in FSP zone.

Bahemat et al., (2008 and 2009) carried out the FSW process on AA2024 for different rotational speeds and tool-pin profiles. The tool-pins used are four flute and taper screw threaded. No defects were found, but observed that the shape of the tool-pin has significant effect on the joint microstructures and final mechanical properties. Also, it was found that the four flute shape exhibited superior tensile properties such as tensile strength and reached upto 90% of base metal mechanical properties. Yong-Jai Kwon et al., (2009) have made successful and defect-free welds at all tool rotational speeds. Especially at 1000, 2000 and 3000 rpm, and the welds exhibited very smooth surface texture in friction stir welding of AA5052 plates. The grain size in the weld nugget was smaller than that in the base metal, and decreased with increasing the tool rotation speed. Finally, the weld nugget exhibited higher average hardness than that of base metal (BM).

Madhusudhan et al., (2011) observed the influence of tool rotational speed and tool-pin profile on defect formation/elimination in AA2014-T6 weld. Two different pin profiles - threaded and thread less have been used during FSW and micro-structural characterizations of weldments produced with different process parameters. The authors mentioned that there is hardly any systematic study which directly compares the effect of tool-pin profile on mechanical properties of AA2014-T6 welds using Taguchi DOE technique.

Qasim et al., (2011) and Palanivel et al., (2011) conducted an investigation to understand the effect of tool-pin profile and tool diameter on microstructure and mechanical

properties in aluminum-alloy, and analyzed five different tool-pin profiles (straight cylindrical, threaded cylindrical, triangular, square, and threaded cylindrical with flat), with three different rotation diameters (3, 4, 5 mm) used to fabricate the joint. Increasing tool-pin diameters from (3 to 5 mm) by a step of 1 mm and keeping all other parameters fixed, resulted in an increase in mechanical properties of the welded joints. The square pin profile gave better tensile properties and a stirred zone with finer grains compared to other weld zones. Jamshidi Aval et al., (2011) investigated the effect of geometric tool parameters on mechanical and micro-structural behaviour during dissimilar friction stir welding of 5 mm thick plates of AA 5086-O and AA 6061-T6. Three tool geometries were used; a conical probe with three grooves, threadless cylindrical probe, and a threaded cylindrical probe. The conical probe with three grooves produced a higher heat input. It also resulted in more homogenous temperatures in the stir zones, resulting in finer grains in the AA 6061 side than those produced in the AA5086 side. Also, decreasing the weld pitch resulted in coarser grains.

The weldability of non-heat treatable and heat treatable aluminium-alloys, which are widely used in fabrication, are compared by analyzing the welds obtained from both materials under a large range of welding conditions (tool dimensions, rotational and traverse speeds, axial loads and tilt angles) chosen to ensure high welding speeds. It can be concluded that high traverse speeds can be achieved in FSW of both, with carefully chosen process and tool parameters. These in turn are strongly dependent on the base material characteristics and plate thickness. In fact the study proves that below certain shoulder dimensions dependent on plate thickness, and for very low tilt angles it is not possible to achieve non-defective welds whatever the process parameters in use.

Based on the above literature survey and the findings by others researchers existing with respect to the tool geometry parameter i.e., tool-pin height (TPH) in the FSW process is not identified and lead to gap area. Besides the FSW process parameters (RS, TS and TPH), the tool geometry plays a significant role in the overall heat input and the resulting plasticized material flow around the rotating tool. There is either little or no information available on the selection of welding processes and geometry parameters for different thicknesses and different grades of the newer materials. Therefore, the development of process maps (process parameters vs final mechanical properties) for any given welding technology is essential for producing quality welds.

FSW technique can produce defect free and high-quality welds with respect to different alloy materials, which otherwise may not be possible to weld with other

conventional fusion welding technologies. So far, FSW has been widely used for low-melting temperature materials, such as aluminium and titanium alloys. Tool steels are used as the welding tool in FSW of aluminium- alloys. It is generally thought that the welding tool is non-consumable in FSW of aluminium -alloys (Nandan *et al.*, 2006). Very few researchers have studied the effect of tool-pin height (TPH) in the FSW process. Also, no one observed the effect of this tool geometry parameter along with the process parameters (RS and TS) and was able to identify the optimum TPH to produce effective and defect free welds which gives the mechanical properties at least up to 90% of the base metal. Also, joining of aluminium-alloys of different series, dissimilar aluminium-alloy with different metals and alloys were researched, but very few researchers worked on AA5052-H32. It should be noted here that the use of AA5052-H32 to produce parts for different light weight products in aerospace, automobile, shipbuilding industries using FSW gave the scope to focus on. The micro-structural studies of FSW of different aluminium-alloys are studied to some extent, but the numerical study of heat input effects on weld geometry, microstructures and mechanical properties of AA5052-H32 is lagging. The existing literature lacks the study of the effects of process parameters, net heat input and also the effect of alloying elements on the resulting microstructures and mechanical properties of AA5052-H32 weldments with respect to tool-pin height (TPH).

Filling the above gaps was the motive of this research work and hence investigating the different phenomena taking place during welding of AA5052-H32 using FSW processes. Towards this, an integrated thermo-mechanical model was developed and validated with the experimental data such that a quantitative data on weldment geometry, thermal and residual distributions, final microstructures and mechanical properties could be obtained through off-line numerical simulations.

### **2.3 Optimization Techniques**

Welding parameters play a very significant role in determining the quality of a weld joint. The joint quality can be defined in terms of final properties such as weld-bead geometry, mechanical properties, and distortion. Generally, all welding processes are used with the aim of obtaining a welded joint with the desired weld-bead parameters, excellent mechanical properties with minimum to no distortion. In this process of achieving desired weld joint quality with minimum experimental trials to reduce the economic considerations, optimization techniques are being used.

Optimization technique is an iterative process of finding the optimal process parameters without violating the set of constraints. Friction stir welding (FSW) process, in general, can also be optimized by obtaining optimal values for parameters such as tool rotational speed (RS), axial force (P), traverse speed (TS), tool dimension and other such parameters. Several optimization techniques can be applied to optimize FSW process. The Taguchi design is an efficient and effective experimental method in which a response variable can be optimized. However, as the FSW is relatively new technology, there have been only a few attempts so far to use the optimization techniques. Some of the optimization techniques applied to FSW process have been summarized in the following paragraphs.

Hardly any systematic study was done by which directly compares the effect of tool-pin profile on mechanical properties of AA2014-T6 welds using Taguchi's DOE technique. Squillac *et al.*, (2006) investigated on the effect of process parameters (RS and TS) on tensile strength and fatigue strength of AA6056 joints by FSW. The influence of process parameters on the weld quality was assessed by Analysis of Variance (ANOVA) methods using the experimental results. A complete two factor factorial experiment, with three replicates was performed. Multi-targeted optimizations with constraints based on genetic algorithm for optimization of stir head dimensions were investigated by Meng *et al.*, (2006). The objective function employed was an analytically derived mathematical model relating heat input coefficient with tool parameters. The goal of optimization was to determine the shoulder diameter and pin diameter of the stirring tool for maximizing the tensile strength of the FSW joints of aluminum-lithium alloy.

The influence of tool rotation speed and tool pin profile on defect formation/elimination in AA2014-T6 welds were studied by Madhusudhan *et al.*, (2011). These authors used two different types of tool-pin profiles; threaded and thread less. Microstructural characterizations of weldments produced with process parameters were discussed.

Venkateswarlu *et al.*, (2013) investigated the effects of threaded FSW tool geometries on AA7039 as well the effect of tool shoulder concavity levels. Tool-pin diameter of 7 mm was found to have maximum influence among the control factors that determine tensile strength of the weld when compared with 6 mm and 8 mm. The 19 mm shoulder diameter was found to be more suitable for obtaining adequate tensile strength and percentage elongation for 6 mm thick plates.

In addition to DOE techniques, some evolutionary algorithms were utilized for optimization of FSW parameters. In FSW process, lap joint resistance optimization using



gradient techniques are established. They combined the gradient technique and the finite difference method to determine the optimal RS and TS in order to maximize the joint strength.

Vidal et al., (2005) used Taguchi's method to find the optimal FSW parameters for improvement of mechanical behaviour of AA2024-T351. An orthogonal array of L9 ( $3^4$ ) was used; ANOVA analysis was carried out to identify the significant factors affecting tensile strength, bending toughness and hardness. It is found that the parameter design of Taguchi method provides a simple, systematic, and efficient methodology for the optimization of the FS welding parameters. The improvement of tensile strength from initial FS welding parameters to the optimal parameters is about 2.8% and the improvement of hardness from initial FS welding parameters to the optimal parameters is about 10%.

Nandan et al., (2006) used the non-linear optimization techniques with constraints, which resulted in convergence of the optimal solution based on the population selected. One of those techniques is the Genetic Algorithm (GA) to determine four process parameters by minimizing the difference between the numerical model and experimental results. The process parameters included variable friction coefficient, the extent of sticking, the heat transfer coefficient, and the extent of viscous dissipation converted into heat. These selected parameters were optimized by a genetic algorithm using a limited volume of measured temperatures at several monitoring locations during FSW of dissimilar aluminum-alloys, AA1200 and AA6061.

The use of Artificial Neural Network (ANN) was proposed by Okuyucu et al., (2007) and obtained correlation between FSW parameters and mechanical properties of aluminum plates. Their attempt was to correlate the parameters rather than to optimize them. The input parameters were RS and TS, while the output parameters included mechanical properties such as tensile strength, elongation, hardness of weld metal and hardness of heat affected zone (HAZ). The obtained model was used to calculate mechanical properties of welded Al plates as a function of RS and TS.

Conventional parametric DOE approach is cumbersome and requires large number of experimental trials. Statistical techniques are often used to reduce the number of experiments conducted. Based on this, one such statistical technique, known as Taguchi method to determine the effect of three process parameters on the tensile strength of friction stir welded RDE-40 aluminum alloy was studied by Lakshminarayanan et al., (2008).

A mathematical model using response surface method (RSM) was used by Elangovan et al., (2008) and developed the relationship between process parameters and tensile strength

for AA6061. Five different tool pin profiles (straight cylindrical, tapered cylindrical, threaded cylindrical, triangular and square) have been used to fabricate the joints at three different axial force levels. The formation of FSP zone has been analysed macroscopically. Tensile properties of the joints have been evaluated and correlated with the FSP zone formation. From this investigation it is found that the square tool pin profile produces mechanically sound and metallurgically defect free welds compared to other tool pin profiles. A defect-free FSP region, smaller grains with uniformly distributed finer strengthening precipitates in FSP region and higher hardness are the reasons for superior tensile properties of the above joints.

A similar study was carried out by others researchers also but on a different aluminum-alloy AA2219 plates (Babu et al., 2008). A similar technique to find the effect of three process parameters on the tensile strength of friction stir welded A319 aluminum alloy was also studied by other researchers. In both of these studies, the authors used Analysis of Variance (ANOVA) to identify statistically significant process parameters (Jayaraman et al., 2009).

Rajakumar et al., (2012) presented FSW joints made using six different grades of aluminium-alloys (AA1100, AA2219, AA2024, AA6061, AA7039, and AA7075) with different levels of process parameters. Macro structural analysis was carried out to identify the feasible working range of process parameters. The optimal welding conditions to attain maximum strength for each alloy were identified using Response Surface Methodology (RSM). Empirical relationships have been developed to predict the tensile strengths of FSW joints at 95% confidence level. The relationships have been developed by incorporating welding parameters using statistical tools such as design of experiments, analysis of variance and regression analysis.

Gupta et al., (2013) carried on AA6061 plates using FSW process and the process parameters were optimized using Taguchi method. The rotational speed (RS), welding speed (TS) and axial force (P) are the process parameters taken into consideration. The optimum process parameters are determined with reference to the tensile strength of the joint. The results indicated that the RS is highest significant parameter in deciding the tensile strength of the joint. The result also shows that optimal values of process parameters are to get a maximum tensile strength of friction stir welded AA6061 and found to be 162 MPa. It was found that the RS played an important contribution of 67 % of the overall response, welding speed and axial force contributed 28% and 1.4 % respectively.

Prasanna et al., (2013) conducted FSW trials using a vertical milling machine on AA 6061 alloy. Four major controllable factors each at four levels, namely, rotational speed,

welding speed, tool-pin height, offset distance were considered. The uncontrollable factors include ultimate tensile strength, percentage of elongation and hardness, which can be converted to signal-to-noise ratios. The grey based taguchi method which is a multiple response process, is used to optimize the factors. A grey relational grade obtained from grey relational analysis is used as the multiple performance characteristic. The resulting optimum process parameters are rotational speed at 800 *rpm*, welding speed at 10 *mm/min*, pin tool length at 5.7 *mm* and offset distance 0.4 *mm* for the best multiple performance characteristics for 6 *mm* thick plates.

Also, numerical analysis of friction stir welding will allow many different welding processes to be simulated in order to understand the effects of changes in different system parameters before physical testing, which would be time-consuming or prohibitively expensive in practice (Xiaocong et al., 2014).

Prakash et al., (2015) optimized the process parameters and obtained better mechanical properties of friction stir welded AM20 magnesium-alloy using Taguchi's Grey Relational Analysis (GRA). The process parameters considered are welding speed, tool rotation speed, shoulder diameter and plunging depth. The experiments were carried out using Taguchi's L18 factorial design of experiment. The ANOVA results showed that the most effective parameter is shoulder diameter for case-1 (RPM -1100, TS -98 *mm/min*, shoulder diameter -24 *mm*) and for case-2(RPM -600, TS -98 *mm/min*, shoulder diameter -24 *mm*) among all the considered parameters.

The observations given by different researchers lead to a gap to optimize the process parameters RS, TS with TPH.

## **2.4 Thermal History and Residual Stresses**

Detailed analysis of heat generation and the temperature history during the FSW process is the first step towards understanding the thermo-mechanical interactions taking place simultaneously. The initial modeling approaches were focused on approximate estimation of heat generated during the FSW process. The preliminary thermal models predicted the temperatures of friction stir welds using the Rosenthal equations (popularly used for moving heat source problems). The amount of frictional heat generated and dissipated into the workpieces determines the strength of the nugget as well as the thermal and residual stresses. The parameters that influence the net heat generation in FSW process includes tool rotational speed (RS), traverse speed (TS) and plunging force (P). FSW nugget is the result of

combined action of frictional heat and mechanical stirring with primary heat source being the frictional heat, which depends on coefficient of friction.

The complex geometry of some type of joints and their three-dimensional nature makes it difficult to develop an overall system of governing equations for predicting the overall behavior of the FSW joints. In addition, material non-linearity due to plastic behavior is difficult to incorporate because the analysis becomes very complex in the mathematical formulation. The experiments are often time consuming and expensive. To overcome these problems, numerical analysis has frequently been used since the year 2000. The focus of all the thermal models was to understand the mechanism of heat generation as well as to predict the temperature distribution in the workpieces as well as the tool. A thermal model forms the basis for the development of mechanical and microstructural models. Some of the findings through numerical studies done by various research groups are discussed below.

Chen *et al.*, (2003) observed thermo-mechanical phenomena during FSW process of AA6061-T6 and the predicted results were compared with the XRD techniques. Chen and Kovacevic (2003) considered the mechanical effects of the shoulder assuming a Coulomb friction law for the interaction between the shoulder and the material.

A sequentially coupled thermo-mechanical model using WELDSIM, and FE code was developed by Zhu and Chao (2004) and used inverse analysis method for thermal analysis based on experimentally measured temperatures. They assumed that the heat flux was linearly distributed on the top surface of the plate and the heat generated at the tool-pin surface was neglected. In subsequent mechanical analysis, the forces from the tool were not considered and also the effect of fixture release, when the weld cooled down to room temperature was studied. Comparison of predicted residual stress fields with the measured values by the neutron diffraction technique at several specific locations showed a good agreement between the two. 3-D, FE model was developed to study the thermo-mechanical process in the butt-welding of aluminium-alloy (AA6061-T6). The heat generation caused by the friction was calculated using experimentally measured contact pressure and a constant value of the friction coefficient. The temperature datum at each time increment was used to evaluate the mechanical and thermal properties.

Zhu *et al.*, (2004) made a non-linear, thermo-mechanical simulation of 304L stainless steel using WELDSIM code. Then, they compared the results obtained from neutron diffraction technique. The effects of temperature dependent properties of aluminium-alloy on the peak temperatures are also studied. Chao *et al.*, (2005) formulated heat transfer simulation into two boundary value problems, a steady-state for tool and transient for the workpiece and

found that majority percentage of frictional heat dissipates into the workpieces. The state-of-the-art of works done on FSW and FSP technologies to study the effects of process parameters on the formation of welds, microstructural refinements and final nugget properties are discussed in the review paper by Mishra et al., (2005).

The moving heat source in FSW process with power input are studied and temperature distribution with and without backing plates are analysed by Khandkar et al., (2005). Colegrove et al., (2007) developed an analytical model for thermal simulation of FSW process. The model included a simulation of the asymmetric heat field under the tool shoulder resulting from viscous and interfacial friction dissipation. The analytical model also considered the influence of hot and cold FSW conditions into the heat flow around the tool. Armentani et al., (2007) evaluated residual stresses in a welding process, by a 2-D non-linear, thermal and thermo-mechanical analysis using FE method. Moreover the technique of element birth and death is used to simulate the welding filler varying with time in weldments. The transient temperature distribution in a welded joint is highly affected by thermal conductivity, large tensile longitudinal residual stresses are present near the welding bead, and the magnitude of these stresses are reduced by 15% when conductivity increasing from 30 W/m-K to 75 W/m-K, low transverse residual stresses are produced near the weldments, but they are affected by thermal conductivity change.

The elements of the birth and death concept to predict the effect of thermal properties on residual stresses in butt joints are analyzed by Rajamanickam (2008). A thermo-pseudo-mechanical model was developed in which the temperature dependent yield stress controls the heat generation (Hattel et al., 2008). Selvamani et al., (2008) clearly observed in FSW weldment that retreating side temperature distribution is relatively higher than the advancing side. The analytical heat input model has been used for the determination of thermal history and based on which finite element analysis has been carried out and the predicted values were confirmed with experimental measured data. The asymmetry in the residual stress distribution is due to the asymmetry in the plasticized material volume along the advancing and retreating side of the stir-zone.

A detailed non-linear finite element method was developed by Rajamanickam et al., (2009) to study thermal history and residual stresses in AA2024 aluminium alloy. The range of RS values (300-1200 rpm) are considered and identified that thermal modelling is useful to predict temperature at the tool shoulder as well as the magnitude of longitudinal residual stresses, which are effected with the RS.

Ulysses et al., (2009) used a three-dimensional, visco-plastic model for FSW process. Forces applied on the tool are computed for various traverse and rotational speeds, but an opposite effect was observed with increasing rotational speeds. Prasanna et al., (2010) compared the thermal simulations on stainless steel using a moving cylindrical coordinate system with the measured temperatures. Jacquin et al., (2011) simplified the thermo-mechanical model for friction stir butt welds of AA2024. Based on kinematically compatible assumptions, this model predicts temperature contours in the welded zone, power dissipation, and the sliding ratio on the interface between the shoulder and the workpiece. A successful comparison with experiments was done and the general tendencies for the influence of operational parameters were well predicted. The analysis of results concerning the contact conditions provides interesting data about the evolution of the relative sliding between the shoulder and the material to be welded. The sliding ratio increases with the tool rotational speed and decreases the temperature in the vicinity of the tool.

A 3-D thermal pseudo mechanical model was developed by Barnik et al., (2012). They formulated an Eulerian frame considering a quasi steady approach to Friction Stir modeling of Aluminium alloy (AA6061) and implemented nonlinear finite element code in Comsol Multiphysics v4.1. The effect of different operating parameters on the temperature distribution was analyzed. The material flow is found to be enhanced with the increase in traverse speed and angular velocity of the pin with a pronounced swirl on the advancing side. Feng et al., (2012) proposed an integrated-thermal-mechanical-metallurgical model to study the formation of residual stresses in FSW welds of AA6061-T6. Binnur et al., (2013) considered modelling a moving heat source with a heat distribution simulating the heat generated from the friction between the tool shoulder and the workpiece; this was used in the heat transfer analysis of AA6061. 3-D simulations were carried out using ANSYS and HyperXtrude commercial software. APDL (ANSYS Parametric Design Language) code is used to model the moving heat source and the corresponding boundary conditions. It was observed that the maximum temperature near the weld increased with increasing the rotational speed as well as with increased tool holding time. Peak temperatures decreased with increased tool traverse speed. Feulvarch et al., (2013) proposed in the literature the finite element method, a simple but robust moving mesh technique for the numerical modeling of the FSW process. It is based on an Eulerian formalism and the mesh was composed of two parts: the first part is fixed around the stirring zone and the second one is fixed at the base material near the tool and moves with a rotational speed corresponding to the tool's velocity.

Therefore, there are no mesh distortions and the Eulerian formalism leads to satisfying computing time.

Madhavi et al., (2014) studied the effect of FSW process parameters on nugget geometry and mechanical properties of aluminium-alloy (AA5052-H32) by performing post-weld mechanical testing and microscopic examinations. Vilaca et al., (2014) presented finite element based thermal model for FSW process. The model included the backing plate and the tool. In their work, the heat input was fitted through iterative process for verification between the predicted and measured values.

The simulation of FSW process is a complex problem, which involves physical couplings between mechanics and heat transfer, very large deformations and strain rates in the stirring zone around the pin. To avoid mesh distortions or very large computing time due to the Arbitrary Lagrangian-Eulerian technique (ALE), an analysis of the material flow and thermo-mechanical phenomena taking place during FSW of polymers are studied by Fernando et al., (2014).

Cartigueyen et al., (2014) developed a 3-D, transient, non-linear thermal model using ANSYS v11 software and tried to predict the thermal history (peak temperatures, heating and cooling periods) during FSP of copper. The simulated temperature distributions were compared with experimental values. The results of the simulation are in good concurrence with that of experimental results. The results showed that the heat generation during FSP strongly depends on both rotational and transverse speed where the peak temperature was observed to be strong function of the rotational speed while the rate of heating was a strong function of the traverse speed. The peak temperature obtained was about 65% of the melting point of base metal.

Hongjun Li et al., (2014) included the heat source into two parts: surface heat flux at the shoulder-workpiece interface and nodal heat generation in the material that should have been displaced by the tool. The heat source algorithm is described through equations and flow charts. The mechanical interaction between the contacting surfaces was modelled with contact elements. However the analysis failed to converge with the contact pairs active. For the analysis without contact pairs, the predicted longitudinal direction stresses matched well with experiment but the transverse direction stresses were significantly different. The contact pressure and temperature dependent heat transfer coefficient significantly affect the thermal analysis. It was found that the proposed adaptive convective boundary condition algorithm is well suited to represent the varying thermal contact conductance at the backing plate-workpiece interface. Miroslav et al., (2014) performed numerical simulations for estimation

of welding plates temperature using finite difference method and explicit scheme with adaptive grid and considered the influence of temperature on material conductivity, contact conditions between welding tool and parent material. The predicted results are in good agreement with the experimental data.

Nikhil et al., (2015) examined the effect of frictional coefficient on the predicted temperature field in FSW process. Additionally, it was concluded that use of a moving heat source technique proved to be a reliable method to simulate friction stir processing as well. Joining of an Al-SiC-Gr hybrid matrix composites through friction stir welding are analyzed by Jeyabalakrishnan et al., (2015). Temperature distribution in the hybrid metal composites was obtained by employing transient thermal analysis.

Hao su et al., (2015) combined the steady-state model with a transient-state model. The total heat generation, heat density and temperature distribution during the welding process with tri-flat tool were elucidated and compared with that of conical tool, and the material flow patterns and deformation regions of various pin orientations are illustrated and found that the deformation zone caused by tri-flat tool is larger than that by conical tool, which is validated by the weld macrographs.

Due to the high transparency of the polymer, poly-methyl-methacrylate (PMMA), it was possible to analyze easily the morphological changes induced by the welding process on it. It was concluded that, due to the polymer rheological and physical properties, the thermo-mechanical conditions during FSW are very different from that registered during welding of metals, leading to completely different material flow mechanisms and weld defect morphologies. Important differences in material flow and temperature distribution between metallic and polymeric material, during FSW were identified and critically analyzed based on Arbegast flow-partitioned deformation zone model.

Friction stir welding is an innovative joining process developed to use in aerospace manufacturing. Like most welding processes, there exist problems with post-weld residual stresses and subsequent geometrical distortion. The residual stress-state of a welded component can be modified using suitably applied mechanical, tensioning and thus distortion can be reduced or eliminated.

A three-dimensional coupled thermo-mechanical model was developed by Rahul et al., (2017) on Lagrangian method to evaluate the performance of two different pin shapes. (smooth conical and threaded conical). Particle tracking method was used to visualize the material flow on advancing side, retreating side, and weld centerline. Results revealed that material flow is nonsymmetrical and unstirred region is lower for the threaded pin as



compared to the smooth. And, also identified that temperature distribution is symmetric over the tool area but asymmetric away from it with a temperature difference of 5°C.

In the present research study, FE based software, ANSYS (APDL), has been used to model the friction stir welding process of aluminium-alloy plates and investigated the effects of process conditions on the residual stress. The finite element modelling has been carried out in two-steps: thermal analysis and stress analysis. In the thermal analysis, the heat input from the friction stir welding process was modelled using a surface heat flux as boundary condition at the top of workpieces. The calculated temperature field was then used for stress analysis. The main focus of the work was to examine the residual stresses generated from various welding conditions. The effects of RS and TS on residual stresses are analyzed at selected locations on the weld surface. It was found that the peak temperatures primarily depends on RS, while the residual stresses depends on TS. Since both RS and TS affects the net heat input per unit length, the use of optimum values are indeed very much important to minimize the residual stresses within the FSW joints.

The predicted results suggested that the application of appropriate mechanical tensioning during welding would reduce the residual stress or even change the residual stresses from tensile state to compressive state. The calculated residual stresses were also compared with experimental measurements and good agreements were found between them.

After the intense literature review we identified few gap areas as shown in Table (2.1) in the FSW process, which led us to work effectively and identified as the objectives of the present research work as discussed in chapter 1.

## **2.5 Research Gaps in FSW Process**

The following are the research gaps identified after the intense literature survey, which led to the objectives of the present research as shown in Table (2.1). Advanced modeling tools can help in the selection of optimal welding process parameters, which in turn reduces the average cost of welding by lowering the rejection rates and reduced demands for pre- and post-heat treatment operations. Also, the selection of right welding process parameters avoids over welding and hence improves quality.

- 1) FSW process is not done extensively experimentally and numerically for the aluminium-alloy (AA5052-H32) which is very pure and difficult to obtain microstructure

- 2) Macro structure, Microstructure analysis and hardness variation is not carried exhaustively with respect to the tool-pin height.
- 3) Mechanical property variations are studied extremely varying all the process parameters which led to the optimization (DOE) of the process parameters for the required workpiece thickness.
- 4) Numerical study of heat input effects on weld geometry, microstructures and mechanical properties of AA5052-H32 is lagging.
- 5) Numerical simulations are done to reduce the tensile stresses by using constraints
- 6) The existing literature lacks the study of the effects of process parameters, net heat input and also the effect of alloying elements on the resulting microstructures and mechanical properties of AA5052-H32

Table (2.1) Gap areas in FSW process

Identified tool-pin profiles and process parameters (Gap: tool-pin height)	Bahemat and Adamowski (2007-2008)
Comprehensive review report and microstructure (Gap: grain size )	Mishra and Ma (2005)
Optimization of process parameters –ANN	Okuyucu and Squillac (2008)
Thermal and Residual stresses (Gap: constraints, TPH )	Zhu and Chao (2003)

## CHAPTER 3

### Experimental investigations of FSW Process

#### 3.1 Friction Stir Welding (FSW) Process

This chapter is focused on the experiments conducted using Friction Stir Welding (FSW) process. Experimental setup has been developed to carry out the experiments on AA5052-H32 workpieces for different process parameters. After performing the experiments, tensile strength, micro-structure and hardness of the welded plates have been measured for ascertaining the influence of the FSW process parameters on the final mechanical properties of the welded joints and quality. The FSW process combines frictional heating and stirring motion to soften and mix the interface between two workpieces, yielding a solid, fully consolidated weld which was discussed in the introduction chapter 1.

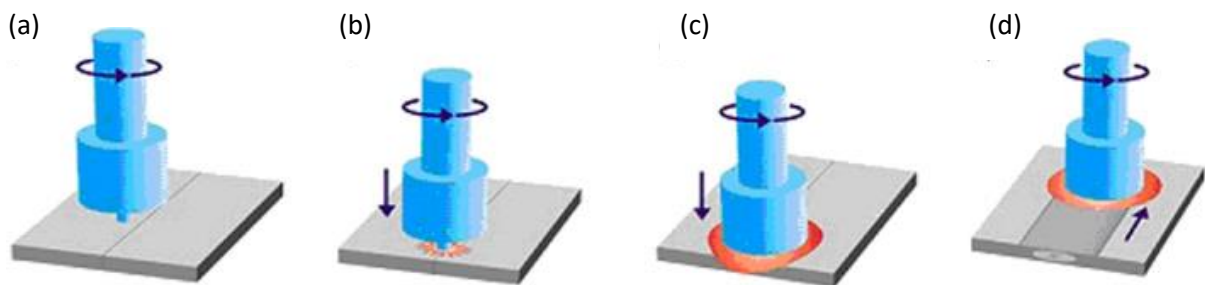


Figure (3.1) Friction Stir Welding stages: (a) initial, (b) plunging, (c) dwelling, (d) welding. (Guerdoux et al., 2009).

In Figures (3.1a-b) a rotating tool is plunged into the workpieces until the tool shoulder comes in contact with the part and in Figures (3.1 c-d) tool is moved forward and joint is formed behind the tool. A total of 27 final welds were studied, either by mechanical properties or microstructural characterization or thermal measurements. Details of the welding parameters are given in Figure (3.2). The welds are divided into three sets. Firstly, a set of welds were produced with three rotational speeds (RS) and traverse speeds (TS) each. Secondly, three welds with tool-pin height (TPH) were produced for the above two sets of RS and TS with thermocouples inserted into the workpieces. All sets were welded on the conventional milling machine such that the welding direction was aligned with the rolling direction of the plates as shown in Figure (3.3).

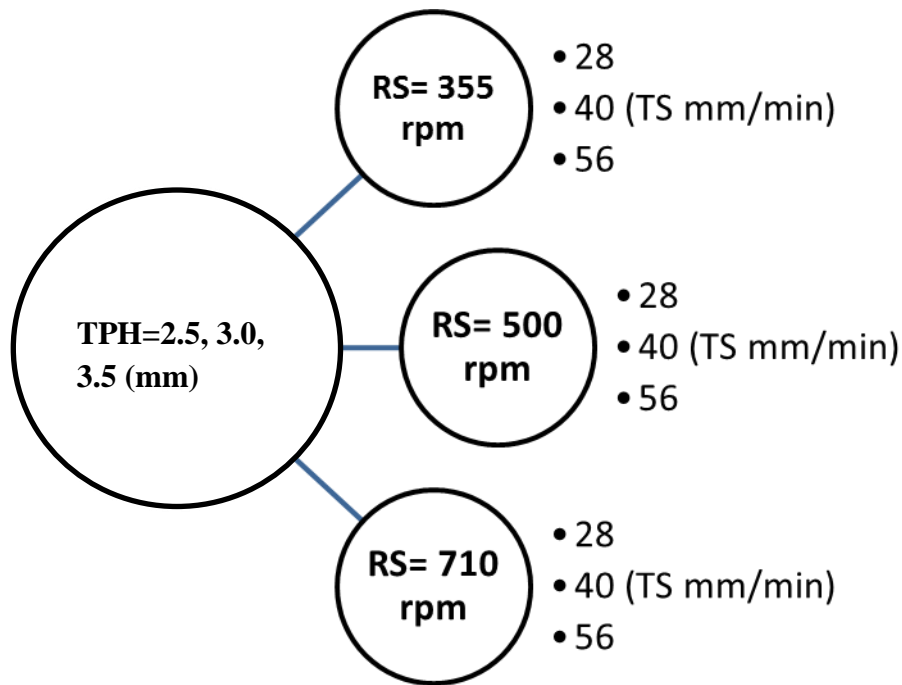


Figure (3.2) FSW welds with range of parameters.

In each welding of the 5052-H32 set, K-type thermocouples were fixed underneath the workpieces on the advancing side (AS) and retreating side (RS) of the welds at distances of 10, 15 and 20 mm from the butting faces of the plates (weld axis). All the thermocouples are bonded using a tape to the workpiece surface as shown in Figure (3.10b).

### 3.2 Workpiece Material Specifications of AA5052-H32

The workpieces to be joined by FSW process are machined to the required dimensions as shown in Figure (3.3). The required dimensions of the plates are prepared based on the bed length and width of the milling machine, length of the backing plate, and the design of the clamping system, so that the arrangements do not allow the distortion of the plates due to forces induced by the rotating tool. However, the aluminum-alloys are designed to be around 300 mm long and 100 mm wide sheet metal cut into the specified dimensions by a shear cutting technique. The final dimensions of the work pieces are 300 mm x 100 mm x 4 mm. The aluminium plates are to be machined at the sides in order to make them flat to ensure accurate face-to-face contact at weld joint. This was accomplished by using the shaping machine and a vice for holding the plates firmly.

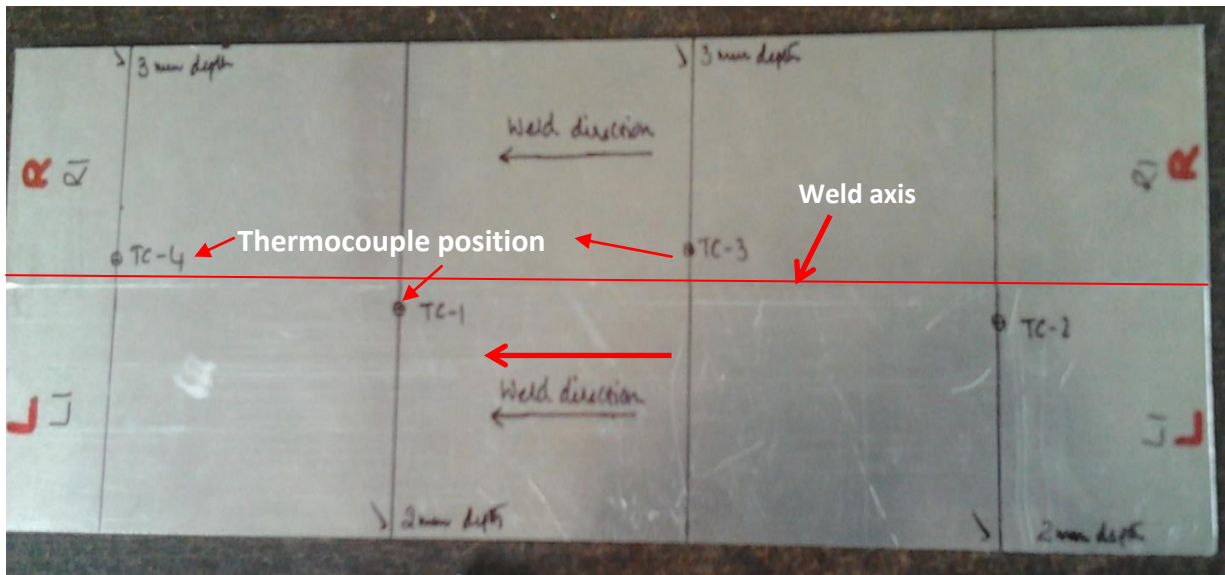


Figure (3.3) AA5052-H32 workpieces with TC locations.

The last stage is to clean the workpiece surfaces close to joint, so as to remove any oxide layers and get clean welds. Fine grind grits were used for surface cleaning. The workpiece material and its chemical composition and base metal mechanical properties are given in Table (3.1)

Base metal: AA 5052-H32 (Al-Mg alloy)

Base metal plate dimensions: 300 mm x 100 mm x 4 mm

The most common tempers for 5052 aluminium is H32 hardened by rolling then stabilized by low-temperature heat treatment to quarter hard.

Table (3.1) Chemical composition and mechanical properties of AA5052-H32.

Chemical Composition (wt, %)										
Cu	Si	Fe	Mn	Mg	Zn	Cr	Ti	Pb	Bi	Al
0.1	0.25	0.4	0.1	2.2-2.8	0.1	0.15-0.35	-	-	-	rest
Mechanical Properties										
Hardness (HV)	Yield strength (MPa)			Ultimate tensile strength (MPa)				% elongation		
60	182			239				12.8		

### 3.3 Preparation of Workpieces and Backing Plate

Backing plates are made out of materials with different thermal diffusivity and strength. They affect the bottom thermal boundary condition of workpieces and resulting joint properties. Backing plate conductivity and axial force both independently affect the process parameters - nugget temperature and tool torque, significantly. The FSW process needs to utilize frictional heat generated efficiently. So, a low thermal conducting metal (backing plate) was placed below the workpieces and thereby less heat diffused to the backing plate. The backing plate material is mild steel (grade-202) of 2 mm thickness for performing the experiments. Hardened backing plate with grooves for TC seating was placed on the bed of the conventional milling machine as shown in Figure (3.4).



Figure (3.4) Backing plate with grooves for thermocouple seating.

### 3.4 Tool Specifications and Design

The tool geometry (shape and size) and material are the important aspects of friction stir welding process. The tool material should have high melting point and hardness than the workpieces. The tool material used for the experiments is high carbon high chromium steel (C-45) with diameter 40 mm and length 65 mm. Based on the tool shoulder design, rod diameter required was 16 mm. A heat treated tool (55HRC) was prepared using facing followed by turning operations to get the required dimensions as given below.

All the machining operations were performed using lathe and milling machines. From literature, it was found that the, FSW welds were carried out by using complicated tool geometries, which are extremely difficult to manufacture. Also, it was observed that the complicated tool pin profiles tend to wear after few numbers of runs leading to conical form.

Hence, in the present work it was decided to use the FSW tools having simple regular geometrical forms, like straight cylindrical, straight tapered cylindrical, etc. On prolonged usage, even if these tools wear out, they will attain either tapered cylindrical or cylindrical shape. Therefore systematic studies of these regular and simple tool-pin geometric shapes are taken up in the present study and the effect of tool-pin height (TPH) on the mechanical properties of FSW joints.

Single pass friction stir butt welds are made using an FSW tool fabricated from tool steel called High Carbon High Chromium (HCHCr- ISO 1.2767, also known as DIN X 45 NiCrMo 4, AISI 6F7, and BS EN 20 B). The tool has a concaved shoulder ( $2^{\circ}$ ) while the tool pin is made cylindrical and tapered with varied tool pin heights of 2.5 mm, 3.0 mm and 3.5 mm, and has a round bottom. The overall height of the pin is having a variation of 0.2-0.5 mm, making slightly shorter than the plate thickness. This section gives all the details and features for designing and implementing friction stir welding tools. The friction stir welding tools for use in this investigation were designed by taking into consideration, the fundamental principles of the FSW process. The performance of the tool depends mainly on four factors, the design of the tool, manufacturing accuracy, proper material selection and proper heat treatment selection. The tool steel is further heat treated to increase the ability of the material to withstand the wear and tear at higher temperatures. The heat treatment provides some properties like wear resistance, and resistance to deformation under high loads and elevated temperatures. The tool-pin material and its properties considered are given in Tables (3.2) and (3.3). The FSW tool nomenclature used for the friction stir welding of AA5052-H32 aluminium- alloy and the fabricated FSW tool for friction stir welding of 4 mm thick aluminium alloy plates are shown in the Figure (3.7) and Figure (3.8) respectively.

Table (3.2) Chemical composition and hardened tool material (AISI D2 Steel) in wt %.

C	Si	Cr	Mo	V	Mn	
1.50	0.30	12.00	0.80	0.90	0.60	
Tempering D2 Steel						
Tempering °C	150	200	250	300	350	400
HRC	62/61	61/60	60/59	57/56	56/55	56/55

Table (3.3) Physical and mechanical properties of tool material (AISI D2 Steel).

Density ( $kg/m^3$ )	Melting point( $^{\circ}C$ )	Poisson's ratio	Elastic modulus( $GPa$ )
7700-8030	1426	0.27-0.3	190-210

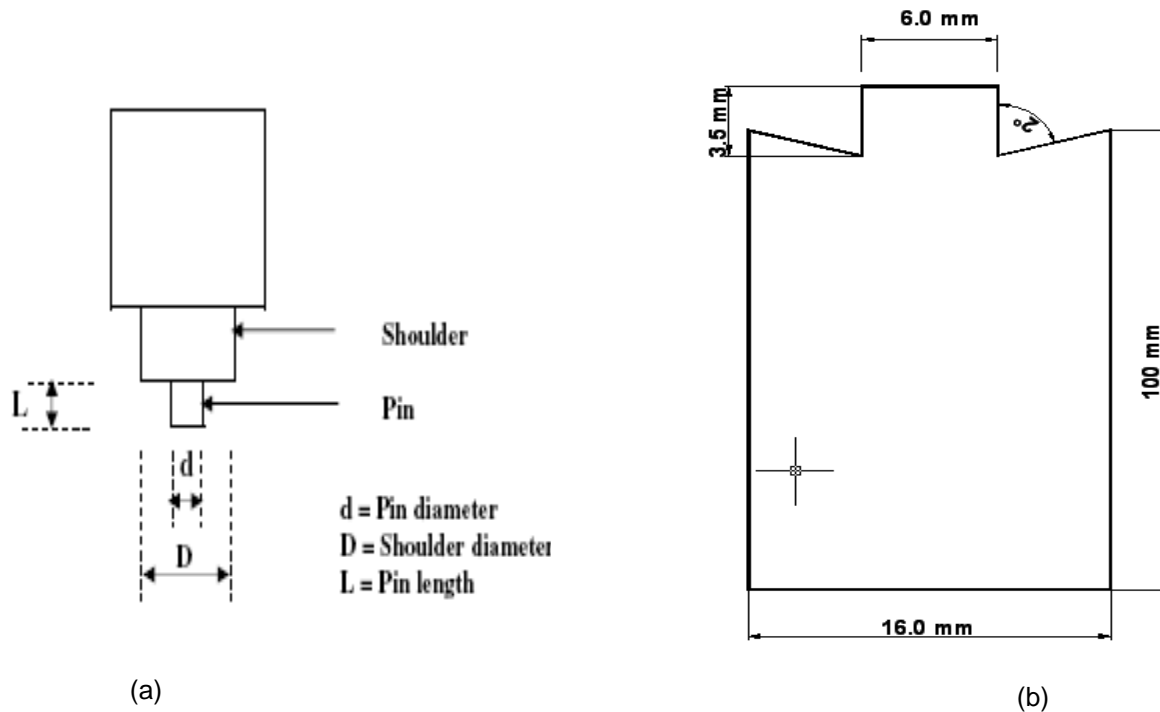


Figure (3.5) Tool geometry with shoulder surface profile used in FSW process.

### 3.5 Advantages of D2 tool-steel

The D2 tool steel was selected because of the following advantages

- High wear and abrasion resistant properties.
- Heat treatable and offers hardness in the range 55-62 HRC.
- Machinable in the annealed condition.
- D2 steel shows little distortion on hardening.
- D2 steel's high chromium content gives it mild corrosion resisting properties in the hardened condition.





Figure (3.6) Tools used with different profiles for FSW welds.

### 3.5.1 Straight cylindrical pin

The FSW tool with cylindrical and tapered pin profiles used to weld 4 mm thick Aluminum AA5052-H32 plates are shown in Figure (3.6). The dimensions of tool and process parameters are shown in Table (3.4).

Table (3.4) Tool geometry and FSW process parameters used.

Parameter	Value
Tool rotational speed, RS ( <i>rpm</i> )	355, 500, 710
Traverse speed, TS ( <i>mm/min</i> )	28, 40, 56
Tool shoulder diameter ( <i>mm</i> )	16
Tool pin diameter ( <i>mm</i> )	6
Tool pin height ( <i>mm</i> )	2.5, 3.0, 3.5
Tool shoulder taper (inwards)	2°

### 3.5.2 Conventional Milling machine

The conventional milling machine was used to carry out the FSW experiments (manufactured and supplied by BATLIBOI; model BFH-5). The tool was mounted in the vertical arbor using suitable collates. The plates to be joined were clamped to the horizontal bed with zero root gaps. The clamping of the test pieces are done such that the movements of the plates are totally restricted under both plunging and translational forces of the FSW tool. The tool rotational speed and traverse speed were set prior to each run of the welding. After plunging the rotating tool at the plate butt and visually ensuring full contact of the tool shoulder with the plate surface, the bed movement was done.

#### *Specifications of milling machine:*

- Spindle motor power: 5.5kW, Model BFH5
- Spindle speed: 2000 rpm
- Cutting feed: 900 mm/min
- Table area: 500 mm x 300 mm Travel (X, Y, Z): 500 mm x 300 mm x 200 mm
- Motor capacity: 7.5 hp



Figure (3.7) Fixture set up on the bed of Conventional milling machine.

The complete fixture set-up on the milling machine is shown in Figure (3.7). The tool used for welding has a cylindrical cross-section, with a tool-pin height of 3 mm which is capable for stirring of the metal and efficient filling of the material in the gap formed during welding process. The three different tool profiles fabricated and used for the current research works are shown in Figure (3.8).

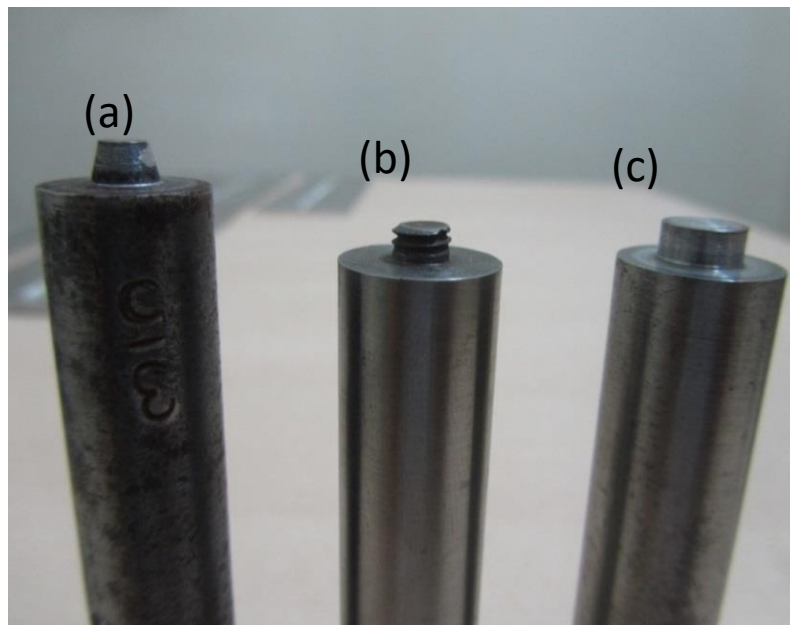


Figure (3.8) Tool profiles used for FSW welds (a) tapered (b) threaded (c) Cylindrical.

Initially, the workpieces (plates) are positioned using mechanical clamps on a conventional milling machine by holding the plates to be welded securely in the fixture in the abutting edges, so that the plates stay in place and do not fly away due to the welding forces. Subsequently, single pass butt welds were made normal to the rolled direction of plates. The rotational motion of the spindle is started and the tool comes in to contact with the surface of the plates and the tool-pin is penetrated to a predetermined depth in between the faying surfaces of the plates to be welded.



Figure (3.9) FSW process on conventional milling machine.

The tool rotates and comes in contact with the surfaces softening the material due to the frictional heat produced, this time is called as pre-heat time and subsequently the tool is traversed in the direction of weld forming the weld joint as shown in Figure (3.9). The tool is withdrawn after the weld is made which leaves a hole at the end of the welded plate.

### 3.5.3 Thermocouples

Temperatures were measured at selected locations, i.e., at different depths from top surface and offset weld axis, during the FSW process. In each experiment a total of six thermocouples at predicted locations (three on advancing side and three on retreating side) were inserted into the workpieces from underneath as shown in Figure (3.10a). Six holes, each 1 mm in diameter and 4 mm in depth, were drilled from the bottom side of the plate for the placement of thermocouples. Actual placement of the thermocouples was assumed to be at a depth of 3.8 mm from the top surface of the plate and width ( $y= 5, 6, \text{ and } 7 \text{ mm}$ ) away from weld centerline. The grooves and seating arrangement for thermocouples is shown in the Figure (3.4). Thermocouples (TCs) are one of the most common sensors used for temperature measurement. They are made up of two different metals coupled together at one or more points. A voltage is produced when there is a variation between the temperature of one of the points and the ambient temperature. There are various types of TCs, depending on the type of metals used and the calibration. The most common types include E, T, K and J. We used K- type thermocouple (chromel–alumel) and is the most common general-purpose thermocouple with a sensitivity of approximately  $41 \mu\text{V}/^\circ\text{C}$ . The thermocouples are inserted from the bottom of the workpiece and at a distance away from the weld centre line so that they cannot be melted and dissolved into the plates. The specifications of the K-type thermocouples are SS316, OD=1 mm and length=50 mm with external cable length of 5 meters, as shown in Figure (3.10b).

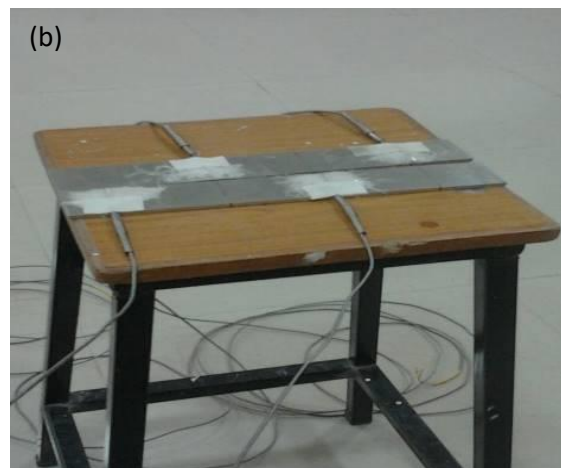
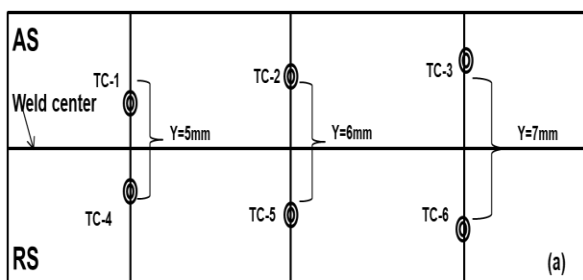


Figure (3.10) (a) TC's at different positions (b) K - type Thermocouples.

### 3.5.4 Data logger

Data logger is an electronic instrument that records measurements at set intervals over a period of time. It displays graphs, and saves the data in formats such as .csv to import into Microsoft Excel. The data logger used is of Model No: TC - 800/ TC – 800D as shown in Figure (3.11), it has eight channels to record, and the temperatures are recorded every two seconds.

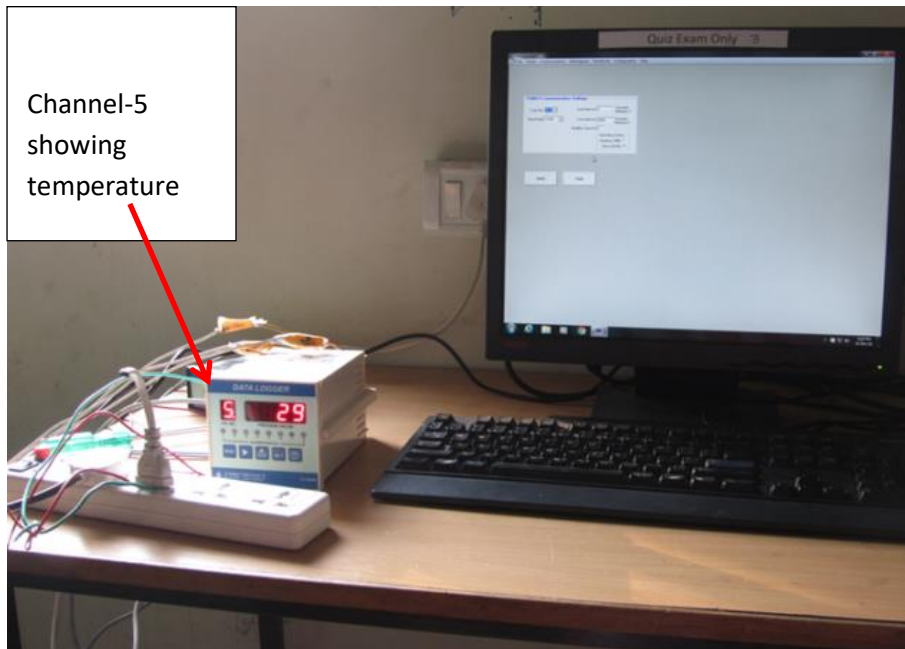


Figure (3.11) Data logger with 8 channels and display.

### 3.5.5 Mold preparation

Specimens of FSW joints for metallographic examination are prepared by cutting the welded joints to the required dimensions using shearing machine and polished using different grades of emery sheets followed by diamond paste. The mold is prepared by adding the cold setting powder and liquid into the mold and leaving it for few hours, till it is hardened the mold with test piece. After removing the mold we get a circular mold with the specimen inserted in the center of the mold as shown in Figure (3.12).



Figure (3.12) Molded test specimens.

### 3.5.6 Polishing and etching

The molded specimens are polished with different grades of emery sheets on a polishing machine (manufactured by M/s BAINPOL and supplied by Metco Pvt Ltd., Chennai). The model no is PMV009, as shown in Figure (3.13) with a fixed RPM of the polishing disc and required time until the specimen is clearly visible without any scratches. Finally they are polished with diamond paste ( $1\mu\text{m}$ ) and then etched with a reagent called Keller's (2% of Hydrofluoric acid) for about 20 seconds to reveal the nugget geometry. Macroscopic examination of welded joints has been carried out using a Trinocular Stereoscope (10X), as shown in Figure (3.14). The required resolution and scale are set to get a clear picture of the various zones in the welded specimens.



Figure (3.13) Polishing disc.



Figure (3.14) Trinocular stereoscope.

### 3.5.7 Zone formation in FSW joint

In general, the heat input to the workpieces plays an important role on the final mechanical properties of the welded joints. In FSW process, due to the material flow more heat is diffused in advancing side than retreating side causing asymmetry in the nugget geometry. Similarly the formation of different zones shown in Figure (3.15) occurs due to heat generated by the mechanical effects of the tool.

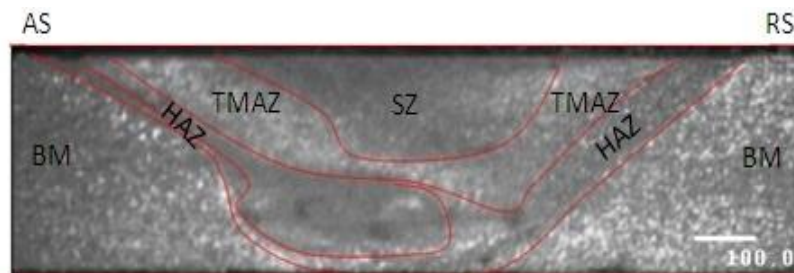


Figure (3.15) Different zones in the FSW joint at RS=500 rpm, TS=40 mm/min, and TPH=3.0 mm

Threadgill *et al.*, (2009) have classified welds into four zones, which are: a weld nugget (WN), a thermo-mechanically affected zone (TMAZ), a heat affected zone (HAZ), beyond which the unaffected base metal (BM) as shown in Figure (3.15). The WN refers to the region previously occupied by the tool pin. In the literature, this region is also referred to as the stirred zone, SZ (Mishra *et al.*, 2005).

The extent of the TMAZ is the trapezoidal region whose geometry depends on the shoulder diameter and the pin diameter, including regions on AS and RS (see Figure 3.15). The stirring action experienced within the TMAZ/WN during FSW leads to the formation of dynamically recrystallized grains in TMAZ due to plastic deformation.

Beyond the TMAZ, a typical narrow HAZ exists, where only a diminishing thermal-field is experienced until reaching the unaffected BM. Because of the rotation direction of the tool, the weld morphology appears asymmetric between the advancing side (AS) to the retreating side (RS). Towards the AS, where the traverse speed and the tangential velocity component of the rotating tool are in the same direction, the TMAZ/HAZ boundary appears sharper compared to the RS where the boundary is more diffuse. Other features include an extended flow arm from the SZ towards the AS, and the concentric circles within the SZ, generally at the bottom (lower half) of the sheet, referred to as onion rings as shown in Figure (3.15).

A brief summary of the zones in the FSW joint with distinct features and phenomena taking place are given below:

***Stir zone (SZ)***

- Recrystallization phenomena occurs
- Smaller grain sizes than that of the base material, resulting in increased hardness.

***Thermo-mechanically affected zone (TMAZ)***

- Severe plastic deformation of grains
- High temperatures induced by RS and TS
- Less number of precipitates

***Heat - affected zone (HAZ)***

- No plastic deformation
- Effect of heat leads to microstructural changes

***Base metal (BM)***

- Unaffected region and hence properties are similar to the base material

## 3.6 Results and Discussion

In this section, the results and discussion of all the experimental works are discussed in detail; which include the nugget geometry, mechanical properties, heat flow, grain size etc.

### 3.6.1 Effect of process parameters vs. nugget geometry

The comprehensive experimental work carried out to study the effect of tool-pin height (TPH) and traverse speed (TS) on the nugget geometry and the final mechanical properties of several welds produced with different combinations of process parameters (TPH and TS) indicate almost negligible material out flow (i.e., no tunnel defects). Subsequent metallographic examinations and UTM tests on post-welded sections revealed a significant variation in mechanical properties (hardness, tensile strength and % elongation) across the nugget cross-section in contrast to that of base metal (BM) values. Overall, it is observed that the increase in TPH resulted in improved mechanical properties such as hardness, YS, UTS and % elongation with few minor defects in some cases. Therefore, an optimum value of TPH has been determined based on the minimum property variation across the nugget for the range of traverse speeds studied and at which defect free welds are achieved.

FSW joints of AA5052-H32 plates (150 mm x 100 mm x 4 mm) were successfully made for different process parameters and the results are discussed below. Figure (3.16) shows the macrographs of weld nugget geometry at different traverse speeds, TS (Figures. 3.16(a)i - 3.16(a)iii) and tool rotational speeds, RS (Figures. 3.16(a) - 3.16(c)) at tool-pin height, TPH=3 mm. For a given RS, increasing TS lowers the net heat input to the plates and also less plasticized material flow around the tool-pin. The decrease in material flow would increase the heat diffusion around the tool-pin thereby increasing the weld penetration beyond the tool-pin tip (i.e., at the weld root). This causes the nugget geometry to become narrow in width and deep in penetration (Figures. 3.16a - 3.16c); it is found at all rotational speeds. Moreover, increasing RS increases the heat input around the tool-pin but due to increased material flow the nugget geometry further becomes narrow and deeper with possible formation and growth of stir zone (SZ).



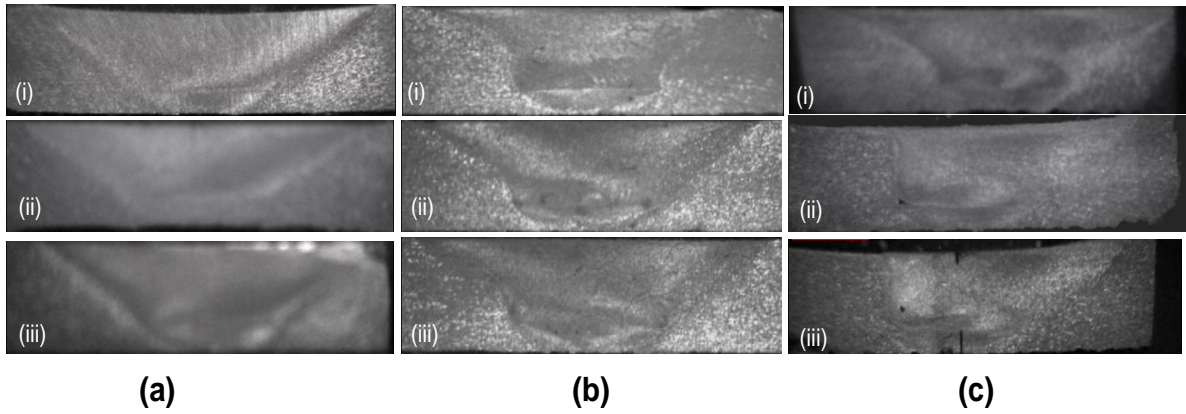


Figure (3.16) Weld nugget geometry for different TS,  $mm/min$  (i=28; ii=40; iii=56) and RS,  $rpm$  (a=355; b=500; c=710).




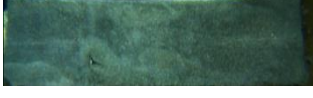



Onion ring patterns are observed with increased rotational speeds (Figures. 3.16b-3.16c). It is also observed that HAZ thickness increased with increase in TS and decreased with increase in RS. Moreover, at lower RS the thermo-mechanical effects are less and hence only two zones (TMAZ and HAZ) were observed (Figure 3.16a). With increased RS, the stir zone (SZ) grew in size. It should be noted here that neither material out flow nor the defects were observed for any of the process parameters studied.

Table (3.5) width and depth of the nugget for different FSW parameters.

TS ( $mm/min$ )	RS = 355 $rpm$		RS = 500 $rpm$		RS = 710 $rpm$	
	Tool-pin Height, TPH = 2.5 $mm$					
	W ( $mm$ )	D ( $mm$ )	W ( $mm$ )	D ( $mm$ )	W ( $mm$ )	D ( $mm$ )
28	10.35	3.25	14.4	3.7	12.6	3.7
40	10.85	3.3	10.9	3.45	11.7	3.4
56	8.35	3.4	8.7	3.35	12.9	3.7
	Tool-pin Height, TPH = 3.0 $mm$					
28	12.9	3.55	11.5	3.65	12.7	3.55
40	13.75	3.65	12.75	3.15	12.14	3.8
56	12.65	3.65	14.14	3.4	10.5	3.5
	Tool-pin Height, TPH = 3.5 $mm$					
28	12.75	3.5	12.75	3.5	10.1	3.5
40	13.45	3.9	12.8	3.8	10.6	3.75
56	12.4	3.75	11.7	3.8	10.44	3.85

To justify further the observations and macrographs in Figure (3.16), Table (3.5) clearly indicate below the variation in the width and depth of the nugget geometry for different process parameters. The variation of increase and decrease in width is observed due to the increase in TS; whereas a steady increase in depth is identified for a tool-pin height of 3.0 mm. The size of the TMAZ increased slightly with the increase in tool rotational speed (RS) due to higher power and higher peak temperatures. The influence of tool rotational speed, traverse speed and tool-pin height on the nugget geometry enables us to find the optimum values of the process parameters to obtain a defect free FSW joint. Some of the above observations and the defects of the welded plates from the experiments are given below in the Table (3.6) from the macrographs. Due to the high RS excess heat input is obtained resulting in the tunnel defect. Pinhole and worm hole are the defects due to insufficient metal transportation and heat generation. These visual observations from macrographs lead to the optimum process parameters and obtained defect free welded joints.

Table (3.6) Macrographs with defects at different RS and TS.

Input parameters	Macrostructure	Defect	Probable reason
355 rpm, TS=28 mm/min, TPH=2.5 mm		Pin hole	Insufficient metal transportation
710 rpm, TS=28 mm/min, TPH=2.5 mm		Tunnel	Excess heat input
500 rpm, TS=40 mm/min, TPH=3.0 mm		Defect free	Sufficient heat input and material transportation
500 rpm, TS=28 mm/min, TPH=3.0 mm		Worm hole	Insufficient heat generation
710 rpm, TS=40 mm/min, TPH=3.0 mm		Defect free	Sufficient heat input and material transportation
500 rpm, TS=40 mm/min, TPH=2.5 mm		Pinhole	Insufficient heat generation
500 rpm, TS=40 mm/min, TPH=3.5 mm		Tunnel	Large mass of flash and excessive thinning due to excess heat input

### 3.7 Tensile Tests on UTM

#### 3.7.1 Electric Discharge Machine (EDM)

The American Society for Testing and Materials (ASTM -E8) guidelines are followed for preparing the tensile test specimens. The wire cut EDM is used to cut the smooth profile of tensile specimens as shown in Figure (3.17).



Figure (3.17) EDM used for UTM specimen.

#### 3.7.2 ASTM standards

Tensile test specimens were made from both rolling and transverse directions of the base metal, and in the transverse direction for the weldments. Due to size limitations, welded section specimens were machined with a shoulder-to-shoulder distance of 100 mm with the weld zone (25 mm shoulder diameter) centered, and width of 12.5 mm similar to the specimen shown in Figure (3.18). The as welded specimens were machined with a gauge length of 25 mm, and width of 10 mm as shown in Figure (3.19). Testing was performed on a MCS screw driven universal machine tester at a crosshead speed of 1 mm/min at room temperature, Figure (3.20). Load-extension curves are plotted using the machine software which recorded data running at a speed of 5 Hz shown in Figure (3.21). At least three tests were performed for each condition. The 0.2% proof stress and tensile strength and percent elongation to failure were determined for each condition.

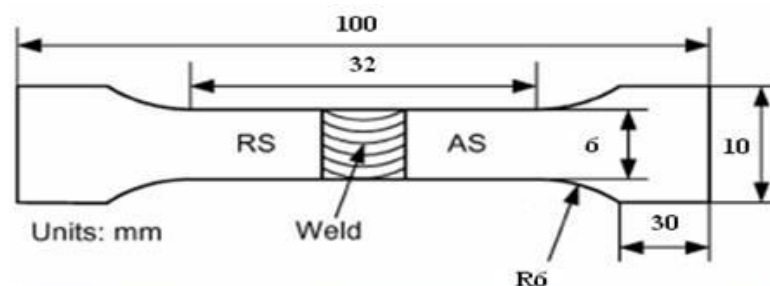


Figure (3.18) ASTM E-8 dimensions.

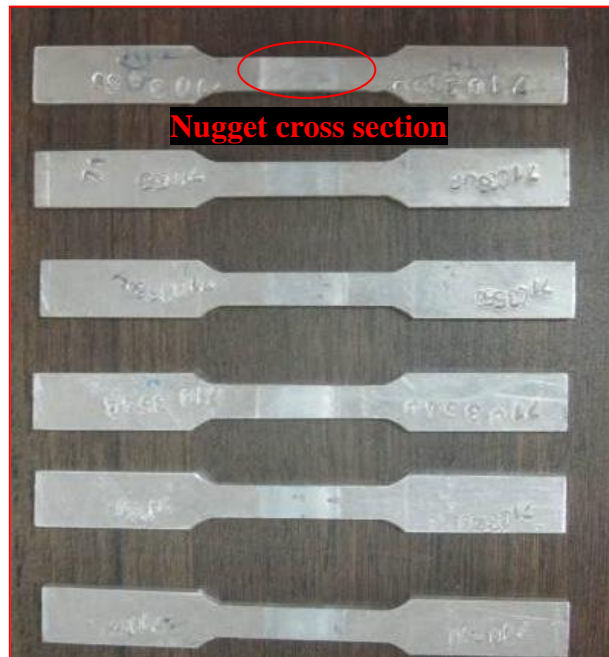


Figure (3.19) Tensile test samples prepared.

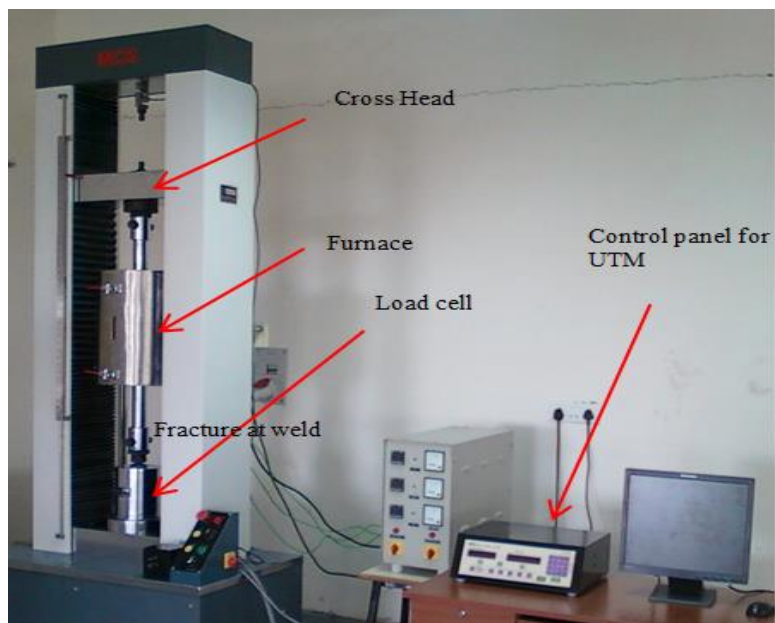


Figure (3.20) Universal Testing Machine.

### 3.7.3 Effect of process parameters vs. mechanical properties

The mechanical properties like yield strength (YS), ultimate tensile strength (UTS) and % elongation of the FSW joints of AA-5052-H32 with different RS and TS are studied from the experimental results and are discussed below in detail. Table (3.7) gives the summary of measured yield strength (YS), ultimate tensile strength (UTS) and % elongation of the FSW joints of AA-5052-H32. It can be observed that % elongation decreased with increasing RS, as expected because hardness increases (see Figure 3.21). Also, the tensile strength decreased slightly with increasing RS. At same RS, tensile strength decreased with increasing TS. However, the tensile strength and mean hardness of FSW joint are closer to the base metal values at 500 rpm and 40 mm/min and therefore considered to be optimum process parameters. Based on the observed trends, it can be concluded that there should be a trade-off between tensile strength and hardness while selecting the optimum process parameters.

Table (3.7) Mechanical properties of the joint at TPH=3.0 mm.

RS (rpm)	YS (MPa)	UTS (MPa)	% E
Traverse speed, TS=28 mm/min			
355	153	229	21
500	126	208	22
710	133	205	17
Traverse speed, TS=40 mm/min			
355	140	205	16
500	144	216	22
710	150	201	16
Traverse speed, TS=56 mm/min			
355	148	211	17
500	118	186	18
710	136	194	14

The tensile test results for the above conditions are shown in Figure (3.21) in terms of load vs. displacement from which various mechanical properties are obtained. It can be observed that for given TS values, increasing TPH increased both YS and tensile strength (UTS), except for TPH=3.5 mm and TS=56 mm/min at which tunnel defects were observed. Since major defects were observed with TPH=3.5 mm and also minor defects at TPH=2.5 mm, the optimum TPH can be considered as 3.0 mm. Also, it can be observed that at TPH=3.0 mm,

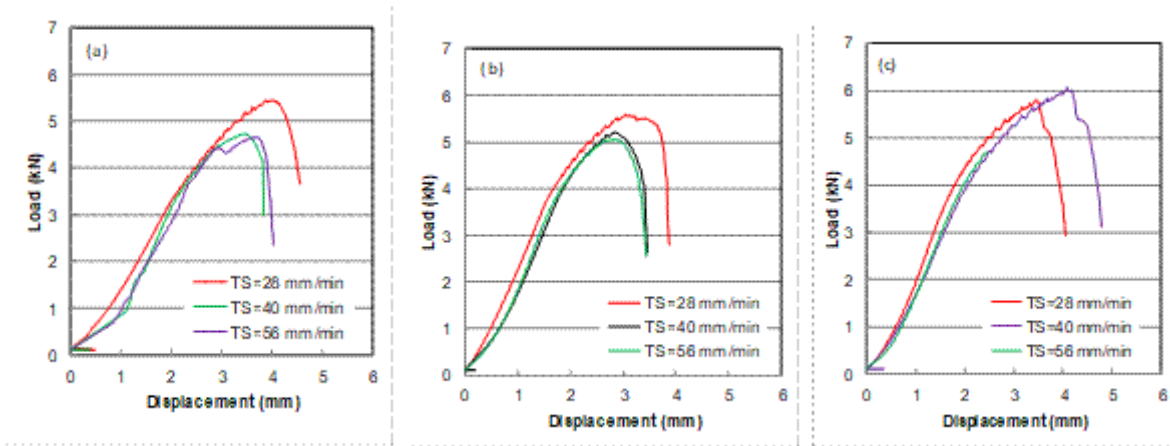


Figure (3.21) Effect of TS on load vs. displacement of FSW joints at different values of TPH, mm; (a) 2.5 (b) 3.0 (c) 3.5. Rotational speed, RS=500 rpm.

the optimum TS found to be between 28-40 *mm/min* for which the % elongation value is closer to the BM value (13%) as observed in Table (3.7). It can be noted here that several researchers considered a gap of about 0.2-0.5 mm. It can be noted that the mechanical properties vary significantly for different TPH values. Also, for 4 mm thick plates of AA50552-H32 the optimum TPH value is 3.0 mm at all different TS indicating that the minimum gap between tool-pin tip and workpiece bottom surface need to be around 1 mm (or 25% of plate thickness) in the present study. From Table (3.6) and Table (3.7) Irrespective of the workpiece thicknesses few weld defects (tunnel) are formed, which could be due to excess material flow because of heat generated with increased TPH values.

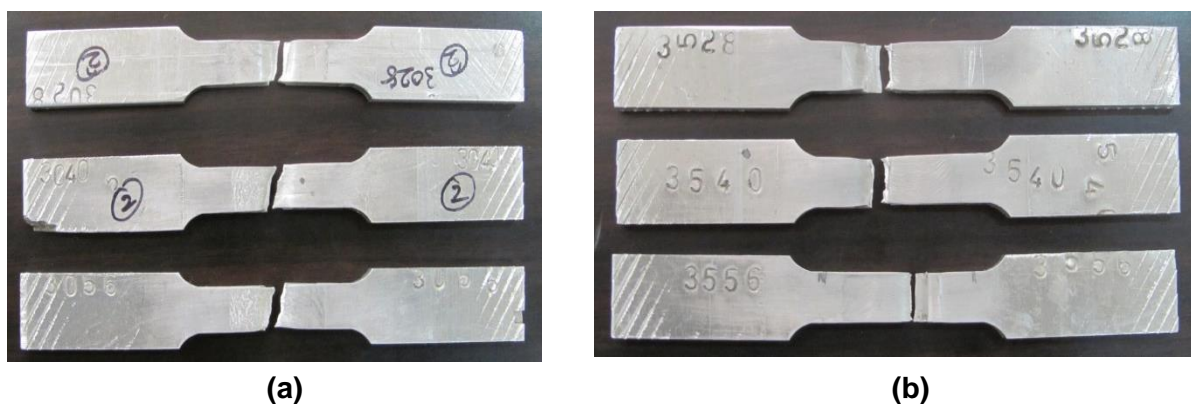


Figure (3.22) Post UTM test specimen of FSW joints for different values of TS, *mm/min* (TS=28; 40; 56); (a) TPH=3.0 mm (b) TPH=3.5 mm.

It can be observed by noting the minimum standard deviation (2-3%) for TPH =3.0 mm, while for all other combinations of process parameters the standard deviation vary between 3-7% and also the % elongation is close to that of the BM value (13%).

Figure (3.22) shows the post-weld tensile test specimens with fracture location for different values of TPH and TS. It can be observed that the fracture location and the profile at the fracture are different for different values of TPH, but are same for different values of TS studied. This indicates that TPH has significant influence on the nugget properties, besides the nugget geometry as mentioned above.

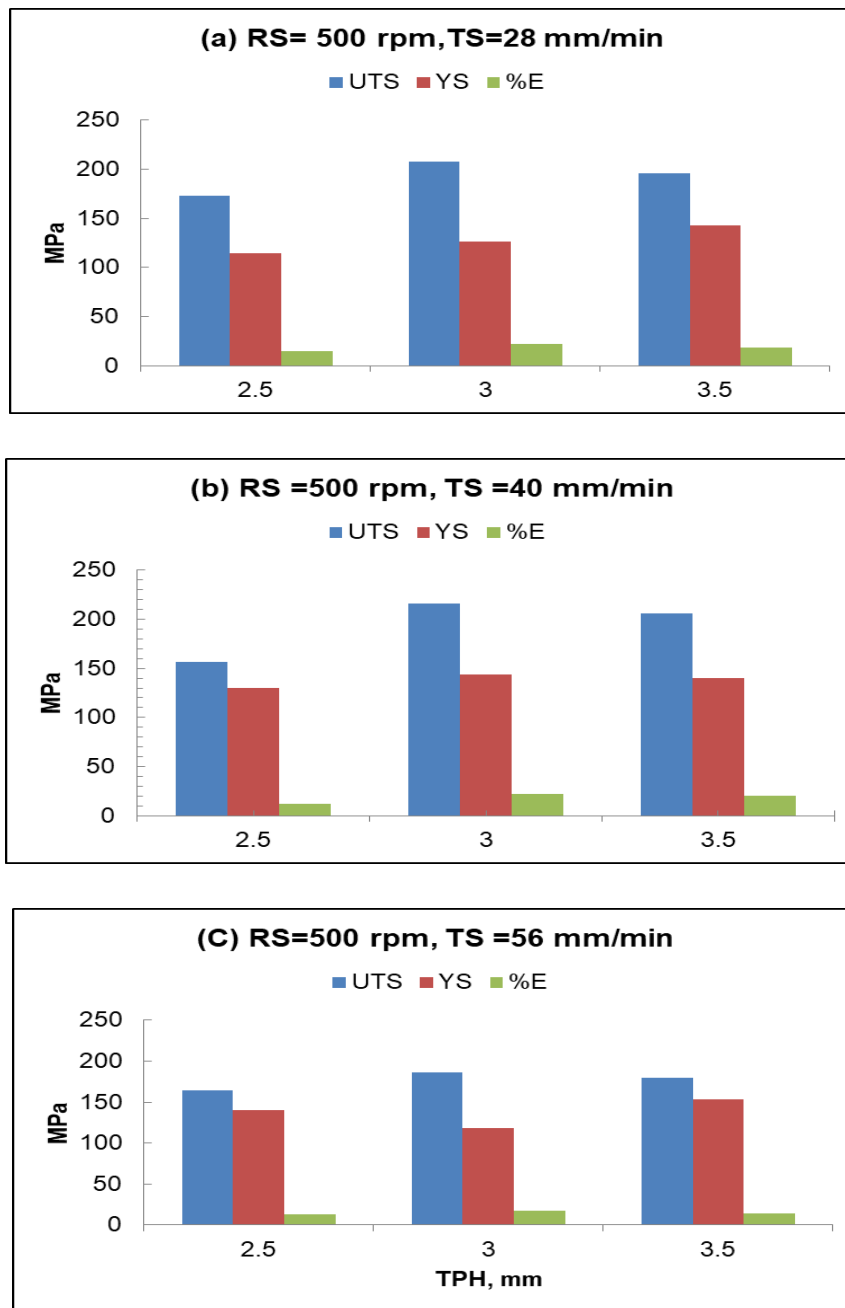


Figure (3.23) Mechanical properties of the FSW joints with different TS (mm/min).

With the increase in TS the fracture locations of the joints are not distant from the weld center, but gradually the fracture distance moved towards the AS. These results indicate that the joints are fractured under the conditions of local and heterogeneous deformation, and the fracture locations of the joints are significantly affected by the welding parameters. Few are fractured at the interface between HAZ (Heat Affected Zone) and TMAZ. Moreover, it should be noted that all the joints are fractured on the advancing side or at the weld center, but not on the retreating side. The tensile properties and fracture locations of the joints are, to a large extent, dependent on the welding defects and hardness distributions of the joints, which, in turn, depend on the welding parameters (Liu et al., 2012).

### **3.7.4 Lüders bands, Strain Hardening and Toughness**

Once the, plastic deformation becomes localized (called necking), and the engineering stresses drop because of the localized reduction in cross-sectional area. However, the true stress continues to rise because the cross-sectional area decreases and the material work-hardens in the neck region. The true-stress-true-strain curves are obtained by converting the tensile stress and its corresponding strain into true values and extending the curve shown in the Figure (3.24). Lüders bands, also known as "slip bands" or "stretcher-strain marks," are localized bands of plastic deformation in metals experiencing tensile stresses, common to low-carbon steels and certain Al-Mg alloys (Roxana et al., 2005). The material in this research is AA5052-H32 is also called as Al-Mg alloy leads to the formation of these bands. In the FSW process the plastic deformation of the material occurs in solid state and deformation is non homogeneous at small plastic strains, concentrated in discrete bands in regions of stress concentration (that yield first) which are undesirable and studied with FSW process parameters which is a gap area. As internal stresses tend to be highest at the shoulders of tensile test specimens, band formation is favored in those areas. However, the formation of Lüders bands depends primarily on the microscopic (i.e. average grain size and crystal structure, if applicable) and macroscopic geometries (width and depth of nugget) of the material. For example, a tensile-tested steel bar with a square cross-section tends to develop comparatively more bands than a bar of identical composition having a circular cross-section. The formation of a Lüders band is preceded by a yield point and a drop in the flow stress. Then the band appears between plastically deformed and undeformed material that moves with the constant cross head velocity (Ananthakrishna, 2007). After the band has passed through the material the deformation proceeds uniformly with positive strain hardening .



Because the nanometer-sized, aluminium particles stabilize the microstructure in elevated temperatures, and has the potential for the joining process by friction stir welding and the joints display excellent mechanical properties when compared to conventional fusion welds, Threadgill et al., (2009). The luder bands are clearly identified in stress-strain graphs for different tool-pin height for which there is a long interruption for 710 rpm and short interruption for 355 rpm as shown in Figure (3.24) which shows clearly the gap area of optimum tool-pin height which is not done by any researcher. Lower RS and TS lead to these slip bands and irrespective of TPH. In addition non-homogeneous plastic flow deformation can be observed at higher degrees of deformation in stress-strain curves in Type-B stretcher strain curves and is clear at TPH =3.0 mm and cannot be eliminated. Type-A can be eliminated by thermo-mechanical treatment(i.e., prior deformation by rolling ). So, in the TMAZ we can see the stretcher strains and to avoid this thermo-mechanical treatment, we need to optimize the process parameters effectively to reduce the TMAZ zone.

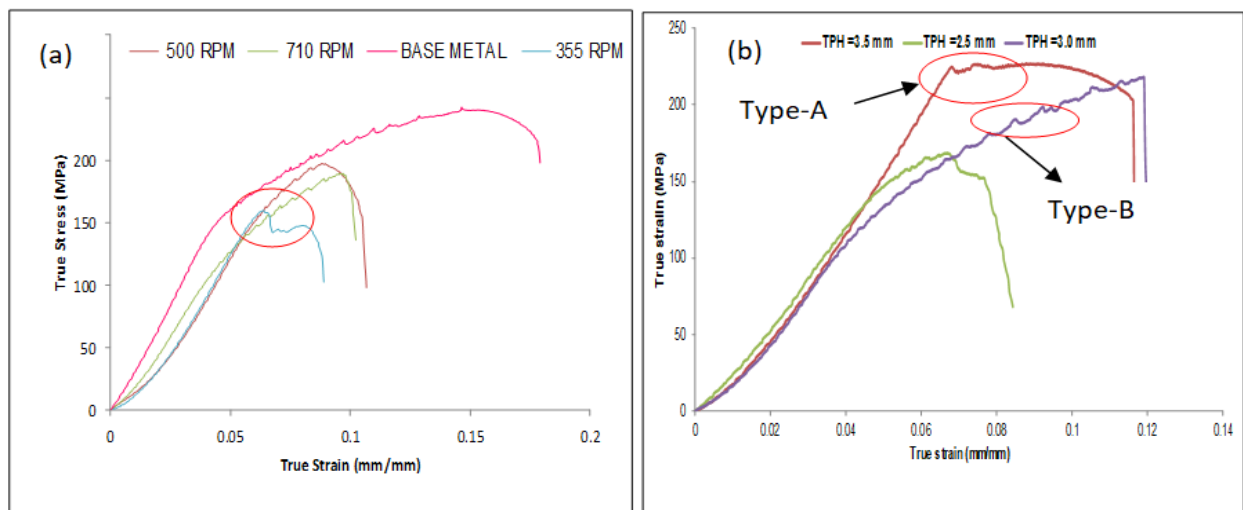


Figure (3.24) (a) Stress-strain curves at different RS (rpm) and TS = 40 mm/min (b) Luder

Strain-hardening behaviour of the FSW joints plays an important role in the material load bearing properties. Strain-hardening is one of the most common methods practiced to enhance the strength of the materials by inducing plastic deformations. Strain-hardening behaviour is greatly influenced by grain size and dislocation density (Elangovan et al., 2008). After the fracture of tensile specimens more on the advancing side, further studies are carried out to find the final mechanical properties such as ductility, toughness and strength of the welded specimens. An assessment of the true stress-true strain curve provides a realistic

characteristic of the material .Therefore, this section presents a detailed work carried out to study the effect of Friction Stir Welding (FSW) process parameters on strain-hardening behaviour of aluminium-alloy plates (AA5052-H32) using hardening capacity and strain hardening exponent concepts. With increasing tool rotation speed and/or decreasing traverse speed, FSW joints show higher hardening capacity and lower strain-hardening exponent. Therefore, the effects of TS and RS on mechanical properties are studied at which defect free welds are achieved. It must be emphasized here that the engineering stress-strain curve does not give a true indication of the deformation characteristics of a metal because it is based on the original dimensions of the specimen. In actuality, ductile materials continue to strain-harden up to fracture, but engineering stress-strain curve gives a different picture. The occurrence of necking in ductile material lead to a drop in load and engineering stress required to continue deformation, once the maximum load is exceeded. An assessment of the true stress-true strain curve provides a realistic characteristic of the material. Beyond maximum load the true stress should be determined from actual measurements of load and cross-sectional area and is expressed by the following expression.

$$\sigma = P/A \quad (3.1)$$

The true strain  $\epsilon$  may be determined from the engineering or conventional strain  $e$  by

$$\epsilon = \ln(e+1) \quad (3.2)$$

This equation is applicable only to the onset of necking for the reasons discussed above.

Beyond maximum load the true strain should be based on actual area and is expressed by the following equation.

$$\epsilon = A_0/A_1 \quad (3.3)$$

Khodaverdizadeh et *al.*, (2012) investigated the copper joints using strain hardening exponent and hardening capacity and revealed that increasing RS or decreasing TS resulted in increased hardening capacity and decreased the hardening exponent. So far, limited studies are reported on the strain-hardening behaviour of Al - alloys, and very few works on the strain hardening of the friction stir welded Al - alloy is seen in the open literature and no works are found on AA5052-H32 which led to study this aspect in this thesis.

In order to calculate the strain-hardening exponent, the relationship between flow stresses and strains in the plastic region are required. The flow stress of a material in the

uniform plastic deformation region is commonly expressed by the Holloman equation as given below in eqns (3.4) and (3.5). In the present study, hardening capacity and strain-hardening exponent are used to investigate the strain-hardening behaviour of samples in the uniform plastic deformation region. The hardening capacity of a material is defined as the ratio of UTS and YS (Luo J et al., 2006) and is given below. With increasing RS or decreasing TS, the FSW nuggets revealed higher hardening capacity and lower strain-hardening exponent in contrast to the base metal (BM) given in Table (3.8).

$$\sigma = K \epsilon^n \quad (3.4)$$

$$H_c = \frac{\sigma_{uts}}{\sigma_y} \quad (3.5)$$

The hardening capacity of FSW nuggets was found to be about twice that of the base metal (BM) value, while the strain-hardening exponent is nearly thrice that of the BM. The hardening capacity ( $H_c$ ) is re-defined as the following normalized equation, (Dorbane et al., 2016) and used in the present analysis.

$$H_c = \frac{\sigma_{uts} - \sigma_y}{\sigma_y} \quad (3.6)$$

Table (3.8) gives the hardening capacity of the FSW nuggets predicted at different combinations of RS and TS. It can be found that the hardening capacity ( $H_c$ ) is high at low strain-hardening exponent ( $n$ ) and vice-a-versa. Also, there is a significant variation of both  $H_c$  and  $n$  with FSW process parameters (RS and TS). It is interesting to note that the higher values of  $H_c$  and  $n$  are found at RS=500 rpm, and TS=40 mm/min at TPH=3 mm, which are concluded by the present authors as the optimum process parameters for a given 4 mm thick AA5052-H32 plates welded by FSW technique (Madhavi et al., 2014).

It should be noted here that all of the above FSW process parameters affects the net heat input per unit weld length. This leads to variation in grain sizes, microstructures, and final mechanical properties across the nugget cross-section. Also, the authors found from experiments that at higher values of TS the average grain sizes in HAZ increased and the hardness decreased (Madhavi et al., 2014), which in turn decreases the YS according to the

Also, the authors found from experiments that at higher values of TS the average grain sizes in HAZ increased and the hardness decreased (Madhavi et al., 2014), which in turn decreases the YS according to the Hall-Petch relationship and depends on hardening capacity and strain-hardening exponent (Dieter 1986, Hosford et al.,2005).

Table (3.8) Strain-hardening exponent, hardening capacity and toughness values at TPH=3mm.

TS (mm/min)	RS = 355 rpm	RS = 500 rpm	RS = 710 rpm
	Strain-hardening exponent, n		
28	0.2556	0.1581	0.1522
40	0.1796	0.2301	0.2037
56	0.1788	0.2615	0.1984
Hardening capacity, H <sub>c</sub>			
28	454.96	391.27	345.92
40	370.33	463.78	393.04
56	380.89	442.26	370.44
Toughness (kJ/mm <sup>3</sup> )			
28	14.23	13.28	10.62
40	10.46	21.99	9.91
56	11.48	21.36	8.58

### 3.7.5 Toughness

Many metals undergo a sharp change in ductility and toughness across a narrow temperature range, called the transition temperature as shown in Figure (3.25). Impact tests are particularly useful in determining the ductile-brittle transition temperature of metals. The transition temperature depends on factors like the composition, microstructure, grain size, surface finish, and deformation rates and most of which vary significantly across the FSW nuggets.

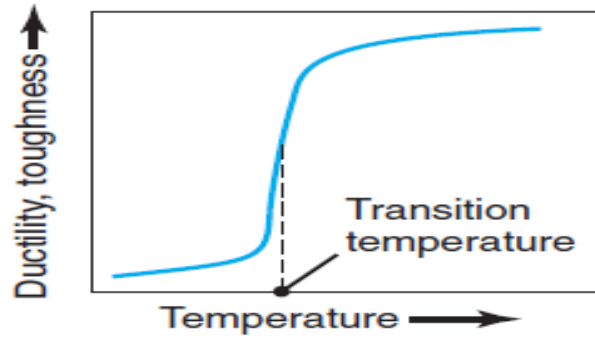


Figure (3.25) Schematic of transition temperature in metals (Kalpakjain *et al.*, 2006).

The toughness of a material is defined as its ability to absorb energy during plastic deformation before fracture occurs. In general, the toughness is measured from the stress-strain graph (see Figure 3.26) and is the total area under the stress-strain curve before it fractures. In the present study, the area under stress-strain curve for different RS and TS are calculated and presented in Table (3.8). It can be observed that the toughness variation of FSW joints with process parameters (RS and TS) is very similar as strain-hardening exponent and hardening capacity, discussed above. Also, interestingly, the toughness is maximum at the same optimum process parameters (RS=500 rpm, TS=40 mm/min, TPH =3.0 mm).

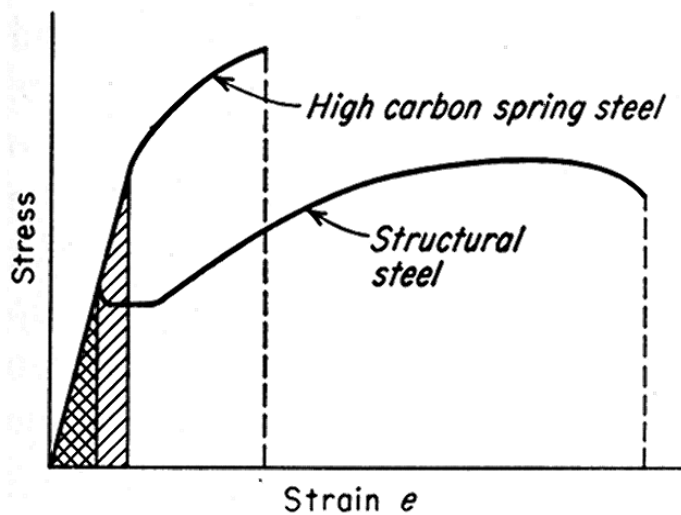


Figure (3.26) shows the stress - strain curve for high and low toughness materials (Mendes *et al.*, 2014).

### 3.7.6 Fractography

The tested tensile specimens, shown in Figure (3.22), are examined using SEM to identify the fracture locations and subsequently characterize the fracture surfaces. SEM observations are made at low and high magnifications to carefully identify the fracture mechanism. Figure

(3.27) clearly indicates the ductile fracture behaviour with crown part, cup, and cone. However, the fracture surface micrographs of these (FSW nugget) tensile specimens exhibited a somewhat different morphology due to the fracture occurring near the TMAZ. However, the ductility drop is drastic, as shown in Figure (3.25). It can be noted from Figure (3.22) that, at same RS, the fracture occurred at the middle of the nugget at higher value of TS and shifted towards advancing side at lower value of TS.

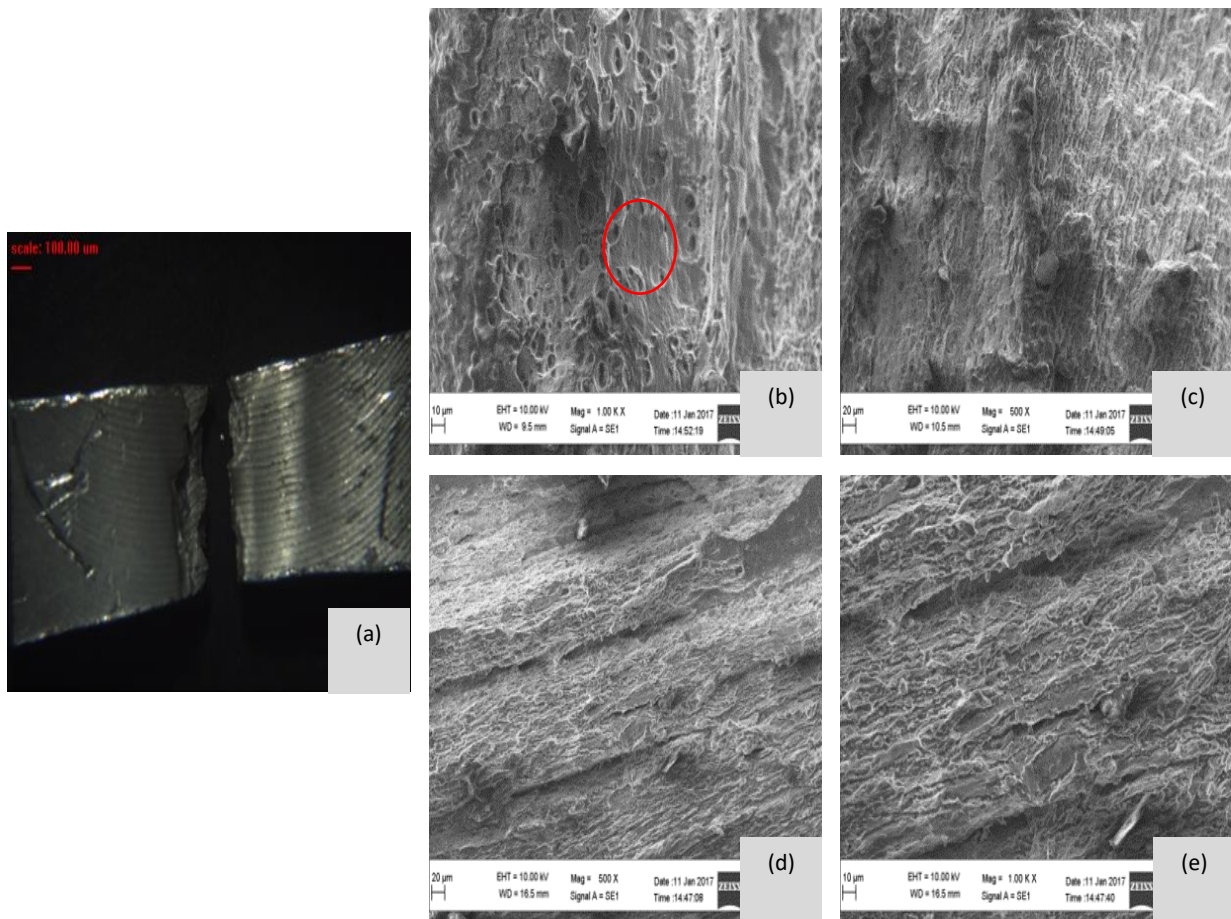


Figure (3.27) SEM micrograph of tensile fracture surface at 500 rpm, TS = 40 mm/min and TPH =3.0 mm.

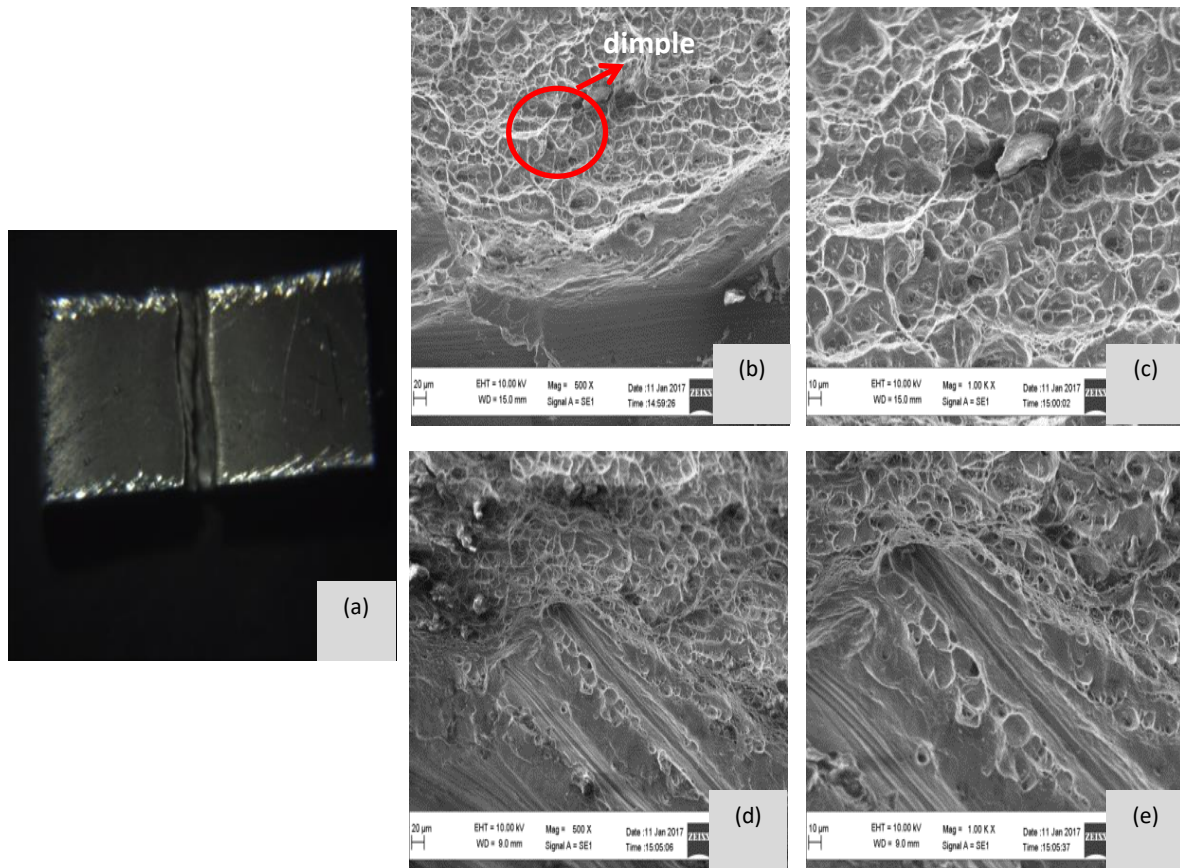


Figure (3.28) SEM micrograph of tensile fracture surface at 355 rpm, TS = 40 mm/min and TPH =3.0 mm.

Figures (3.27-3.29) presents the SEM micrographs of fractured surfaces, as part of fractography analysis. It can be observed that the fracture mechanism is dimpled rupture. It is a known fact that the dimpled rupture fracture mechanism indicates some degree of ductility and the existence of the defect can cause a stress concentration around the defect zone during the tensile test. In contrast, FSW nuggets show both small and large size dimples (see Figures 3.27-3.29). The secondary cracks are observed inside the dimples. From the fractography, it can be inferred that the FSW nuggets failed under ductile mode. The TMAZ near weld periphery undergoes high grain deformation and lower hardness (Wang et al., 2014). The size of the voids in the joint suggests that a smaller stretch zone (HAZ) is present at the tip of the crack. This leads to a small plastic zone ahead of the crack and a rather low ductility, as shown in Figure (3.27). Also, the fracture surfaces are populated with very fine dimples, revealing a more ductile behaviour before failure. Figure (3.27) shows long and flat regions on the fracture surface corresponded to the elongated grains, separated by ductile tear ridges.

Figure (3.29) shows the facets that formed in the fracture section of FSW nugget, which is one of the aspects of cleavage fracture for the specimen at 710 rpm and 40 mm/min. However, finer dimples are observed in this case compared with the other two values of RS. Figures (3.27-3.29) In overall the above figures clearly shows that the fracture surfaces are composed of deep dimples, shallow dimples, sheared dimples, and cleavage facets.

In Al-alloys, there are some characteristics in the fracture surfaces of FSW specimens, which show the ductile and cleavage fracture mechanisms. Likewise, fractography of the FSW nuggets confirm the higher elongation at higher heat input conditions (high RS and low TS). SEM micrographs are taken from the whole joint and the root of weld. All the fractured surfaces consist of dimples having various sizes and shapes, which means the ductile failure. Compared with the middle and bottom slices, the dimples in the top slice are deeper and tearing edges are thicker with lots of micro pores. Therefore, the top of weld yields the maximum mechanical properties.

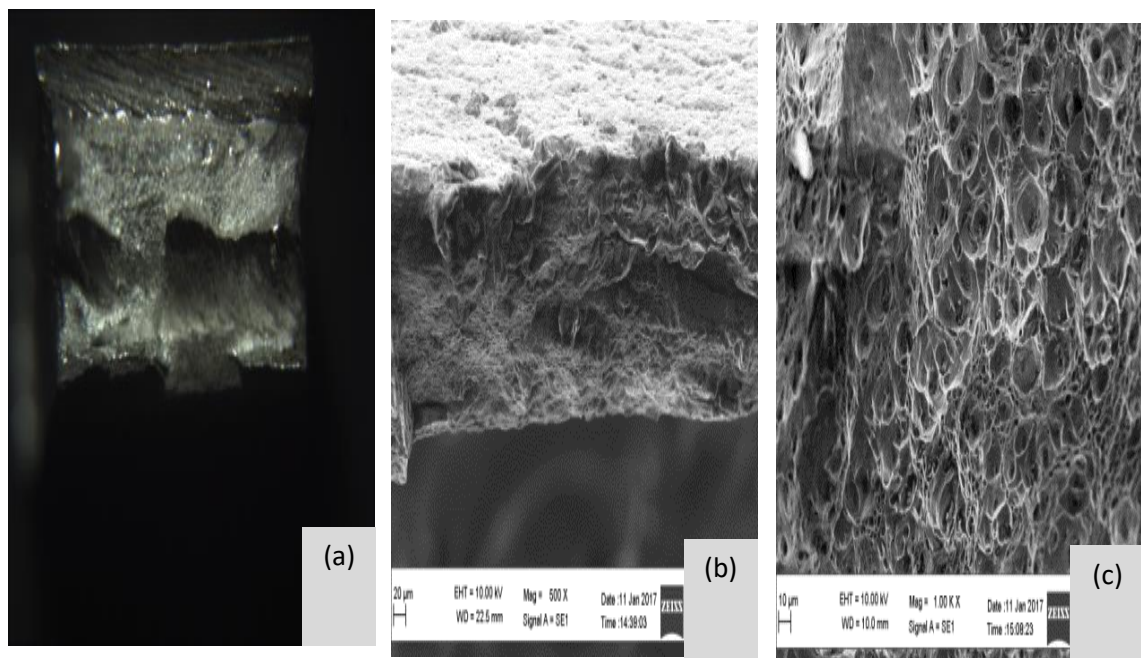


Figure.3.29 Fracture surface of FSW nugget at 710 rpm, 40 mm/min ,TPH =3.0 mm (a) macrograph of fracture surface; (b) SEM image of fracture surface; (c) enlarged SEM image of (b).



### 3.7.7 Summary of $H_c$ , $n$ and Toughness

The following are the conclusions of the SEM pictures at different FSW process parameters to study the nature of fracture, ductility and toughness.

- With increasing RS or decreasing TS, friction-stir welded joints showed higher hardening capacity and lower strain hardening exponent.
- The fracture surfaces are populated with very fine dimples, revealing a ductile behaviour of the material.
- Tensile fracture mode of the FSW joints is clearly a quasi-cleavage type, including both dimples and facets. Also, FSW joints at low values of TS revealed more ductile as compared to that of joints with higher TS.
- Hardening capacity, strain-hardening exponent and toughness behaviour at different RS and TS clearly indicated the sensitivity of FSW process parameters and the maximum values are attained at the optimum process parameters.

### 3.8 Effect of Process Parameters vs. Thermal Cycles

In this section, the detailed experimental analysis carried out on the heat generation due to the friction between the tool-pin and workpiece are studied. The material flow movement from advancing side to retreating side due to stirring effect is clearly noticed. The effect of RS and TS are significant in producing heat and material flow; they are then compared with experimental values.

Over the past decade and half, researchers have investigated on FSW of different aluminium-alloys and the effects of process parameters on resulting macro and micro-structures and final mechanical properties of the nugget. In particular, this experimental research works revealed several aspects of different phenomena affecting the peak temperatures at different thermocouple positions for a given RS, TS and TPH. Tool-pin height is responsible for the total load with which the tool exerts on the weld plates in the downward direction. As this force exceeds a certain limit, it causes higher heat input which leads to excessive thinning.

When this force is lower than required, cracks may appear because of no vertical flow of material (Vidal *et al.*, 2009). Therefore, tool rotational speed, welding speed and tool-pin height are responsible for the good quality of welds, mechanical properties, and

microstructure of the weld. In order to quantify the heat effects on microstructures, K-type thermocouples are used to measure the temperatures at selected locations within the workpiece during FSW process. Further, the overall thermo-mechanical effects due to rotation of the tool are studied by examining the variations in the nugget geometry for different weld traverse speeds (Figure 3.16). Finally, the peak temperatures are qualitatively measured at different places from the weld center line and values are discussed in the Table (3.10).

In general, the temperature at any given point within the workpiece rises as the heat source approaches it and decreases once it moves away. Therefore, the thermal cycle consists of heating and cooling periods. The maximum temperature (peak temperature,  $T_p$ ) attained at any given point depends on its location from the weld center line, i.e., depth (y-value) from top surface and width (z-value) away from the weld axis in the cross-sectional view of the nugget. In FSW process, due to material flow, more heat would be transported and diffused in the direction of tool rotation making the weld nugget asymmetric with respect to the weld axis.

Therefore, the nugget geometry consists of an advancing side (AS) on the left and retreating side (RS) on the right for clockwise rotation of the tool and vice versa. Figure (3.30) shows the measured temperatures during butt welding of AA5052-H32 plates at different traverse speeds. Figures (3. 30a-3. 30c) on the left shows the temperatures measured at different locations in advancing side (AS) while on the right shows for the same locations in retreating side (RS). It can be observed from Figure (3. 30) that for same locations, the peak temperatures are higher in AS than RS and the difference in peak temperatures increase in the depth direction.

It is a known fact the net frictional heat input per unit length of the weld depends on weld traverse speed (TS) and is high at low TS value. The increased heat input at low TS values increases the material temperature and thereby increases the material flow. The increased material flow results in an increased distribution of the total frictional heat within the workpiece.

This manifests as less variation in peak temperatures and can be clearly observed in Figures (3. 30a-3. 30c) at  $TS=28 \text{ mm/min}$  for all depths. Further, it can be observed that the decrease in material flow at higher TS results in increases peak temperatures on AS and decreased peak temperatures on RS. Also, the decrease in material flow resulted in increased temperatures in depth direction indicating more material flow in the lateral direction.

Increasing TS increased the width and depth of the nugget and the same locations become closer to the zones, thereby increasing the peak temperatures and is clearly observed in Figures (3. 30a-3. 30c). Table (3.9) gives the summary of peak temperatures ( $T_P$ ) at selected locations in AS and RS and at different weld traverse speeds. It can be observed that the peak temperatures are higher in AS than RS. Also, It should be noted here that the TCs were positioned nearer to HAZ (i.e., at  $y=1\text{mm}$  and  $z =5, 6, 7 \text{ mm}$  from weld surface) and towards the BM at all conditions.

Table (3.9) Peak temperatures at width,  $z=6\text{mm}$  and different traverse speeds, (mm/min), at fixed RS = 500 rpm

Depth, y (mm) From top surface	Adv. Side (AS)			Ret. Side (RS)		
	TS=28	TS=40	TS=56	TS=28	TS=40	TS=56
y=1	287	238	307	293	269	279
y=1.5	393	356	348	390	356	347
y=2	363	380	326	289	303	303
y=2.5	353	391	366	399	308	337
y=3	295	400	328	285	320	302

Variations of peak temperatures for various process parameters and at different positions are discussed briefly. Before, introducing the more quantitative details of friction stir welding, it is worthwhile to summarize the results from an experimental perspective. A brief summary of some experimental works done by different authors on deformation and material flow during friction stir welding are discussed briefly. The experimental results were broadly summarized by Seidel et al., (2001) and Reynolds, (2008), as (a) deformation at the tool shoulder and workpiece interface, and (b) deformation at the tool-pin and workpiece interface.

The nature of deformation at tool shoulder/workpiece interface is illustrated schematically in Figure (3.0) where the FSW tool transfers the material from advancing side to the retreating side. The material at the retreating side on the other hand moves to the advancing side. A key difference being the circular movement of advancing side material is directed vertically downwards into the workpiece, while the retreating side material is pushed vertically up towards the workpiece surface. In fact, depending upon the conditions of welding, some of the material may even be pushed out as flash on the workpiece surface.

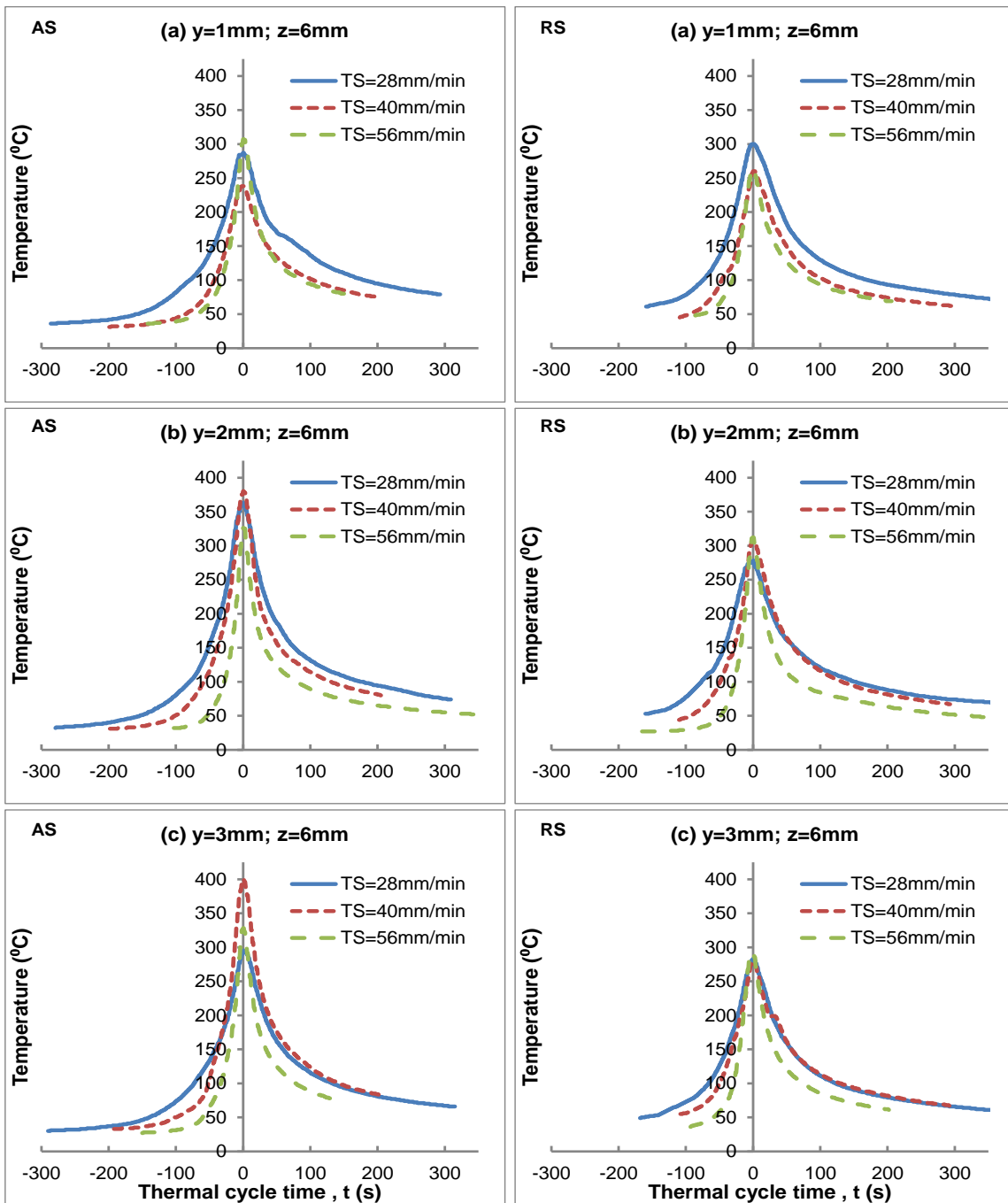


Figure (3.30) Thermal cycles at selected locations in AS and RS for different traverse speeds, (TS) and same RS and TPH.

The amount of heat conducted into the workpiece dictates a successful process which is defined by the quality, shape and microstructure of the processed zone, as well as the residual stress and the distortion of the workpiece. The amount of the heat gone to the tool dictates the life of the tool and the capability of the tool to produce a good processed zone. For instance, insufficient heat from the friction could lead to breakage of the tool-pin as the material is not soft enough. Therefore, understanding the heat transfer aspect of the friction stir welding is

extremely important, not only for the science but also for improving the process. In general, increasing TS lowers the net heat input to the material resulting in less plasticized state and hence insufficient material flow around the tool-pin surface. For a constant RS and TPH, increasing TS decreased the peak temperature.

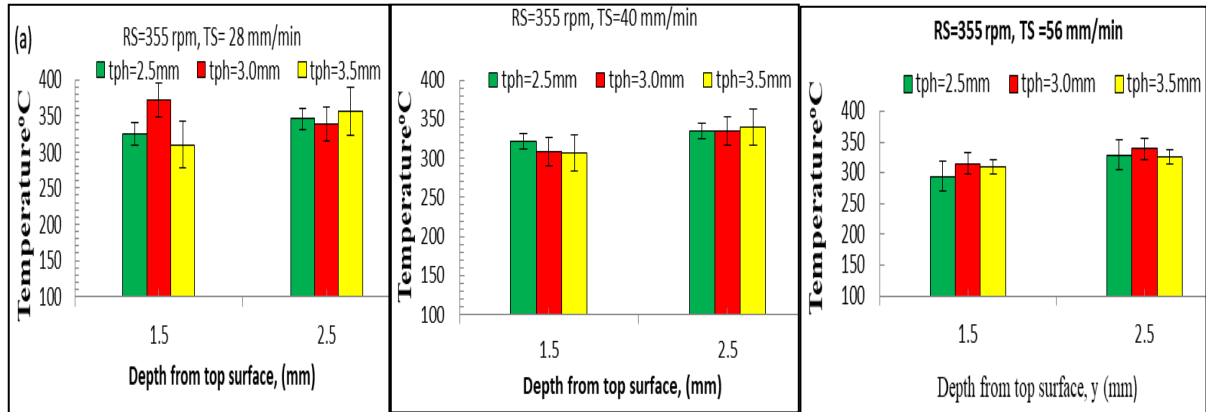


Figure (3.31) Peak temperatures across nugget cross-section and at various depths ( $y=1.5, 2.5$  mm) from top surface for RS=355 rpm, TS= (a) 28 (b) 40 and (c) 56 mm/min.

The peak temperatures for the FSW joints made using various traverse speeds across the nugget cross section are shown in Figures (3.31 and 3.32). With the increase in depth from top surface across the nugget cross-section the peak temperatures increased. Keeping the other parameters (TS, TPH) constant, by decreasing the RS, the average peak temperature decreased. Meanwhile, with increase in TS, the peak temperature decreased. Also, increasing the TPH increases the total frictional heat around the tool-pin resulting in more plasticized material flow which tends to change the nugget shape and size, as well change the grain size. This in turn dictates the hardness and other mechanical properties.

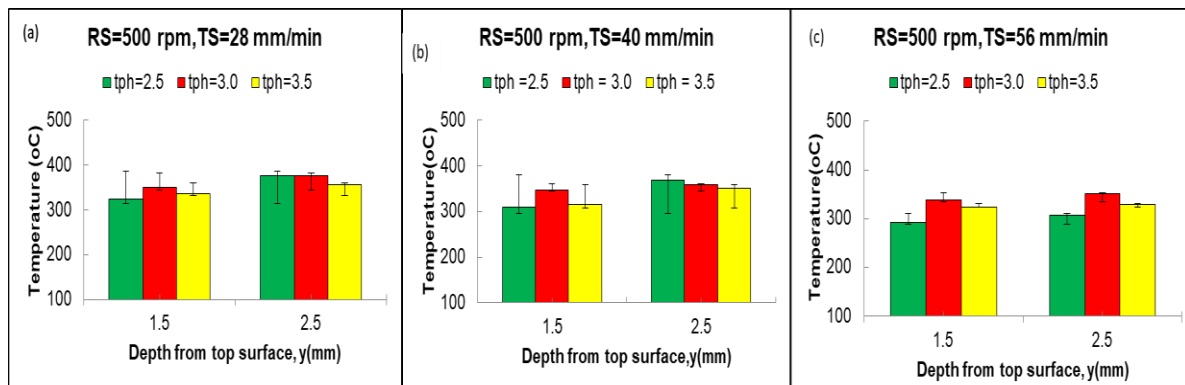


Figure (3.32) Peak temperatures across nugget cross-section and at various depths ( $y=1.5, 2.5$  mm) from top surface for RS=500 rpm, TS= (a) 28 (b) 40 and (c) 56

## **3.9 Grain Size and Hardness in FSW Nugget**

### **3.9.1 Grain Size**

The overall thermo-mechanical effects due to rotation of the tool are studied by examining the grain size variations in the nugget geometry for different weld traverse speeds. Finally, the peak temperatures and grain sizes are qualitatively related to the final hardness and the key observations are discussed below.

In FSW process, due to thermo-mechanical effects, recrystallization phenomenon occurs and forms fine and equiaxed grains in FSW zones. The optimum range of the rotational and traverse speeds will be an important parameter to achieve high quality weld, since the variation of these parameters will affect the thermo-mechanical condition for the microstructural changes in the specimen.

The grain sizes and distribution are subjected to the thermal and mechanical conditions that the material experiences during FSW process vary from zone to zone as well as point to point within the zones. According to the literature, it is clear that grain size in the stir zone affects the quality of the joints. The grain growth in the stir zone is caused by the temperature rise during the FSW process.

The specimens for metallographic examination are cross-sectioned perpendicular to the welding direction and prepared for micro structural investigation. After preparation, metallographic specimens were etched for 10 s with Keller's solution (2% HF). The mean grain sizes are measured according with ASTM linear intercept method. Optical microscopy was used for microstructural characterization.

The experimental results from Figure (3.33) show that the grain size distribution in different zones is very clear, and that the grains are fine and uniform in SZ and somewhat coarser in TMAZ. It can also be observed that the grains are much larger in HAZ and comparable to that of base metal (BM) indicating no mechanical effects in HAZ and grain size changes are subjected to thermal conditions, only.

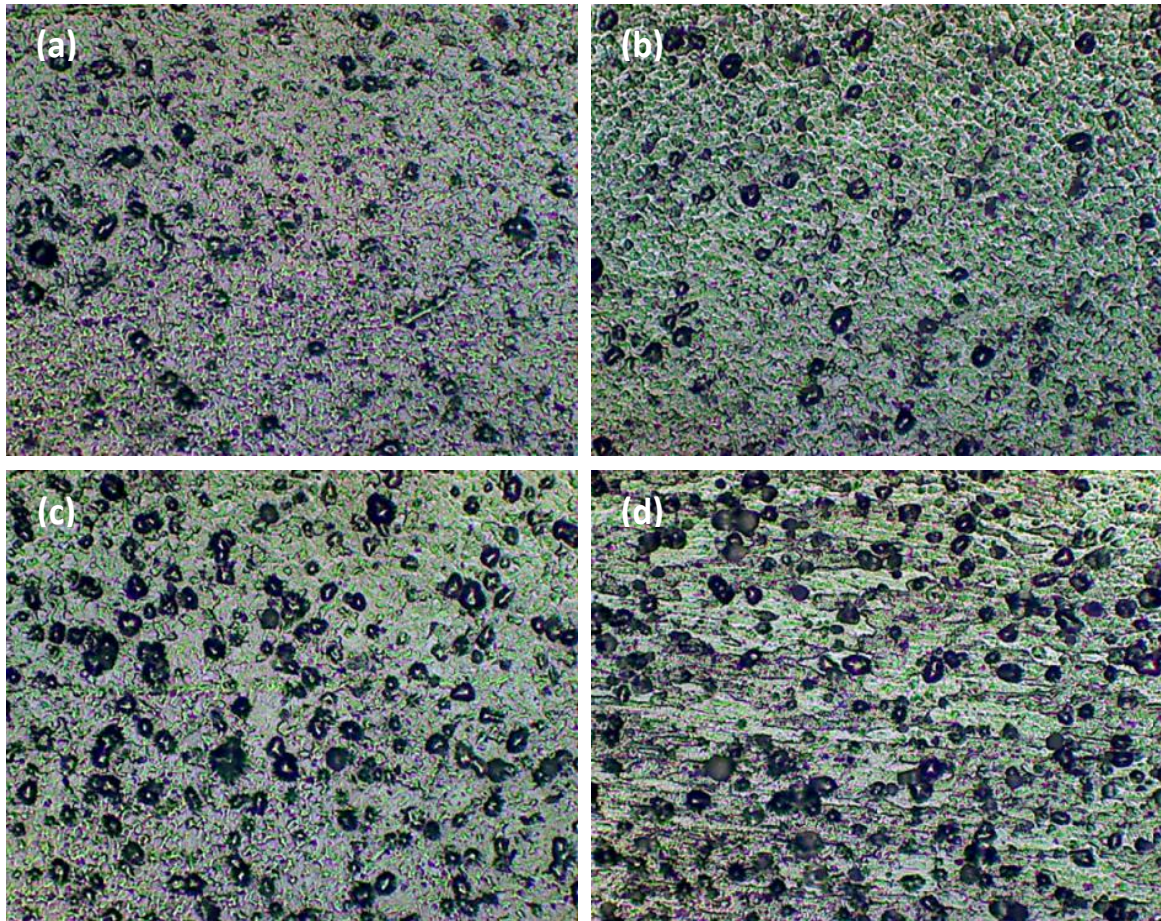


Figure (3.33) Grain size variation in different zones at TS=56 mm/min, TPH =3.0 mm and RS=500 rpm; (a) SZ (b) TMAZ (c) HAZ (d) BM.

However, the grains vary from point to point and may observe significant variation near the interface. It is observed from Figure (3.33) that the secondary particle density is low in SZ and TMAZ as compared to the HAZ and BM and is due to increased diffusion at higher temperatures. Also, the particle density increased with increasing TS values. Different patterns and grain sizes of the nugget zone in the welding region depend on the conditions and parameters used during the FSW process.

From the observations of macrographs, we identified the optimum process parameters which enabled us to find defect free weld. The optimum rotational and traverse speeds are 500 rpm and 40 mm/min, respectively. A combination of three rotational speeds and three traverse speeds are applied. Microstructural evaluation using optical microscopy is studied.

During friction stir welding, material undergoes severe plastic deformation at elevated temperature which results in the formation of fine grains. Figure 3.33 (a–d) shows optical micrographs obtained from weld nugget zone of the joints including reinforcements. This

phenomenon is known as dynamic recrystallization (DRX) .The dominant factor in determination of grain size is the heat input; higher temperatures promote grain boundary migration. Figure (3.33) shows the microstructure of specimen at 500 rpm and 56 mm/min in which SZ, TMAZ, and HAZ are clearly distinct. The grains in the base metal(AA5052-H32) are elongated and are bigger in size compared to grains in SZ, TMAZ and HAZ as shown in Figure (3.34). In other words, higher heat input associated with increase in rotational speed or decrease in traverse speed, facilitates grain growth and consequently coarsens the crystallized grains as shown in Figure (3.35) . At a rotational speed of 710 rpm, an increase in traverse speed, resulted in larger grain sizes. This result suggests the key role of stirring action in controlling the grain size.

In Figure (3.34) the grains in base metal are larger in size and elongated. According to the literature, there are limited works done on the effect of tool geometric parameters on grain sizes of AA 6xxx and AA 5xxx plates. Jamshidiaval et al., (2011) studied the effect of tool geometric parameters on mechanical and microstructural behaviours during dissimilar friction stir welding of 5 mm thick plates of AA5086- O and AA6061-T6 and identified that the tool with a concave shoulder and a conical pin with grooves produced higher heat input and resulted in more uniform grains in the stir-zone than with the other tool-pins (cylindrical with and without threads). Also, the grain sizes in the stir- zone on AA6061 side of all the welds are finer than those produced on AA5086 side. Further, the grains in the stir-zone became coarser with decrease in weld pitch (a ratio of traverse and rotational speeds).

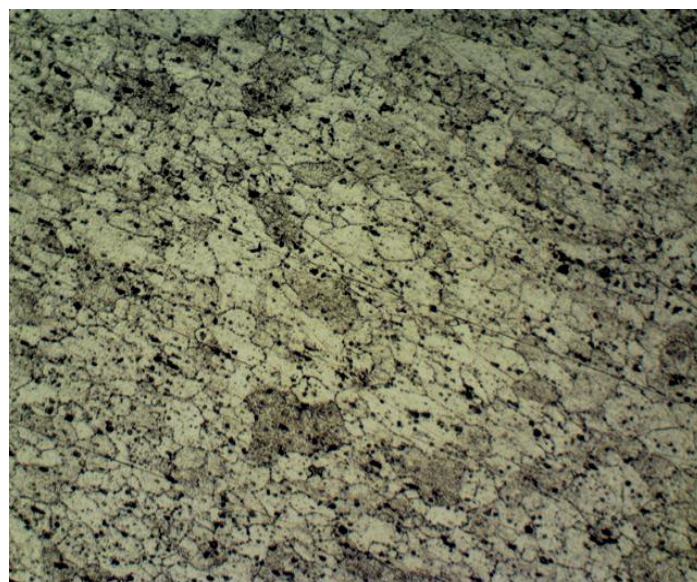


Figure 3.34 Elongated base metal grains(AA5052-H32).



In this thesis, the grain size at given location on the cross-section of the weld nugget is measured by Hey's line intercept method (ASTM E1382-97/E112) using optical microscope. The average grain sizes are measured both on advancing side and retreating sides at regular intervals of 1 mm from the weld center line towards the base metal and at different depths in the thickness direction ( $y=1.5$  and 2.5 mm from weld top surface). It can be observed from the Figure (3.35a) that the stir zone had equiaxed grains with an average grain size less than that of the base metal Figure (3.34) and is attributed to the recrystallization phenomenon during FSW process. Figure (3.35b) shows the grains in TMAZ, whose shape is much similar to that of the grains in the base metal but the average grain size is smaller. Moreover, the secondary particles (precipitates) are uniformly distributed unlike in stir-zone. Figure (3.35a). Figure (3.35c) shows the interface between the TMAZ and HAZ.

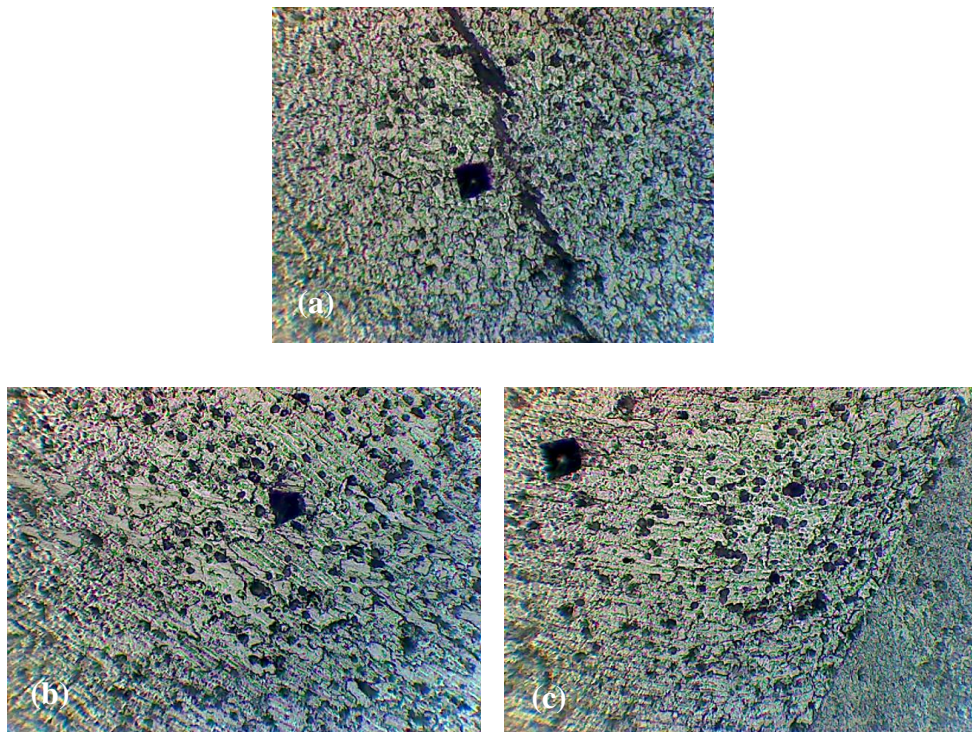


Figure (3.35) Grains at 710 rpm and 40 mm/min of FSW joints; (a) SZ (b) TMAZ (c) TMAZ/HAZ.

The effect of tool-pin height on the average grain diameter at locations in the depth direction of the nugget cross section ( $y=1.5, 2.5 \text{ mm}$ ) in the advancing side and retreating side are shown in detail in the Figure (3.36) given below. We can clearly observe the difference in the average grain size variation both in the AS and RS as well in the depth direction.

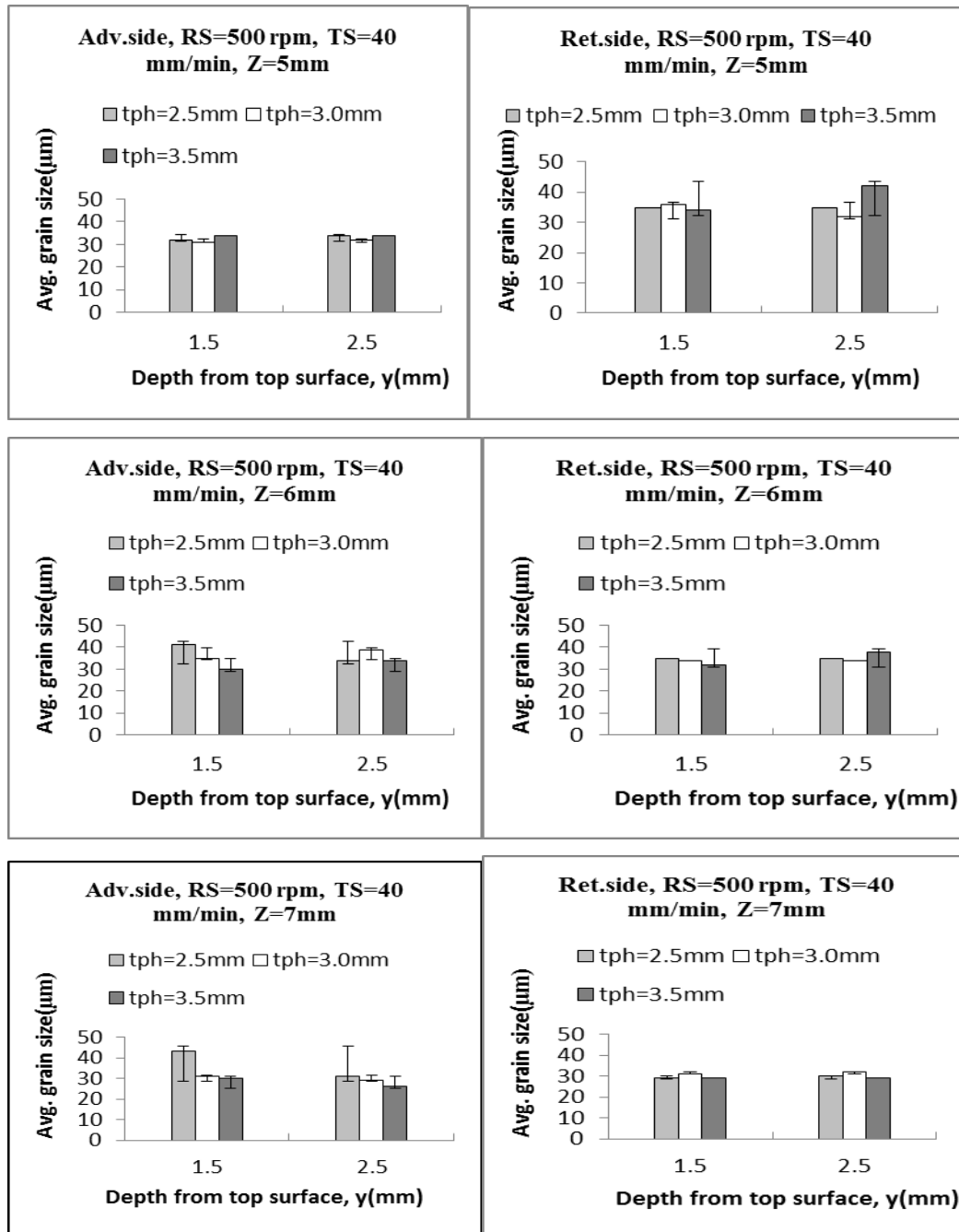


Figure (3.36) AGD at 500 rpm and 40 mm/min at  $z = 5, 6, 7 \text{ mm}$  on AS and RS.

Variations in grain sizes are caused by the peak temperatures and cooling rates. With high temperature and slow cooling rate, the re-crystallized grain growth increases. So, the increase

in RS and or decrease in TS results in a high peak temperature in weld nugget zone and further it increased the degree of deformation due to thermo-mechanical effects, which increases the grain size during FSW process. HAZ is a mechanically unaffected zone where heat diffusion is very high with no further increase in grain size. This implies that peak temperatures have a role in determining grain sizes in FSW joint. It is observed that the average grain diameter (AGD) reduced with increasing in TS, since the peak temperatures are lowered. As shown in Table (3.10) there is a slight increase in AGD with increase in RS from 355 rpm to 710 rpm which clearly explains the fact that RS has little effect on the grain size in the weld nugget zone (WNZ). There was also a tendency for the difference in the grain size from top and bottom surfaces of nugget cross section. The AGD decreased from top to bottom of the WNZ with increase in RS. But at 355 rpm and 710 rpm there is a slight variation of increase in AGD with increase in depth from top to bottom at high RS. Increase in TPH, drastically decreased the AGD. With the increase of TS, AGD first decreases and then increases.

Table (3.10) Average grain diameter ( $\mu\text{m}$ ) in FSW joints.

RS(rpm)	TPH=2.5 mm	TPH=3.0 mm	TPH=3.5 mm
Traverse Speed, TS=28 mm/min			
355	29	26	30
500	29	28	28
710	36	35	28
Traverse Speed, TS=40 mm/min			
355	30	24	26
500	33	31	28
710	30	30	30
Traverse Speed, TS=56 mm/min			
355	30	30	30
500	30	31	28
710	32	36	30

It can be observed from Figure (3.37) that the secondary particle density is low in SZ and TMAZ as compared to the HAZ and BM and is due to the increased diffusion at higher temperatures at a depth of  $y=2.5\text{ mm}$ . Also, the particle density increased with increasing TS values. Figure (3.38) shows the grain size distribution at same location in AS and RS but for

two different traverse speeds (40 and 56 *mm/min*). It can be observed that the grains are smaller in AS (average grain size is 24 and 26  $\mu\text{m}$ , respectively) than in RS (average grain size is 28 and 30  $\mu\text{m}$ , respectively) and is attributed to recrystallization phenomenon at these peak temperatures.

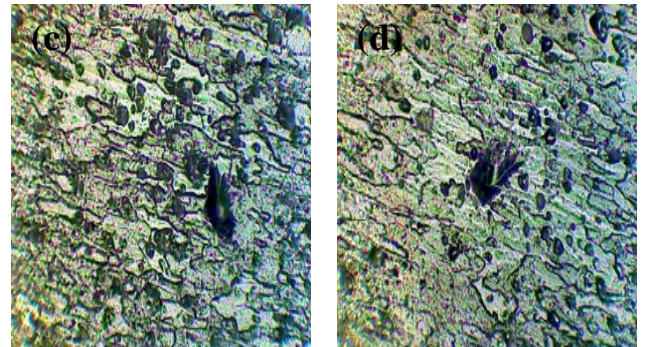
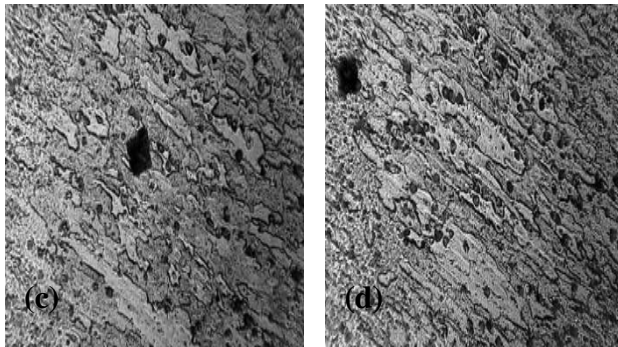
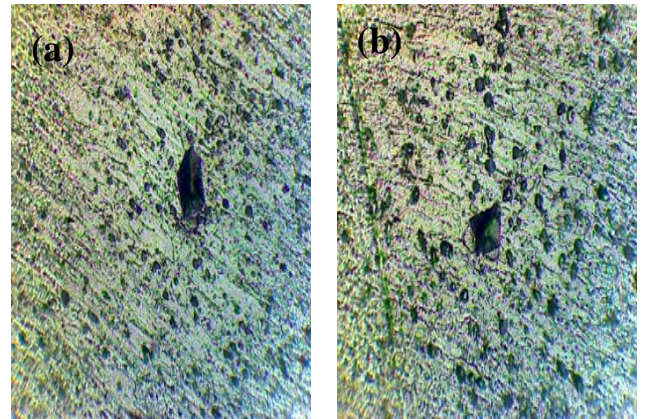
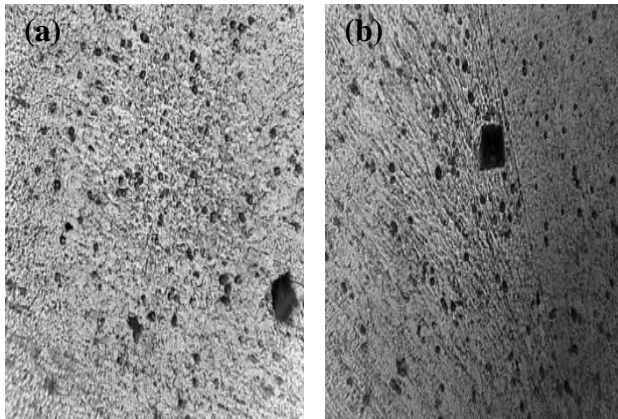


Figure (3.37) Grain size variation in different zones at TS = 56 *mm/min* and RS=355 rpm; (a) SZ (b) TMAZ (c) HAZ (d) BM.

Figure (3.38) Grain sizes at selected location ( $y=2.5\text{mm}$ ,  $z=5\text{mm}$ ) in AS and RS; (a, b) at TS=40 *mm/min*, (c, d) at TS 56 *mm/min*.

### 3.9.2 Hardness variations in FSW joint

The hardness at a given location depends on peak temperature as well the zone in which the point lies, i.e. whether mechanical effects are present or not. In general, heat input to the workpieces plays an important role on the final mechanical properties of the welded joints. In FSW process due to material flow more heat is diffused in advancing side than retreating side causing asymmetry in the nugget geometry. The increased heat flow with mechanical effects due to rotating tool-pin enhances the recrystallization phenomenon resulting in fine grains in the advancing side.

It can be found from Figure (3.39) that the hardness in advancing side is significantly higher than those values in the retreating side and is attributed to recrystallization phenomenon. Also, the hardness variation is more in retreating side than in advancing side.

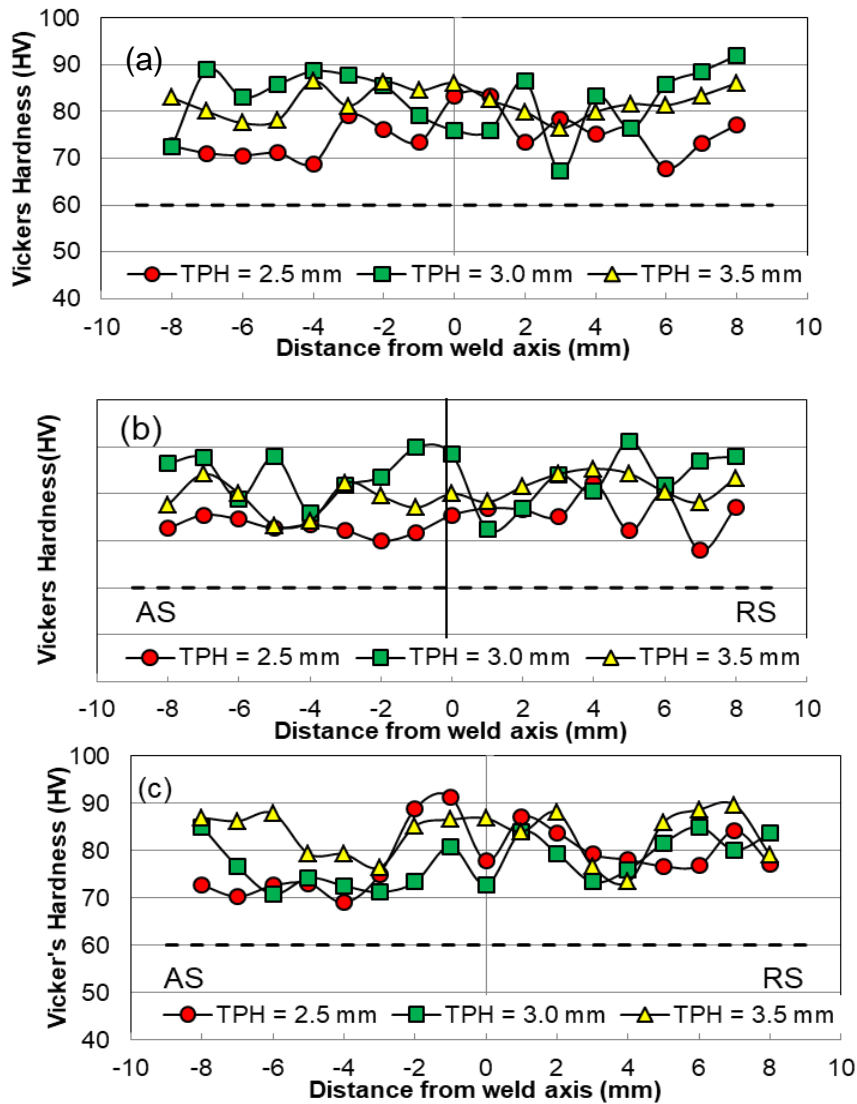


Figure (3.39) Hardness variation across nugget cross-section and at various depths from top surface; (a) 1 mm (b) 2 mm (c) 3 mm. Rotational speed, RS=355 rpm.

Further, it can be observed from Figure (3.39) that the hardness values on the retreating side are lower than the base material at 355 rpm and decreases further with increasing TS. Also, the mean hardness increased with RS and decreased with TS both on advancing and retreating sides, as observed by other researchers too. Figure (3.40) gives the summary of mean hardness values at different depths across the nugget cross-section for different RS and TS. It can be observed that the mean hardness values are higher at a rotational speed of 500 rpm as compared to 355 rpm and 710 rpm and at all traverse speeds. Moreover, at 500 rpm

the hardness variation across the nugget is less (std. dev.:  $\pm 5$ ) as compared to 355 rpm (std. dev.:  $\pm 10$ ) and 710 rpm (std. dev.:  $\pm 8$ ).

Table (3.11) Mean hardness at TS = 40 mm/min

Distance below top-surface (mm)	TPH=2.5 mm		TPH=3.0 mm		TPH=3.5 mm	
	Mean Hardness (HV)	Standard Deviation ( $\pm N$ )	Mean Hardness (HV)	Standard Deviation ( $\pm N$ )	Mean Hardness (HV)	Standard Deviation ( $\pm N$ )
Rotational speed, RS=500 rpm						
y=1.0	73.9	3.9	81.2	4.8	84.4	5.3
y=2.0	75.6	5.5	79.8	4.4	83.3	3.6
y=3.0	80.5	6.3	81.4	3.4	86.3	2.8

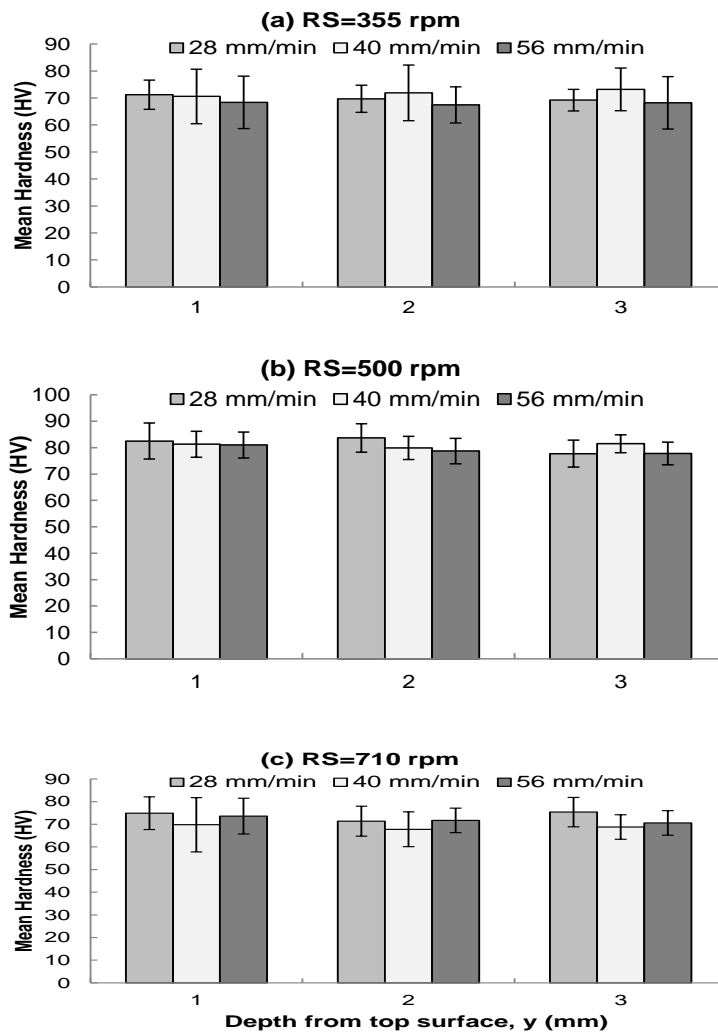


Figure (3.40) Mean hardness variation across nugget cross-section and at various depths from top surface.

Also, at same RS the variation in mean hardness with TS is very low. Therefore, it can be concluded that tool rotational speed significantly influences the mean hardness of FSW joints of AA5052-H32 as compared to the weld traverse speeds. It is clear from Table (3.11) the above said variation is true with respect to hardness at optimum traverse speed of 40 mm/min. We observed that mean hardness increased with increase in TPH across nugget cross-section and also at various depths from top surface.

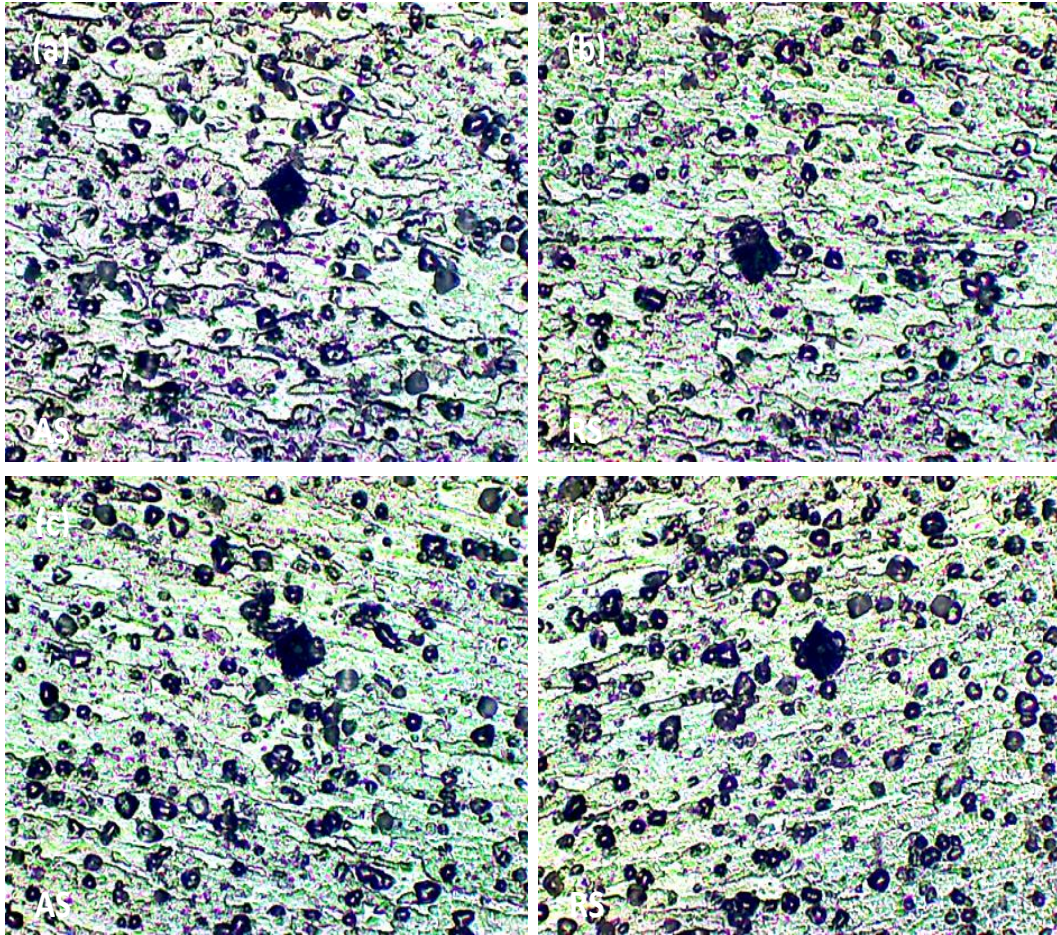


Figure (3.41) Grain sizes at selected location ( $y=3$  mm,  $z=6$  mm) in AS and RS; (a, b) at TS=28 mm/min, (c, d) at TS=56 mm/min.

In order to study the heat effects on hardness variation, indents were made at selected locations for which temperature profiles are measured. Figure (3.41) shows the grain size distribution around the indent at same location in AS and RS and at two different heat inputs. The increased grain sizes in AS results in decreased hardness as compared to that of RS and is clearly observed in Figure (3.40) at all rotational speeds.

### 3.10 Residual Stress Measurement Using XRD

Residual stress measurement and control are very important for the safety of structures of high-speed trains, and airplane wings, which is critical for the structure design. Residual stresses can be tensile or compressive depending up on the location and type of non-uniform volumetric change taking place. Differential heating or cooling in welding and heat treatment, or localized stresses like in contour rolling, machining and shot peening can result in residual stresses. We measured the Friction Stir Welded plates at ambient temperature to identify the tensile and compressive stresses at particular locations in the transverse and longitudinal directions which affect the mechanical properties of the joint at different process parameters

Table (3.12) Residual stresses on the top surface of the plate.

<b>RS=355 rpm; TS=28, 40, 56 mm/min;TPH=3 mm</b>			
<b>Dist (width), mm</b>	<b>S<sub>x</sub>=0 (transverse),28</b>	<b>S<sub>x</sub>=0, 40</b>	<b>S<sub>x</sub>=0 ,56</b>
1	-8.85E+01	-127.9	-6.16E+01
2	-8.83E+01	-96.2	-6.84E+01
3	-1.37E+02	-104.6	-1.14E+02
4	-1.00E+02	-172.6	-8.10E+01
5	-9.37E+01	-119.9	-1.23E+02
6	-1.03E+02	-199.1	-9.88E+01
7	-9.61E+01	-106.7	-1.18E+02
8	-1.12E+02	-19.6	-1.39E+02
9	-7.77E+01	-42.6	-1.24E+02
10	-7.43E+01	-152.8	-9.61E+01

From the Table (3.12) we obtained the residual stresses at different traverse speeds at constant tool rotational speed and tool-pin height in the transverse direction of the FSW joints. The graph results show that residual stresses varied with increase in TS and the stresses showed the trend of compressive and tensile state when moved away from the weld centerline, resembling the shape of 'W'. It is clearly visible from the Figure (3.42) the large variation of stress ( $\pm 25$  MPa) with increase in traverse speed and follow the wave form .



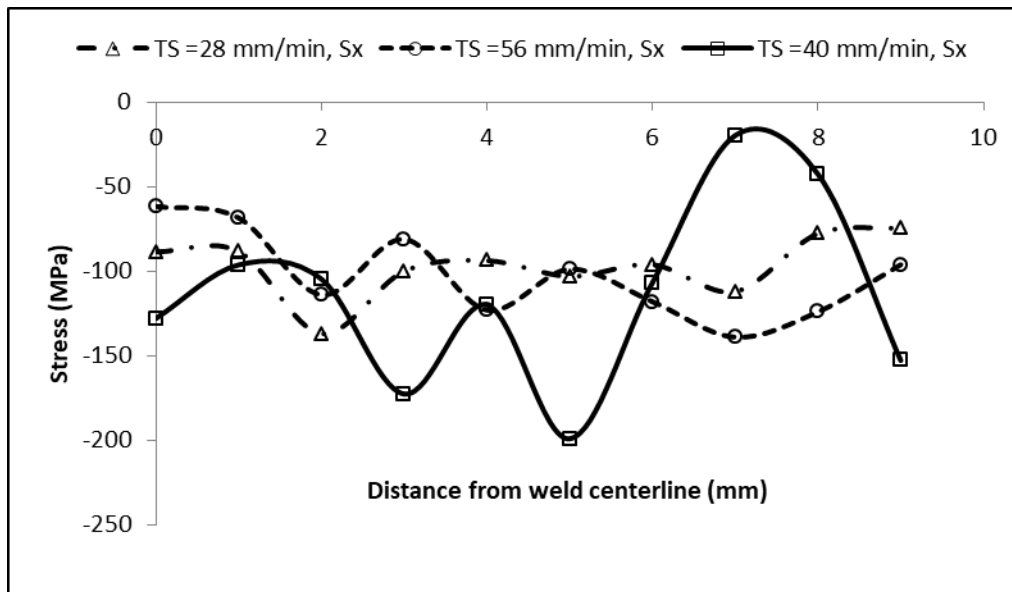


Figure (3.42) Residual stress on top surface of the plate at 355 rpm and TPH=3.0 mm.

### 3.11 Conclusions

The following are the brief conclusions drawn from the experiments.

- 1) The tensile strength of the FSW joint increased with increase in tool rotational speed (RS).
- 2) Tensile fracture mode of the FSW joints is clearly a quasi-cleavage type, including both dimples and facets.
- 3) The average peak temperature decreased with decrease in the RS, and also with increase in TS.
- 4) Mean hardness values are higher at a rotational speed of 500 rpm as compared to 355 rpm and 710 rpm and at all traverse speeds. The deviation of the hardness variation across the nugget is less at 500 rpm (std. dev.:  $\pm 5$ ) as compared to 355 rpm (std. dev.:  $\pm 10$ ) and 710 rpm (std. dev.:  $\pm 8$ ).
- 5) Mean hardness increased with increase in TPH across nugget cross-section and also at various depths from top surface.
- 6) The increased grain sizes in advancing side results in decreased hardness as compared to that of retreating side and is clearly observed at all rotational speeds.

## CHAPTER 4

### Optimization of FSW Process Parameters

#### 4.1 Introduction to Taguchi Method

The quality of welded joints by Friction Stir Welding (FSW) process has been evaluated by examining the ultimate tensile strength (UTS) as the characteristic feature of the joint efficiency. Besides the FSW process parameters (rotational speed- RS, traverse speed - TS and axial load - P), the tool-pin geometry (shape and size) significantly influences the net heat input to the joint and the resulting plasticized material flow around the rotating tool. This chapter discusses on the application of Taguchi method as a statistical technique for DOE and optimizes the FSW process parameters. The three parameters studied in this thesis are rotational speed (RS), traverse speed (TS) and tool-pin height (TPH).

The experiments are arranged using Taguchi's L27 orthogonal-array for three levels and three parameters. The signal-to-noise (S/N) ratio and the analysis of variance have been considered to study the influence of different parameters on the strength of FSW joints. The optimization results clearly indicated that RS is the most sensitive parameter affecting the FSW joint strength and hence the joint quality. The optimal values of parameters studied are such that the tensile strength of the joint is comparable to that of base metal (239 MPa). The effects of individual FSW process parameters on overall mechanical properties of aluminium-alloy (AA 5052-H32) plates are analyzed and discussed below in detail.

Researchers have put a lot of effort to understand the effect of FSW process parameters on material flow behavior, microstructure formation and mechanical properties of FSW joints (Sahu et al., 2015). Most of them followed the traditional experimental techniques, i.e. varying one parameter at a time while other parameters were constant; this conventional parametric design of experiment approach is time consuming. Taguchi's statistical design is a powerful tool to identify significant factor from many factors by conducting relatively less number of experiments.

Though research work applying Taguchi method on various processes has been reported in the literatures, it appears that the optimization of FSW process parameters of AA5052-H32 aluminium - alloy has not been reported yet. Considering the above facts, the

Taguchi method is adopted to analyze the effect of each processing parameters (RS, TS and TPH) for optimum tensile strength of FSW joints of AA5052-H32 aluminium alloy.

Advantages of Taguchi's optimization technique:

- Reduce cycle time of test phase and cost.
- Find maximum defects with minimal test cases.
- A method for quantitatively identifying the right inputs and parameter levels.

## 4.2 Taguchi's Method of Design of Experiments

Since the introduction of DOE by Fisher in the 1920's, Taguchi also started his research with DOE. This statistical technique had come a long way from a theoretical perspective, but nevertheless practical usage in industry was rare. To make the technique easy to apply, he standardized the application method. For laying out the experiments, he created a number of unique orthogonal arrays, each of which can be employed to a number of experimental situations. To analyze the results of the experiments, he introduced the signal-to-noise (S/N) ratio, for analyzing and predicting the optimal levels of the input parameters for optimize response. This new design was also able to include the influence of uncontrollable factors in the investigation, thereby making the design very robust. Taguchi proposed a mathematical formula, called the loss function for estimating the monetary loss caused by lack of quality. The loss function estimates loss even if parts are made within specification limits. That is, there is some loss associated with a population of parts no matter how well they are produced. As long as any parts differ from the target specifications, there is some loss. This loss function value is further converted into a signal-to-noise (S/N) ratio. Basically, the performance characteristic has the following three categories of the S/N ratios;

- The Lower-the-better
- The Larger-the-better
- The Nominal-the-better

### 4.2.1 The Smaller-the-Better (STB)

This category of S/N ratio is selected when the performance characteristic like "defects ", etc. is required for which the ideal desired value is zero. The generic formula for calculating the S/N ratio is as follows;

$$\frac{S}{N} = -10 \log_{10} [ \text{mean of sum of squares of measured data} ] \quad (4.1)$$

#### 4.2.2 The Larger-the-Better (LTB)

This case is opposite to the smaller the best case and it is obtained by taking the reciprocals of measured data. The general formula for calculating the larger the better S/N ratio is as follows;

$$\frac{S}{N} = -10 \log_{10} \left[ \text{mean of sum of squares of reciprocal of measured data} \right] \quad (4.2)$$

#### 4.2.3 The Nominal-the-Better (NTB)

This case arises when a specified value is most desired, meaning that neither a smaller nor a larger value is desirable. The general formula for calculating the nominal the better S/N ratio is as follows;

$$\frac{S}{N} = 10 \log_{10} [\text{square of mean / variance}] \quad (4.3)$$

The effect of each variable on the output, and the signal-to-noise ratio, need to be calculated for each experiment conducted.  $y_i$  is the mean value and  $s_i$  is the variance.  $y_i$  is the value of the performance characteristic for a given experiment. The S/N ratios for each level of process are calculated depending upon the S/N analysis results. Not taking account of the class of quality characteristic of interest, a larger S/N ratio of the parameters is selected for better quality characteristic of interest. Therefore, the best level of the product or process factors is the level which has the highest S/N ratio. Moreover, another statistical technique called, analysis of variance (ANOVA) is employed to observe the percentage effect of selected parameters on the output response. The ANOVA analysis also separates the selected parameters into statistically significant and insignificant parameters.

Finally, with the ANOVA and S/N ratio analyses, the best combination of the level of the selected parameters of the product or process can be forecasted. Also, a confirmation test based on the best predicted combination of parameters levels is carried out to estimate the error between the actual and the predicted value of output response. The goal of this research was to investigate the process parameters to produce optimum values in the FSW joints.

Larger response value represents better or improved UTS, so the S/N ratio category larger the better is selected for this study.

Taguchi method is therefore a test based procedure that employs the following steps to recognize the design factors that minimize or maximize the desired quality characteristic (e.g., productivity or surface roughness, etc).

- Identify the objective function to be optimized.
- Identify the controllable and uncontrollable (noise), if any, factors and their levels or ranges.
- Choosing the orthogonal array matrix suitable to the number of factors and their levels taken for design of experiment.
- Carry out the experimentation for collection of data.
- Analyze the experimental data collected for determining the optimum levels of controllable and uncontrollable factors.
- Conduct the experimentation with predicted optimal level of factors for verification.

Taking into account multiple parameters simultaneously, the Taguchi parameter method utilizes orthogonal array for experimental run combinations to reduce the product or process development cycle that consequently minimizes the cost and time. Taguchi method is applied in conventional manufacturing techniques, such as, welding, drilling, turning and milling to find the best possible combination of parameters for improved performance. In this process researcher's like Saurabh Kumar Gupta et al., (2013) identified the joining of 6061-T4 Al alloy plates using friction stir welding (FSW) process and optimized process parameters using Taguchi method. The rotational speed, welding speed and axial force were the process parameters considered. The optimum process parameters were determined with reference to tensile strength of the joint. The results indicated that the rotational speed is the highest significant parameter in deciding the tensile strength of the joint. Also, the optimal values of process parameters are to get a maximum tensile strength of friction stir welded AA 6061 is 162 MPa. The contribution of RS is 67 % of the overall response, welding speed and axial force contribute 28% and 1.4 % respectively of the overall response.

The effects of threaded tool geometries on AA7039 FSW welds are discussed by Venkateswarlu et al., (2013). The effects of tool shoulder concavity levels are also investigated. Tool-pin diameter was found to have maximum influence among the control

factors that determine tensile strength of the weld. The 19 mm shoulder diameter was found to be more suitable for obtaining adequate tensile strength and percentage elongation. The influence of tool RS and TPH on defect formation in AA2014-T6 weld was observed by Madhusudhan et al., (2011). Two different types of pin profiles- threaded and thread less have been used during FSW. Micro-structural characterizations of weldments produced with process parameters have been discussed. The authors mentioned that there is hardly any systematic study which directly compares effect of tool-pin profile on mechanical properties of 2014-T6 Al alloy welds using Taguchi DOE technique.

Researchers have not used Taguchi method to discuss the effect of TPH on defect formation in the AA5052-H32 welds, and hence that is one of the objectives in the present research.

### **4.3 Design of Experiments**

The most important difference between a classical experimental design and a Taguchi method-based robust design technique is that the former tends to focus solely on the mean of the quality characteristic, while the later considers the minimization of the variance of the characteristic of interest. Although the Taguchi method has drawn much criticism due to several major limitations, it has been able to solve single response problems effectively.

#### **4.3.1 Taguchi method for FSW Process**

It has been clearly shown in the literature [Madhavi et al., (2014); Palanivel et al., (2011); Pawar et al., (2013); Rajakumar et al., (2012)] that FSW process parameters such as tool geometry, rotational speed, welding speed and axial force significantly influence the process and play a major role in deciding the quality of the weld.

The list of FSW process and tool-pin geometry parameters given below are used in the optimization technique by researchers.

1. Rotational speed of the tool (*rpm*)
2. Welding speed (*mm/min*)
3. Axial force
4. Tool geometry
  - (a) Tool-Pin length (*mm*);(b) Tool-pin shape (c) Tool shoulder diameter

In the present work, experimental work has been designed in a sequence of steps to assure that data is obtained in a way that its analysis will lead immediately to valid statistical interpretations. Taguchi techniques use standard Orthogonal Arrays (OA) for forming a matrix of experiments. Using an OA to design the experiment helps to study the influence of multiple factors on the average of quality and the variations in a fast and economic way. OA's allow identifying few important main effects from the many less important ones. Also, it allows us to estimate interaction effects if any and determine their significance.

In the present investigation three operating parameters, each at three levels, are selected to evaluate tensile strength effects on the FSW joints. The factors to be studied are mentioned in Table (4.1). Based on Taguchi method, the L27-OA was constructed. The reason for using L27-OA is to evaluate the significance of interaction terms. Interaction means the influence of an operating variable on the effect of other operating variable.

When the rotational speed is lower than 355 *rpm*, low frictional heat is generated which results in poor plastic flow of the material, and defects like pinhole or tunnel are formed in the weld zone. Rotational speed higher than 710 *rpm* causes excessive release of stirred material to the upper surface, which leaves voids in the weld zone and we observe a poor surface quality, as shown in Figure (4.1).

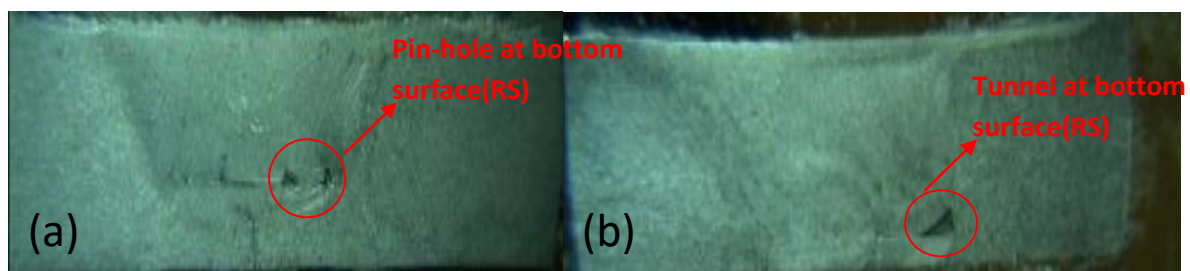


Figure (4.1) Defects in FSW joints at (a) RS =355 rpm (b) RS=710 rpm at TS =28 mm/min and TPH =2.5 mm.

According to the L27 orthogonal array, three experiments in each set of process parameters have been performed on AA5052-H32 aluminium plates. The three factors used in this experiment are the tool rotational speed, traverse speed and tool-pin height. The factors and the levels of the process parameters are presented in Table (4.1) and these parameters are taken based on the trials to weld the FSW of Al-alloy plates. The experiment's notation is also included in the L27 orthogonal array which results in an additional column, in order to represent the parameters, as presented in Table (4.2).

Table (4.1) Process parameters with their range and three levels.

Level	Rotational speed(A), <i>rpm</i>	Traverse speed(B), <i>mm/min</i>	Tool-pin height(C), <i>mm</i>
Range	355-710	28-56	2.5-3.5
Level 1	355	28	2.5
Level 2	500	40	3.0
Level 3	710	56	3.5

The FSW butt joint weld being performed on Al-alloy needs careful experimentation, and hence the tool is plunged slowly into the work piece, till the tool shoulder comes in contact with the surface of the work piece. When the tool is inserted, the stirring action starts to occur, and only the pin penetrates deep into the work piece while the tool shoulder touches the top surface. Frictional heat occurs along with the stirring action. Twenty seconds dwell time is given before the start of each welding, and then the automatic feed is given. With reference to the ASTM- E8 standard, the tensile specimens are prepared.

The tensile tests for 27 specimens are conducted and they yielded a variety of results. The tensile failure has occurred in between the regions of HAZ and TMAZ. FSW joints of Al-alloy have been welded, and the average tensile strength of the three tensile specimens from the same sample was obtained. It reveals that the FSW parameters do not lead to a significant variation, tunnel and crack like defect at the weld zone are observed; when the tool-pin height is higher than 3.0 *mm*, large mass of flash and excessive thinning are observed due to higher heat input.

Hence, the range of process parameters such as tool rotational speed is selected as 355-710 *rpm*, the traverse speed is selected as 28-56 *mm/min* and tool-pin height is selected as 2.5-3.5 *mm*. Based on the number of factors and levels a suitable Taguchi orthogonal array (L27) for the experiment is selected by using MINITAB 17 statistical software as shown in Table (4.2).



Table (4.2) Experimental layout –L27 orthogonal array.

S No	Rotational Speed (A)	Traverse Speed (B)	Tool-pin height(C)
1	355	28	2.5
2	355	28	3
3	355	28	3.5
4	355	40	2.5
5	355	40	3
6	355	40	3.5
7	355	56	2.5
8	355	56	3
9	355	56	3.5
10	500	28	2.5
11	500	28	3
12	500	28	3.5
13	500	40	2.5
14	500	40	3
15	500	40	3.5
16	500	56	2.5
17	500	56	3
18	500	56	3.5
19	710	28	2.5
20	710	28	3
21	710	28	3.5
22	710	40	2.5
23	710	40	3
24	710	40	3.5
25	710	56	2.5
26	710	56	3
27	710	56	3.5

### 4.3.2 Selection of Orthogonal Array (OA)

Before the selection of particular OA following points must be considered.

- The number of factors and interactions of interest
- The number of levels and interactions of interest

As three levels and three factors are taken into consideration, L9 will not allow the consideration of interactions. L27 OA is considered to identify the effect of process parameters on the tensile strength and of the FSW joints as shown in Table (4.3).

Table (4.3) Process Parameters –L27 orthogonal array

S.No	RS(rpm)	TS(mm/min)	TPH(mm)	UTS(MPa)	Temperature( <sup>0</sup> C)	Hardness(HV)
1	355	28	2.5	199	302	60
2	355	28	3	229	312	55
3	355	28	3.5	232	320	59
4	355	40	2.5	178	300	59
5	355	40	3	205	310	57
6	355	40	3.5	209	315	59
7	355	56	2.5	184	297	58
8	355	56	3	211	319	54
9	355	56	3.5	225	313	58
10	500	28	2.5	176	332	62
11	500	28	3	208	343	58
12	500	28	3.5	203	352	60
13	500	40	2.5	177	329	60
14	500	40	3	216	340	58
15	500	40	3.5	187	345	59
16	500	56	2.5	169	326	60
17	500	56	3	186	348	56
18	500	56	3.5	200	342	59
19	710	28	2.5	162	366	72
20	710	28	3	205	378	60
21	710	28	3.5	161	387	69
22	710	40	2.5	165	362	62
23	710	40	3	201	372	58
24	710	40	3.5	172	378	63
25	710	56	2.5	163	357	65
26	710	56	3	194	380	57
27	710	56	3.5	184	372	71

The maximum tensile strength, temperature and hardness developed in each set of combinations is noted and tabulated in Table (4.3). For each experiment in the orthogonal array, signal to noise (S/N) ratio is calculated. The quality response is mainly divided in to three main types; the larger-the better (LTB), the smaller-the better (STB) and the nominal-the best (NTB). The respective output values in Table (4.3) represent the ultimate tensile strength which determines the strength of the FSW joints.

## 4.4 Results and Discussion

### 4.4.1 Analysis of data

In the present work, second order interaction terms viz., (RS\*TS), (TS\*TPH), (RS\*TPH) and the third order viz., (RS\*TS\*TPH) where [RS = rotational speed, TS = traverse speed, TPH = tool-pin height] are considered. The experiments were carried out according to the L27-OA. The tensile strength is considered as the response in the Taguchi array. Response Table for Signal to Noise Ratios and means is shown in Table (4.4) for the response factor UTS. The mean ratio is calculated based on LTB criterion and the S/N ratio is calculated based on STB criterion. After conducting the experiment, the results were converted into S/N ratio values. The final L27-OA displaying response values and their corresponding S/N ratio values for UTS are shown in Table (4.4).

Table (4.4) Response table for Means and S/N ratio - UTS

Level	Means			S/N Ratio		
	A(RS)	B(TS)	C(TPH)	A(RS)	B(TS)	C(TPH)
L1	222.9	210.8	194.6	46.93	46.42	45.76
L2	201.9	198.1	199.7	46.08	45.92	45.99
L3	188.7	204.6	219.2	45.50	46.18	46.76
Delta	34.2	12.7	24.7	1.42	0.51	1.00
Rank	1	3	2	1	3	2

Response Table for Signal to Noise Ratios and means is shown in Table (4.5) for the response factor temperature and it is the same rank as obtained for UTS and shows that RS is the most sensitive process parameter during the FSW process for the response factor temperature .From the Tables (4.5) and (4.6) we can conclude that as the response factor is different, the ranks are not changing for the process parameters but levels are different for S/N ratio which is explained above .

Table (4.5) Response table for Means and S/N ratio - Temperature

Level	Means			S/N Ratio		
	A(RS)	B(TS)	C(TPH)	A(RS)	B(TS)	C(TPH)
L1	344.4	382.2	367.1	50.74	51.62	51.27
L2	378.1	377.0	383.5	51.55	51.50	51.65
L3	414.2	377.5	386.1	52.34	51.51	51.71
Delta	69.7	5.2	19.0	1.60	0.12	0.44
Rank	1	3	2	1	3	2

Response Table for Signal to Noise Ratios and means is shown in Table (4.6) for the response factor hardness and is similar to the ranks obtained for UTS and temperature. This shows that RS is the most sensitive parameter as well TPH for the response factor hardness.

Table (4.6) Response table for Means and S/N ratio -Hardness

Level	Means			S/N Ratio		
	A(RS)	B(TS)	C(TPH)	A(RS)	B(TS)	C(TPH)
L1	64.67	69.00	69.22	36.21	36.75	36.79
L2	66.11	66.44	64.00	36.40	36.45	36.12
L3	70.67	66.00	68.22	36.96	36.38	36.67
Delta	6.00	3.00	5.22	0.75	0.37	0.67
Rank	1	3	2	1	3	2

#### 4.4.2 Signal to Noise Ratio

The signal to noise S/N ratio is calculated based on the quality of characteristics intended. The objective function described in this investigation is maximization of the tensile strength, so the performance characteristic, larger the better S/N ratio is calculated. The formula for S/N ratio is given below.

$$S/N = -10 * \log(\Sigma(1/Y^2)/n) \quad (4.4)$$

where, n is number of experiments and y is observed response value.

In this study, the tensile strength value and its effects on the FSW joints are analyzed to study the effects of the FSW process parameters. The experimental results are then transformed into means and signal-to-noise (S/N) ratio. In this work, 27 means and 27 S/N ratios are calculated and the estimated tensile strength, means and signal-to-noise (S/N) ratio are given in Table (4.7) It is clear that a larger S/N ratio corresponds to better quality characteristics. Therefore, the optimal level of process parameter is the level of highest S/N ratio. The average mean and SN ratio values of all levels are calculated and listed in tables (4.4),(4.5) and (4.6)

Based on both mean and S/N ratio, it is clear that the maximum tensile strength occurs when rotational speed, welding speed and tool-pin height are at different levels for tensile strength, temperature and hardness. For S/N ratio, the larger the better criteria is selected as it is suitable for improving the mechanical behavior of AA5052-H32 plates and it is taken for obtaining optimal welding performance in the FSW joint. From the initial trial experiments, the results obtained from the macrographs and tensile tests, the optimum process parameters identified are at rotational speed of 500 *rpm*, traverse speed of 40 *mm/min* and tool-pin height of 3.0 *mm*. We found few defective and defect free samples as compared with the combination of other process parameters.

Table (4.7) Response table for S/N ratio – UTS, TEMP,HV

S No	Rotational Speed (A)	Traverse Speed (B)	Tool-pin height (c)	SNRA1 (UTS)	SNRA1 (TEMP)	SNRA1 (HV)
1	355	28	2.5	46.92706	50.52679	36.5215
2	355	28	3	47.19671	50.80659	35.84783
3	355	28	3.5	48.23239	51.029	36.39088
4	355	40	2.5	45.9333	50.44888	36.39088
5	355	40	3	46.10703	50.75638	36.1236
6	355	40	3.5	47.34712	50.88136	36.39088
7	355	56	2.5	46.1926	50.37028	36.25827
8	355	56	3	46.44439	51.00457	35.7066
9	355	56	3.5	47.9588	50.83158	36.25827
10	500	28	2.5	45.84512	51.35464	36.77698
11	500	28	3	46.14992	51.63444	36.25827
12	500	28	3.5	47.08217	51.85685	36.5215
13	500	40	2.5	45.88932	51.2625	36.5215
14	500	40	3	45.29636	51.56361	36.25827
15	500	40	3.5	46.36127	51.68662	36.39088
16	500	56	2.5	45.48316	51.20052	36.5215
17	500	56	3	45.66602	51.76543	35.98681
18	500	56	3.5	46.9661	51.6185	36.39088
19	710	28	2.5	45.10545	52.19616	38.1697
20	710	28	3	46.1926	52.46705	36.5215
21	710	28	3.5	45.05706	52.67543	37.72981
22	710	40	2.5	45.29636	52.09748	36.77698
23	710	40	3	45.34343	52.33371	36.25827
24	710	40	3.5	45.66602	52.47532	36.90196
25	710	56	2.5	45.20143	51.97581	37.14665
26	710	56	3	45.48316	52.51859	36.1236
27	710	56	3.5	46.1926	52.33161	37.02517

### 4.4.3 Main Effect Plot

Main effects plot for the main effect terms viz. factors RS, TS and TPH are shown in Figure (4.2). From the main effect plots, it has been observed that tensile strength increases with increase in RS from 355 rpm to 710 rpm. From Fig (4.2) it is observed that tensile strength is highest at level 1 of rotational speed(A1) , level 1 of traverse speed(B1) and level 3 of tool-pin height(C3) and shows that increase in tool-pin height increases the tensile strength.

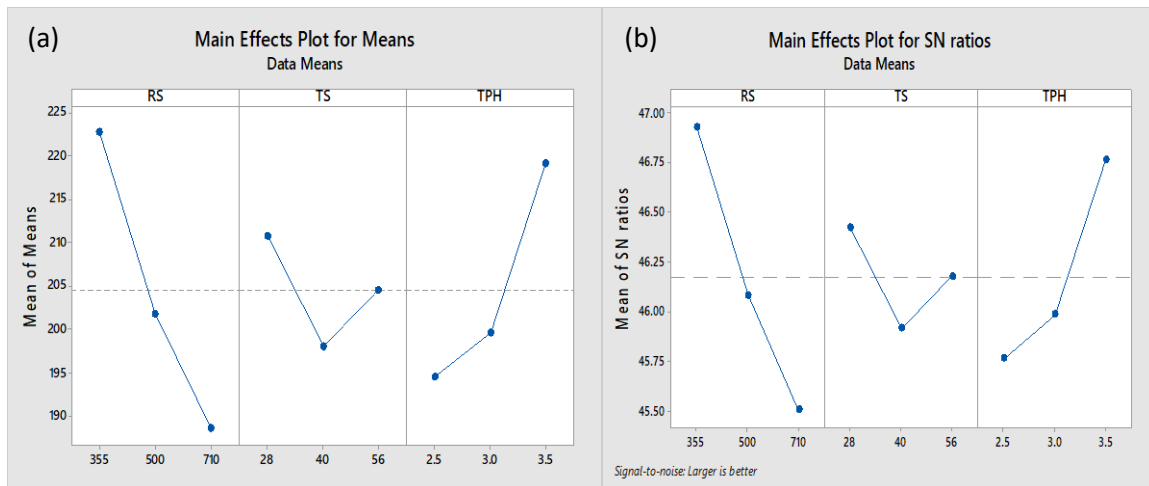


Figure (4.2) Main effects plot for (a)Means and(b) S/N ratio on UTS.

Main effects plot for the response factor temperature for the means and SN ratio are shown in Figure (4.3 a) and (4.3b). Here we clearly observe the difference in the levels of the process parameters influence on the temperature during FSW process. It is identified that the levels are different in means as per the criteria of STB as A1B2C1 and for S/N ratio(LTB) it is A3B1C3. It shows that as RS increases the temperature increases .

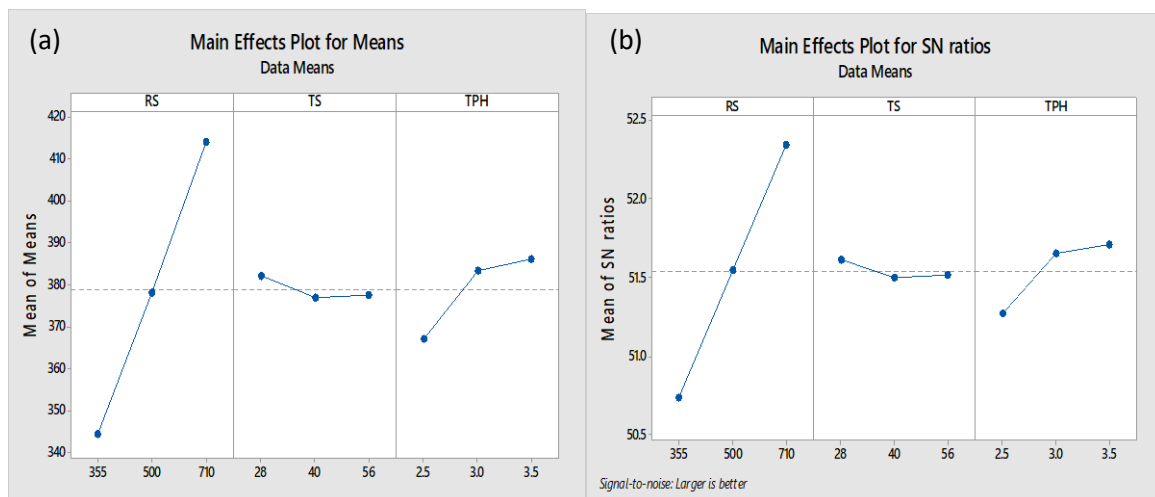


Figure (4.3) Main effects plot for (a)Means and (b)S/N ratio on Temperature.

Similarly for the response factor hardness the variation the main effects plot are shown in Fig (4.4). The levels are varied with respect to the process parameter influence on the hardness.

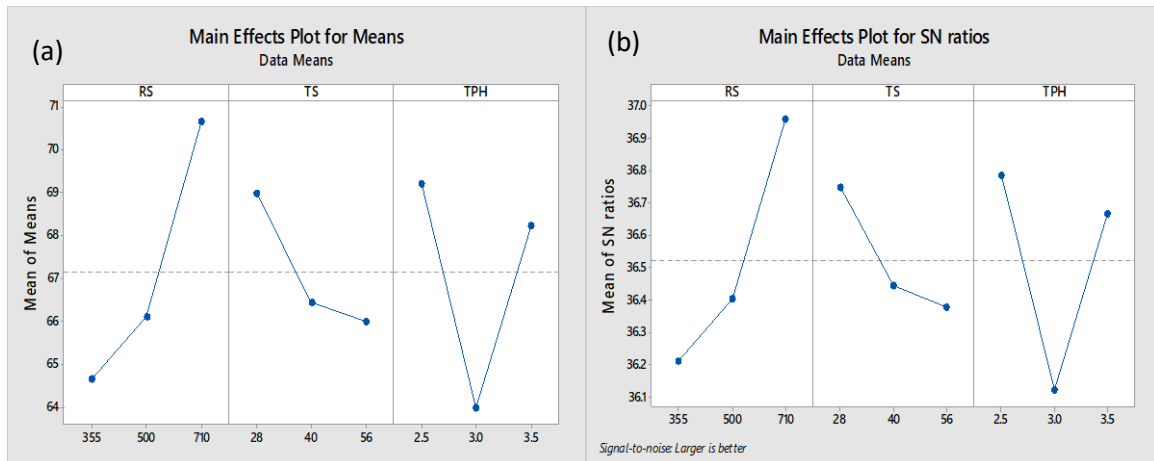


Figure (4.4) Main effects plots for and(a) means, (b) S/N ratio for hardness.

#### 4.4.4 Interaction Plot

Whether interactions between factors exist or not can be shown by plotting a matrix of interaction plot. Parallel lines in an interaction plot indicate no interaction. However, the interaction plot doesn't tell if the interaction is statistically significant. Interaction plots are most often used to visualize interactions during DOE. Matrix of interaction plot for UTS is shown in Figure (4.5). It can be seen visually that there are non-parallel lines between RS and TS. Also, TPH does not show any significant interaction (parallel lines) for UTS.

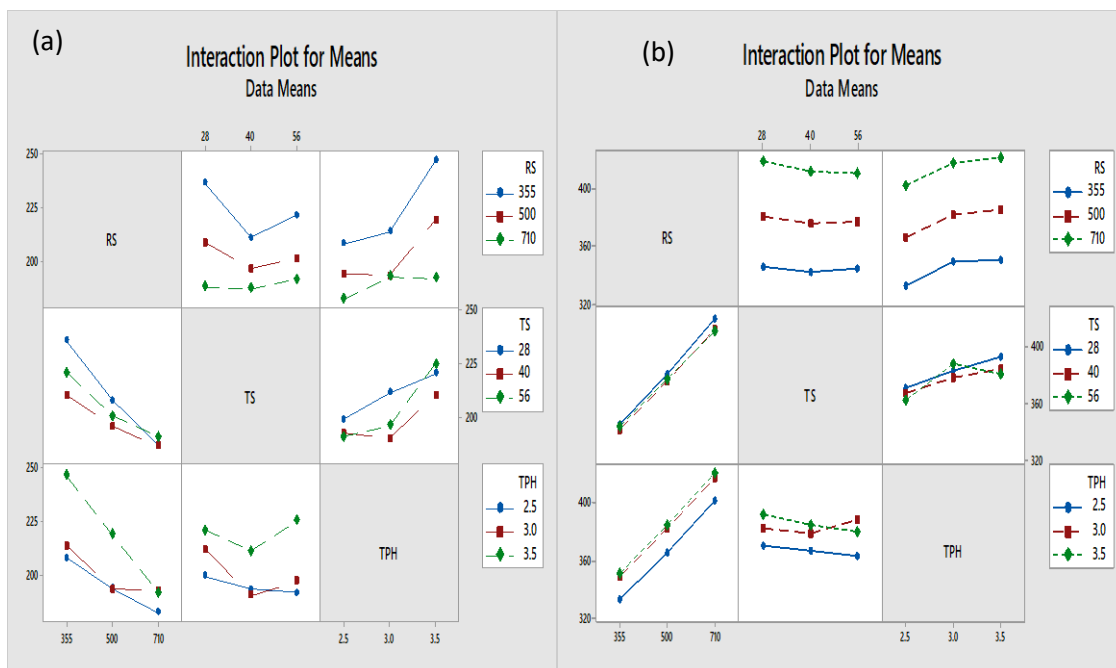


Figure (4.5) Interaction plot for means(a) UTS, (b) Temperature.



#### 4.4.5 Result Evaluation

The two different methodologies in carrying out the complete OA analysis are (i) common approach is to analyze the average result of repetitive runs, or (ii) a single run, through ANOVA analysis. Since in the present work there is only one replication, further analysis of OA is done through ANOVA. Once the data for a designed experiment has been collected, the sample information is used to make inferences about the population means associated with the various treatments. The method used to compare the treatment means is known as analysis of variance, or ANOVA.

An ANOVA Table breaks down the effect of each factor and the experimental error. In addition, it will also break down all of the possible interactions of the factors. In the present work ANOVA Table for UTS has been shown in Table (4.6) using MINITAB 17 software. In this process, it is seen that the significant factors are RS (A), TPH (B), interaction between RS and TPH (RS\*TPH) and TS (C).

The mean and (S/N) ratio are the two effects which influence the response of the factors. The influencing level of each selected welding parameter can be identified. The tensile strength of the FSW weld is taken as the output characteristic. The response table for the S/N ratio shows that the tool rotational speed ranks first in the contribution of good joint strength, while tool-pin height and traverse speed take the second and third ranks. The same trend has been observed in the response table of the mean. The tensile strength is estimated to be the maximum at 355 *rpm*, rotational speed, 3.5 *mm* tool-pin height and 56 *mm/min* traverse speed; which is optimal from the plots obtained.

The main aim of the analysis is to estimate the percentage of the individual contribution of the welding parameter on the tensile strength of the weld, and also to give accurately the combination of the process parameters. Individual optimal values for the process parameters and their specified performance characteristics can be obtained. The relative importance of the welding parameters is presented in Table (4.6). The analysis of variance for tensile result shows that the tool rotational speed (RS) is the most influential parameter with a percentage of 47%, followed by the tool-pin height (TPH) of 27% and traverse speed (TS) of 6%. The optimum parameters obtained can be due to the two following possibilities; either the combination of the process parameters as prescribed may be present in the experimental combination, or may not be present in the combination.

The purpose of ANOVA is to find out the significant process parameters which affect the tensile strength of FSW joints. The ANOVA results for both mean and S/N ratio is calculated and given in Table (4.8) and (4.9) respectively. The F-test is being carried out to study the significances of process parameters. The high F value shows that the factor is highly significant in affecting the process response. In this study, results of ANOVA show that the rotational speed is a significant factor and plays an important role in affecting the tensile strength of FSW joints.

Table (4.8) ANOVA for Tensile Strength (Means).

Source	DF	Adj SS	Adj MS	F-Value	P-Value
RS	2	5361.0	2680.48	77.55	0.000
TS	2	722.1	361.04	10.45	0.006
TPH	2	3051.0	1525.48	44.13	0.000
RS*TS	4	503.7	125.93	3.64	0.057
RS*TPH	4	1132.1	283.04	8.19	0.006
TS*TPH	4	466.4	116.59	3.37	0.067
Error	8	276.5	34.56	-	-
Total	26	11512.7	-	-	-

Interaction (RS\*TS\*TPH) had small variance. The final ANOVA Table for percentage contribution (exact value in percent) of each of the significant factors in affecting the response value, which is calculated on the basis of ANOVA Table, is shown in Table (4.8). The significant main effect terms and interaction terms in the ANOVA Table (4.9) are computed using the F-ratio as a test statistic. Tensile strength prediction and optimization can eliminate the need for performing experiments on the basis of the conventional trial and error method which is time consuming. The present study is aimed at to identify the most significant parameter and percentage contribution of each parameter on tensile strength of friction stir welded aluminium joints by conducting minimum number of experiments using Taguchi orthogonal array.

Table (4.9) ANOVA for S/N Ratio of UTS.

Source	DF	Adj SS	Adj MS	F-Value	P-Value
Regression	10	8232.6	823.216	12.05	0.000
RS	1	0.0	0.004	0.00	0.994
TS	1	75.71	75.713	1.11	0.308
TPH	1	54.04	54.040	0.79	0.387
RS*RS	1	236.98	236.985	3.47	0.081
TS*TS	1	482.72	482.716	7.07	0.017
TPH*TPH	1	253.50	253.500	3.71	0.072
RS*TS	1	6.34	6.343	0.09	0.765
RS*TPH	1	106.49	106.494	1.56	0.230
TS*TPH	1	1.87	1.867	0.03	0.871
RS*TS*TPH	1	19.13	19.132	0.28	0.604
Error	16	1093.16	68.323	-	-
Total	26	9325.32	-	-	-

Based on the highest values of the S/N ratio and mean levels (Tables 4.8 and 4.9) for the significant factors A, B and C, the overall optimum conditions thus obtained are A1, B3 and C2. Similar results were obtained by few researchers who studied on different process parameters using Taguchi analysis. But no one has worked on TPH as one of the process parameters along with RS and TS. When an experiment is conducted and the optimum treatment condition within the experiment is determined, one of two possibilities exists:

- 1) The prescribed combination of factor levels is identical to one of those in the experiment;
- 2) The prescribed combination of factor levels is not included in the experiment.

It must be noted that the above combination of factor levels A1, B3, C2 are among the combinations tested for the experiment. This is expected because of the multifactor nature of the experimental design employed from possible combinations. Based on the experiments, the optimum level setting is A2B2C2. The additive model to evaluate the predicted tensile strength is taken from the literature (Kadian *et al.*, 2014). Similarly we observed the factor levels for temperature and hardness as A3B1C3 and A3B1C1 which is clearly shown in above figures.

#### 4.4.6 Mathematical modeling

A general regression for the complete model was performed using MINITAB 17 software. Regression in MINITAB 17 uses the ordinary least squares method which derives the equation by minimizing the sum of the squared residuals. In the present study, there are three operational factors each at three levels. The number of terms in the model depends on the degree of freedom of the main effect terms and the corresponding interactions.

A simpler reduced model of lower order which provides sufficient information for the prediction of  $y$  was found using the F-test statistic. (W. Mendenhall et al., 1989). If  $F > F_{\alpha}$ ,  $\alpha=0.05$ , then the reduced model does not provide sufficient information and is rejected. A t-test of individual parameters in the regression model was further performed. The t value for each parameter is enlisted in the MINITAB 17 software program as shown in Table (4.10).

Table (4.10) Estimated Model Coefficients for Means(UTS)

Term	Coef	SE Coef	T-Value	P-Value	VIF
Constant	424	207	2.05	0.058	
RS	0.003	0.326	0.01	0.994	889.79
TS	-4.32	4.10	-1.05	0.308	875.57
TPH	-86.6	97.4	-0.89	0.387	625.20
RS*RS	0.000208	0.000111	1.86	0.081	121.53
TS*TS	0.0469	0.0176	2.66	0.017	116.85
TPH*TPH	26.0	13.5	1.93	0.072	433.00
RS*TS	-0.00215	0.00706	-0.30	0.765	1473.98
RS*TPH	-0.125	0.100	-1.25	0.230	948.47
TS*TPH	-0.21	1.26	-0.17	0.871	939.10
RS*TS*TPH	0.00123	0.00233	0.53	0.604	1640.37

The level of confidence is 95 % i.e. p- value should be less than 0.05. If p-value is less than 0.05 it shows doubt on null hypothesis, which says all sample means equal and effect of that factor on the result is statistically significant (W. Mendenhall et al., 1989). The final prediction equation obtained from MINITAB 17 software for the UTS is given below

Regression Equation:

$$UTS = 424 + 0.003 RS - 4.32 TS - 86.6 TPH + 0.000208 RS*RS + 0.0469 TS*TS + 26 TPH*TPH - 0.00215 RS*TS - 0.125 RS*TPH - 0.21 TS*TPH + 0.00123 RS*TS*$$

The coefficients of model for means are shown in Table (4.11).

Table (4.11) Coefficients of model for means

	S	R-sq	R-sq(adj)	R-sq(pred)
UTS	5.87918	97.60%	92.19%	72.64%
TEMPERATURE	4.16662	98.86%	98.14%	95.91%
HARDNESS	1.14665	97.78%	92.78%	74.69%

R-sq = 97.60 % indicate that the model is able to predict the response with high accuracy. R-sq(adj) is a modified R-sq that has been adjusted for the number of terms in the model. If unnecessary terms are included in the model, R-sq can be artificially high, but adjusted R-sq(adj) = 92.19%.) may get smaller. The standard deviation of errors in the modeling, S = 5.87918. This indicates that the model can explain the variation in UTS which makes an adequate representation of the process. The same process is repeated for identifying the regression coefficients for temperature and hardness.

$$\text{TEMP} = -32 + 0.341 \text{ RS} - 1.50 \text{ TS} + 178.4 \text{ TPH} - 0.000170 \text{ RS}*\text{RS} + 0.01651 \text{ TS}*\text{TS} - 27.38 \text{ TPH}*\text{TPH} + 0.00072 \text{ RS}*\text{TS} + 0.0207 \text{ RS}*\text{TPH} + 0.090 \text{ TS}*\text{TPH} - 0.00045 \text{ RS}*\text{TS}*\text{TPH}$$

$$\text{HV} = 233.6 + 0.0299 \text{ RS} - 0.32 \text{ TS} - 111.3 \text{ TPH} + 0.000033 \text{ RS}*\text{RS} + 0.00661 \text{ TS}*\text{TS} + 18.89 \text{ TPH}*\text{TPH} - 0.00098 \text{ RS}*\text{TS} - 0.0100 \text{ RS}*\text{TPH} - 0.040 \text{ TS}*\text{TPH} + 0.000180 \text{ RS}*\text{TS}*\text{TPH}$$

The residual plot for means of this process is shown in Figure (4.6). This layout is useful to determine whether the model meets the assumptions of the analysis. The residuals are the deviations of the observed data values from the predicted value  $\hat{y}$  and they estimate the error terms ( $e_i$ ) in the model. The  $e_i$  are assumed to be random and normally distributed with mean equal to zero and constant standard deviation. If the error terms follow a normal distribution, they will fall on a straight line on the normal probability plot. Because they are estimates of the error terms, the residuals should exhibit similar properties. If the assumptions are valid, plots of the residuals versus run sequence, predicted values, and other independent variables should be random and structure less. If structure remains in the residuals, residual plots may suggest modifications to the model that will remove the structure. Investigation of residuals has been used to evaluate the model adequacy. Residuals are found to be scattered and without any definite pattern which prove the adequacy of the model.

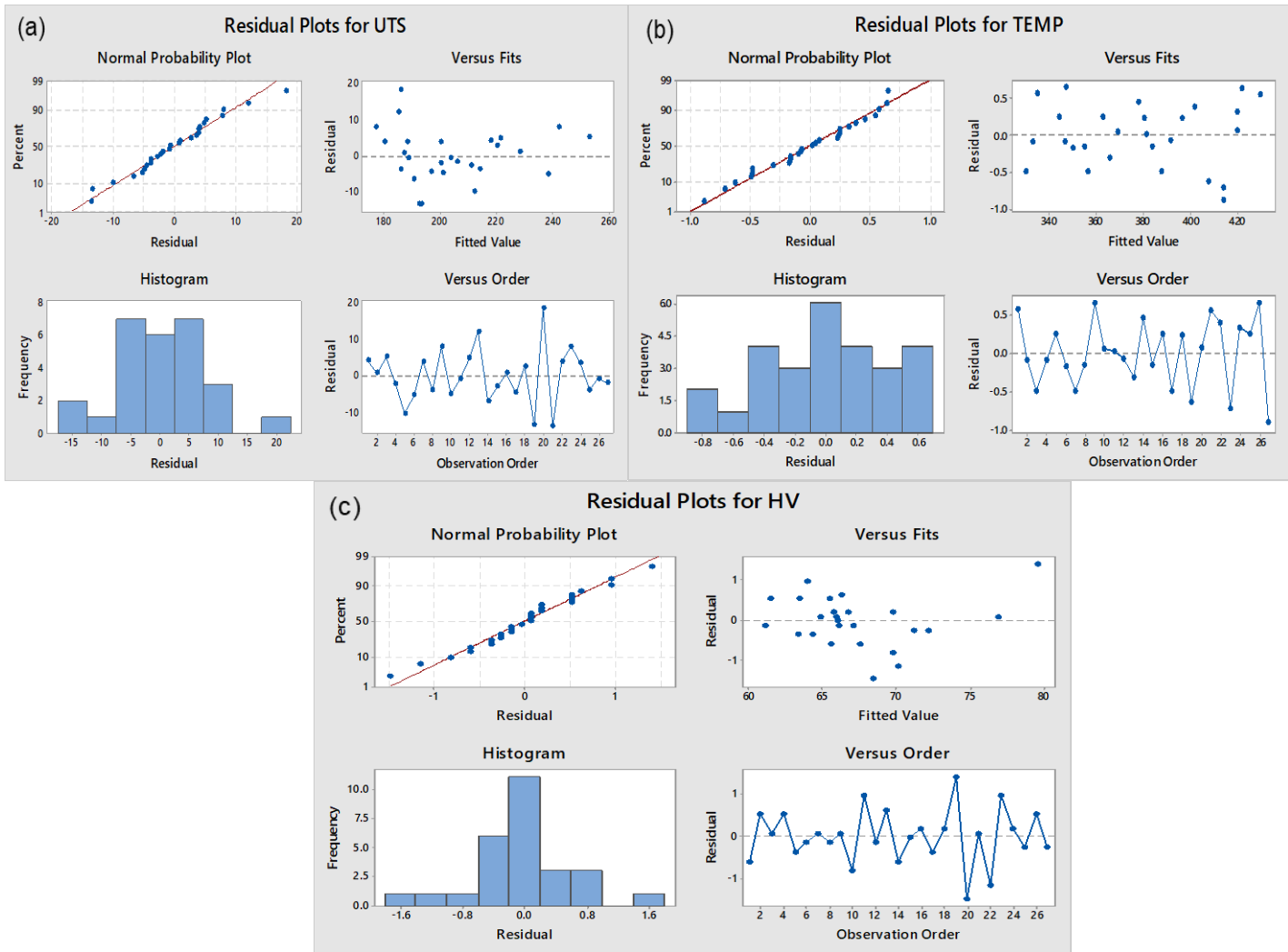


Figure (4.6) Different residual plots for testing the adequacy of the proposed model.  
(a) UTS, (b) Temperature, and (c) Hardness

The residual plots in the Figure (4.6) and the interpretation of each residual plot for the present experiment is given below:

- Normal probability plot indicates the data are normally distributed and the variables are influencing the response. Outliers don't exist in the data
- Residuals versus fitted values indicate the variance is constant and a non-linear relationship exists.
- Histogram proves the data are not skewed and no outliers exist.
- Residuals versus order of the data indicate that there are systematic effects in the data due to time or data collection order.

#### 4.4.7 Confirmation Run

Once the optimal level of the process parameters is selected, the final step is to verify the improvement of the performance characteristics using optimal level of process parameters. Therefore, a confirmation experiment was carried out to validate the developed algebraic model. Table 4.12 shows the results of the confirmation experiment using the FSW process parameters.

Table (4.12) Optimal values from Taguchi method

	UTS (MPa)		Temperature (°C)		Hardness (HV)	
RS (rpm)	A1	355	A3	710	A3	355
TS (mm/min)	B1	28	B1	28	B1	28
TPH (mm)	C3	3.5	C3	3.5	C1	2.5
Optimal Value	223		392		71	
Predicted Value	228		420		76	
Percentage Error (%)	2.24		7.14		6.57	
Confirmation Run	230		400		67	

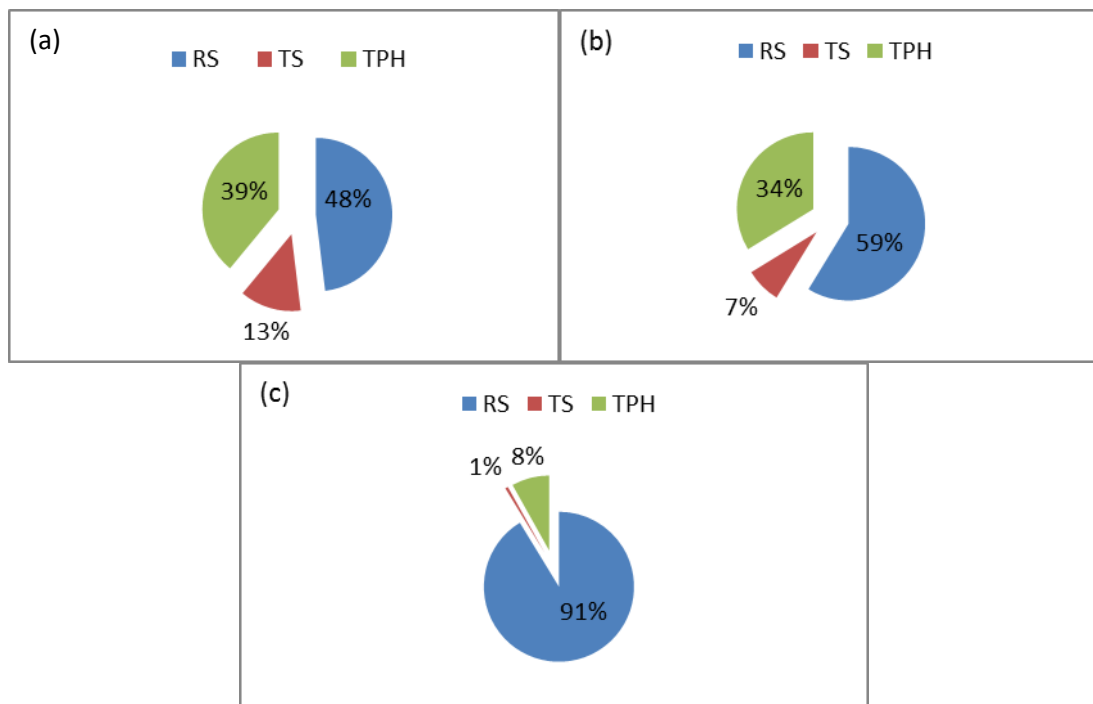


Figure (4.7) Percentage contributions of process parameters in model. (a) UTS, (b) HV, and (c) Temperature

The contribution percentages of each process parameters are shown in Figure (4.7). In both tensile strength and hardness analysis it is observed that the tool-pin height is a contributing factor to promote good performance during the FSW process. The percentages are calculated neglecting the second order combination and error which are least significant when compared to RS, TS, and TPH alone. This factor (TPH) is related to typical defects called small root defects which can greatly decrease the resistance to tensile test of the FSW joints and RS is the most sensitive parameter.

#### **4.5 Conclusions**

This study has shown the application of Taguchi method on the performance evaluation of a FSW process for the UTS. The level of importance of the process's parameters is determined by using ANOVA. Moreover, regression modeling has helped us generate an equation to describe the statistical relationship between the process's parameters and the response variable (UTS) and to predict new observations.

1. The L27 Taguchi orthogonal designed experiments of FSW on aluminium alloy AA 5052 are successfully conducted.
2. The FSW process parameters are optimized with an objective to maximize the tensile strength, temperature and hardness of the joint.
3. The rotational speed plays an important role and contribution of the overall response is 48%; welding speed and tool-pin height contribute 13% and 39 % respectively of the overall response for the tensile strength.



## CHAPTER 5

### Finite Element Modeling and Simulations

#### 5.1 Thermal and Residual Stresses

In this chapter, numerical and experimental investigations of heat generation during friction stir welding (FSW) of aluminium alloys are studied. FSW experiments are conducted with different process parameters like tool rotational speed, traverse speed and tool-pin height. In the friction stir welding (FSW) process, heat is generated by friction between the tool and the workpiece. This heat flows into the workpiece as well as the tool. The amount of heat conducted into the workpiece determines the quality of the weld, residual stress and distortion of the workpiece. The amount of the heat that flows to the tool dictates the life of the tool and the capability of the tool for the joining process.

This study aims to experimentally explore the thermal histories and temperature distributions in a workpiece during a friction stir welding (FSW) process involving the butt joining of aluminum 5052-H32. To quantify the physical values of the process, the temperatures in the workpiece and the tool are measured during FSW process using K-type thermocouples. Successful welding processes are achieved by appropriately controlling the maximum temperatures during the welding process.

Using the measured transient temperature fields finite element numerical analysis was performed to determine the heat flux generated from the friction to the workpiece and the tool. Detailed temperature distributions in the workpiece and the tool are presented. Discussions relative to the FSW process are then given. In particular, the results show that (1) the majority of the heat generated from the friction, i.e., about 95%, is transferred into the workpiece and only 5% flows into the tool and (2) the fraction of the rate of plastic work dissipated as heat is about 80%.

Apart from these the heat sources inherent to the FSW process are the energy released during the viscous/plastic flow deformation around the tool and the friction between the tool surface and the workpiece plates to be welded. The heat sources are considered to be concentrated at mid-thickness, simulating the approximate typical location for the center of

the nugget, in accordance with observed transversal sections, the point heat source follows the butt joint line, with constant translation velocity, and thus a steady-state heat flow condition is considered as shown in Figure 5.1. One important contribution for the overall thermal field is seen as the simulation of the asymmetric temperature distribution effect in the vicinity of the periphery of the tool base.

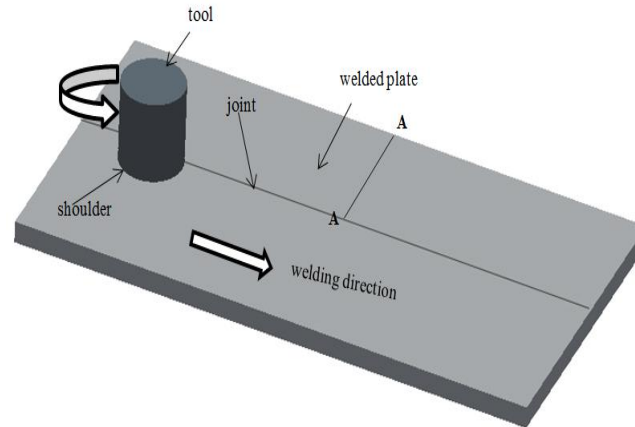


Figure (5.1) Schematic of Friction Stir Welding.

From Chapter 3, it can be established that for the material, the advancing side is hotter than the retreating side. This fact is consistent with geometric characteristics typical of weld zone features of the nugget. Here the recrystallized zone develops almost axisymmetric from the mid-thickness in an onion rings-like arrangement. Closer to the top surface of the weld (near the shoulder) this form grows towards the periphery of the shoulder but more so towards the advancing side (shearing side). This fact can be attributed due to the asymmetric velocity field resulting from the composition of both rotational and translation velocity of the tool. The classification to establish hot and cold weld conditions is based on the value of the ratio between rotational and translational, velocities of the tool relatively to the parts being welded.

In reality, and for the typical FSW apparatus, the loss mechanisms may differ from the top surface conditions, where the heat is predominantly lost by convection and radiation to the surrounding environment, which includes the tool, and the bottom surface, where the heat is mostly lost by conduction to the anvil.

During the establishment of the particular solutions from the differential equation governing heat flow conducted into solid bodies, it was assumed that density, specific heat and the conductivity coefficient do not vary and are thus independent of position and temperature. This assumption in a solid state welding process does not induce significant deviations into the final results, at least when compared to the deviation which can be expected for fusion welding. Wherein this approach was developed and had been used since the mid1940's.

(i) The thermal source was simulated as a linear source, with a length of about the diameter of the tool base defining the solutions for three domains - prior to the arrival of the source, within the source domain, and after the source has passed.

(ii) Thermal source simulated as a point source representing the thermal field in the entire domain with the exception of the diameter correspondent to the tool base, where the tool geometry is represented.

From both solutions the second was adopted because it does not compromise the initial objectives of the code developed, and results obtained require lower computational time. It also leads to an increase in quality when visualizing the results. The asymmetry due to the composition of the rotational and translational velocities of the FSW tool, introduces the concept of advancing and retreating sides for the material and heat flow during the FSW process.

### **5.1.1 Introduction to ANSYS V14.5**

A three dimensional (3D), transient, non-linear thermo-mechanical model was developed using ANSYS 14.5 software to simulate the thermal history during FSW of AA5052-H32. The simulated temperature distributions (profile and peak temperatures) are compared with experimental values to predict a temperature history which is in good agreement with experimentally measured results. The maximum temperature in the FSW process increases with the increase of the rotational speed. The results show that the heat generation during FSW strongly depends on both rotational speed and traverse speed. Further, the tool shoulder restricts the out flow of plasticized material and applies substantial forces to consolidate the weld joint. In order to produce quality welds by FSW technique, it is important to understand the role of process parameters and their effects on the macro- and micro-structures and final mechanical properties of the weld nugget. In FSW technique, the key process parameters

includes tool rotational speed (RS), weld traverse speed (TS), axial load (P), tool-pin height (TPH) and tool-pin profile.

Due to the complexity of the FSW process it is very difficult to gain insight into the joint during the actual welding process. Numerical simulation helps overcome this problem by providing an effective way of analyzing the formation of FSW joints. Ulysses (2002) used a three dimensional visco-plastic modeling to model FSW process. Forces applied on the tool are computed for various welding and rotational speeds, but the opposite effect was observed for increasing rotational speeds. Kovacevic (2003) have introduced a moving co-ordinate system in a 3-D heat transfer model using finite difference method to reduce the difficulty of modeling the moving tool during FSW. Rajamanickam (2009) developed a thermo-mechanical finite element model for FSW of aluminium alloy and observed that thermal modeling is useful to predict temperature near tool shoulder.

Chao et al., (2003) formulated heat transfer into two boundary value problems, a steady-state for tool and transient for the workpiece and found that majority of frictional heat dissipates into the work pieces. Prasanna et al., (2009) performed thermal simulations on stainless steel using moving cylindrical coordinate system and compared the results with experimental data. Zhu and Chao (2002) studied the effect of temperature dependent properties of aluminium-alloy on peak temperatures. Madhavi et al., (2014) presented on the effect of FSW process parameters on nugget geometry and mechanical properties of aluminium-alloy (AA5052-H32) by performing post weld mechanical testing and microscopic examination. Nikhil et al., (2015) examined the effect of coefficient of friction in the FSW process.

### **5.1.2 FSW process modelling using APDL**

Tool rotational speed (RS) and traverse speed (TS) have a major influence on the nugget geometry (shape and size) and the final weld quality. Increase in RS would result in increased heat generation and dissipation at the tool-shoulder and pin-surface regions. Similarly, increase in TS would result in decreased net heat input per unit length of the weld. Apart from these two process parameters, the tool geometry (tool- pin height) would also affect the net heat generation due to total frictional contact area between work piece and tool material which is very small but when combined with the other two parameters, its influence will

affect the mechanical properties as discussed in chapter-3 and chapter-4. An inverse analysis approach has been adopted to predict weld quality of FSW joints of aluminium-alloy (AA5052-H32) plates for different combination of process parameters (RS, TS and TPH). A detailed comparative study of the predicted and measured thermal cycles and peak temperatures within TMAZ/HAZ indicated that quality of weldment is influenced by rotational speed (RS) and traverse speed (TS), axial load (P) and therefore must be considered as sensitive process parameters.

### **5.1.3 FSW computational analysis**

Since a detailed account of the procedure was provided in chapter 3 only the key aspects of this procedure will be presented in the remainder of this section.

#### *5.1.3 (a) Computational Domain*

The computational domain used consists of a (150.0 mm length, 4.0 mm thickness) rectangular plate and a tool with circular pin and a 16 mm diameter solid right circular cylindrical shoulder. The tool geometry was selected to match the one used in the experimental investigation of the FSW behavior of AA5052-H32. Two work-pieces, (150 x 35 x 4 mm<sup>3</sup>) are modeled using commercially available code using ANSYS (APDL) V14.5. The element used is solid 226, which gives both mechanical and thermal properties. The numbers of mesh elements used are 30,000 using asymmetrical hexahedral mesh. Mesh sensitivity was done in FE simulations. However, the number of elements used was fixed (48x25x25) due to node limitation in the available licensed software at that point of time and moreover it was taking long time for each run. Mesh sensitivity was done by considering non-uniform elements with fine mesh around heat source ( $\Delta y_1=0.1$  mm and  $\Delta z_1=1$  mm) and coarse mesh ( $\Delta y_2=0.25$  mm,  $\Delta z_2=3$  mm and  $\Delta z_3=5$ mm) away from the heat source. A uniform size of  $\Delta x=3$  mm was considered along the length direction, as the heat source is moving one. Convection was applied on all sides and transient thermal process was used. A moving heat source is incorporated in the present model. The temperature dependent material properties are used which reflect the variation of values with change in temperature as shown in Table (5.1). The collected temperature–time data enabled a detailed quantitative analysis of the thermal process in FSW. The movement of FSW tool is implemented by creating a local cylindrical coordinate system and calculated heat load at each node and at each instance in time.

In order to simplify the moving tool effects on the work-piece in ANSYS, and to obtain reasonably accurate results, further time steps of shoulder area (circular) are formulated to move the tool along the weld line, as shown in Figure (5.2). Here, each shoulder circle has heat generation and time step, also each circle represents one step. The FSW process was assumed to start at a spot 10 mm away from the edge of the workpiece and stop after transformation of 134 mm along the weld line for all process studies as shown in Figures 5.2(a) and 5.2 (b).

The computational domain is meshed using ~30,000 first-order eight-node reduced integration hexahedral thermo-mechanically coupled solid elements. The meshed model is as shown in Figure (5.12).

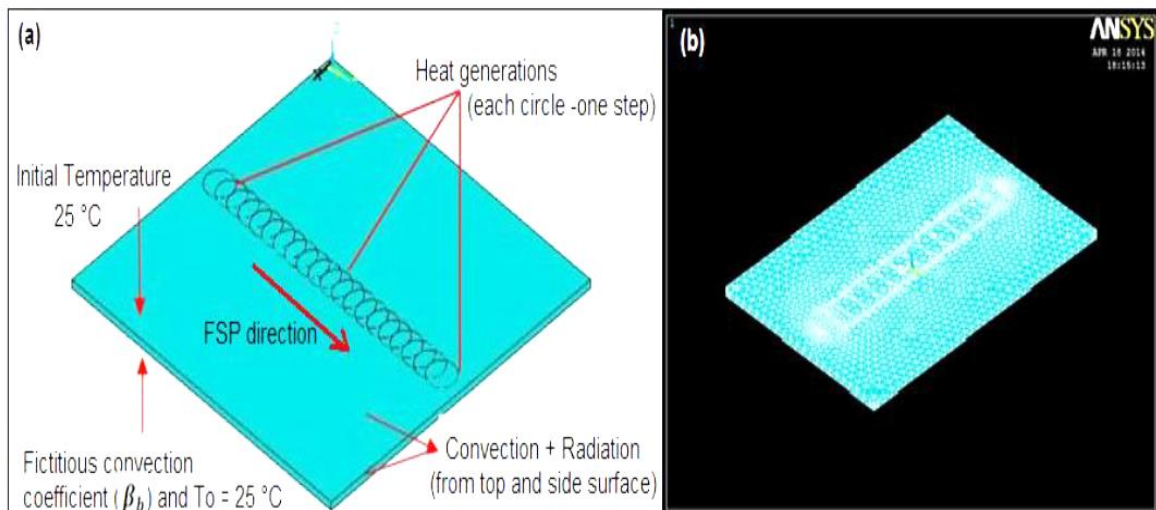


Figure: 5.2(a) Schematic representation of BC's; (b) Modeled 3D mesh in ANSYS program.

A moving coordinate system was used for modeling the tool movement during the FSW process. A detailed comparative study of the predicted and measured thermal cycles and peak temperatures within TMAZ/HAZ indicated that quality of weldment is influenced by rotational speed (RS) and traverse speed (TS), axial load (P) and therefore must be considered as sensitive process parameters. The advantage of ANSYS software is that temperature outputs can be obtained at every desired time step during FSW. The coefficient of friction has been varied with process parameters like RS and TS. The TS has little influence in contrast with RS.

Table (5.1) Temperature dependent material properties

S. No	Temperature, T (°C)	Thermal conductivity, k (W/m °C)	Specific heat, C <sub>p</sub> (J/Kg °C)	Yield strength, YS (MPa)
1	25	91	915	193
2	104	98	979	191
3	208	102	1031	134
4	312	107	1069	77
5	416	111	1100	20
6	520	120	1141	10

### 5.1.4 Mathematical modelling

Temperature measurements within the stirred zone are very difficult to make because of the intense plastic deformation produced by the rotation and translation of the tool. Therefore, it is important to obtain information about the temperature distribution during the FSW process by numerical simulations and analysis. The thermo-mechanical simulations of the FSW process can predict the transient temperature field, maximum temperatures, thermal stresses, active stress forces and even extended to determine the residual stresses. APDL (ANSYS Parametric Design Language) code was developed to model a moving heat source with appropriate boundary conditions for FSW process. FE numerical analyses are performed to determine the heat flow generated by the friction between the work-piece and the tool. The results showed that about 95% of the heat generated by friction is transferred into the work-piece and only 5% flows into the tool. Total heat generation during FSW is mainly due to the friction between tool and work-piece and intense plastic deformation around the rotating tool-pin. The heat generated by the plastic deformation of tool near the pin was neglected in this study because of negligible magnitude and is difficult to analyze. Therefore in this model, the heat generated by friction between tool-pin surface and work-piece, as well between the tool shoulder and work- piece are considered. The net heat generated per tool rotation in the heat region is uniformly distributed in cells located at a radial distance equal to pin radius ( $R_p$ ) and is expressed by the following equations;

$$Q_s = \frac{2}{3} \mu \Pi P (R_s^3 - R_p^3) (1 + \tan \alpha) \omega \quad (5.1)$$

$$Q_p = \omega * R_p * F_v \quad (5.2)$$

where,

$$F_v = \mu * d_{pin} * h_{pin} * \sigma_{y80} \quad (5.3)$$

Total heat

$$Q = Q_s + Q_p \quad (5.4)$$

where,  $R_s$  is radius of shoulder,  $R_p$  is radius of pin,  $\alpha$  is tool tilt angle,  $\mu$  is coefficient of friction between tool pin and work piece,  $\omega$  is rotational speed,  $P$  is axial load.

### 5.1.5 Computational analysis type

The FSW process is analyzed computationally using an un-coupled thermo mechanical finite-element algorithm within which heat dissipation associated with plastic deformation and tool/work-piece interfacial friction-sliding is treated as a heat source in the governing thermal equation while the effect of temperature on the mechanical response of the work-piece material is taken into account through the use of a temperature-dependent work-piece material model/properties.

#### *a) Initial conditions*

The analysis is carried out by prescribing from the onset a constant rotational speed, a zero tool translational speed along the butted surfaces and a constant downward pressure to the tool. Since the tool is not allowed to travel, the work-piece material is assigned the translational velocity of the tool but in the opposite direction. Thus, Figure 5.2 represents not the entire work-piece but rather a circular region around the tool in the otherwise infinitely-long/wide work-piece. Both the work-piece and the tool are initially set to the ambient temperature.

#### *b) Boundary conditions*

To mimic the role played by the rigid backing plate in preventing the flow of the work-piece material in the downward direction, zero normal velocity boundary conditions are applied over the bottom surface of the work-piece. To comply with the requirement for a constant translational speed of the tool, the appropriate inflow and out-flow velocities are prescribed over the circumferential portion of the work-piece surface (in a direction opposite to that of tool travel). Over the top portion of the work-piece as well as over the surface of its centre-hole, the material normal velocities are set equal to their mesh counterparts. As far as the thermal boundary conditions are concerned, standard convective boundary conditions are applied over free surfaces of the work-piece and the tool while enhanced convection



boundary conditions are applied over the bottom face of the work-piece (to mimic the effect of enhanced heat extraction through the work-piece backing plate).

*c) Heat-generation and partitioning*

As mentioned earlier, both plastic deformation and frictional sliding are treated as heat sources. To account for the fact that a small fraction of the plastic-deformation work is stored in the form of crystal defects, 95% of this work was assumed to be dissipated in the form of heat. Partitioning of this heat between the tool and the work-piece is then computed using the appropriate thermal properties of the two materials.

*(a) Tool material*

As mentioned earlier, tool material selection for FSW is quite challenging due to high strength and low thermal conductivity of the work-piece material. Consequently, FSW tools are typically made of sintered advanced carbon materials such as high carbon or chromium carbides. Due to high strength of these materials, the tool does not typically suffer much deformation on the FSW process. However, tool wear may become a serious issue. Since an analysis of tool wear is beyond the scope of the present work, the tool material is considered as being rigid. Consequently, and considering the fact that the tool acquires a portion of the heat generated due to slip at the tool-workpiece interface, the thermal properties and density for the tool material still have to be specified. For the HCHCr tool material considered in the present work, the following properties were used: thermal conductivity,  $k=120 \text{ W/m}\cdot\text{K}$ , specific heat,  $cp=140 \text{ J/kg}\cdot\text{K}$ , and density,  $\rho=18,900 \text{ kg/m}^3$ .

*d) Workpiece material*

The workpiece material AA5052-H32 is assumed to be isotropic, linear-elastic and strain-hardenable, strain-rate sensitive, thermally softenable plastic material. Essentially, strain hardening is still assumed to be related to the equivalent plastic strain discussed in chapter 3. Overall, the results presented in this section reveal correlations between the FSW process parameters (e.g., rotational and travel velocities of the tool, tool-pin height, tool tilt-angle and tool-design/material) and percentage of constraints, etc.). It should be noted that all the results shown pertain to the steady-state FSW regime and not to the transient regime corresponding to the start-up of the FSW process.

### 5.1.6 Thermal histories during FSW process

Typical spatial distribution of temperature over a medial longitudinal section of the work-piece is displayed in Figure (5.2). The results like the ones displayed in this figure can be used in the FSW process optimization in order to ensure that the workpiece material has been sufficiently softened throughout the work-piece thickness (without being subjected to excessively high temperatures) which is a prerequisite for getting good quality FSW joints.

- (a) Depending on the FSW process conditions such as tool contact pressure, tool rotational and translational speeds, temperatures in a range between 200<sup>0</sup>C and 400<sup>0</sup>C are obtained.
- (b) The highest temperatures are always found in the work-piece material right below the tool shoulder and the temperatures progressively decrease from this region as a function of the distance in the radial and through-the-thickness directions.
- (c) As the tool rotational speed increased, higher temperatures are observed and temperature differences between the top and bottom surfaces of the work piece are reduced.
- (d) By computing the energies dissipated via the plastic deformation process and that dissipated through friction between the tool/workpiece interfaces, it is found that plastic deformation typically contributes around 30% to the overall heat generation and this contribution increases slowly with an increase in the translational velocity of the tool.

With increased RS, the stir zone (SZ) grew in size. It should be noted here that neither material out flow nor the defects were observed in all the process parameters studied. The comparison of numerical and experimental results showed that the equivalent plastic strain can approximately correlate with the microstructural evolution. The high temperature region around the stirred zone extended with increasing rotational speed. The simulation results on the temperature field are in agreement with the experimental results. The temperature distributions on the surface and through thickness of the specimens are measured for different rotational and traverse speeds. It is observed that the maximum temperature is about 400<sup>0</sup>C and occurs at the middle of the nugget and is slowly reducing away from the center. A similar phenomenon is observed at different RS and TS and is shown in the Table (5.2). It was found from both the numerical simulations and experiments that the quality of the FSW can be improved when the rotational speed (RS) is increased or the traverse speed (TS) is decreased. The temperature decreased with increase in distance (z) away from weld centerline and at a depth (y) of 1.5 mm from the top surface.

Table (5.2): Average peak temperatures at TS=40 mm/min and different RS.

S. No.	Distance (mm)	Peak Temperature, $T_p$ ( $^{\circ}\text{C}$ )					
		355 rpm		500 rpm		710 rpm	
		Expt.	Sim.	Expt.	Sim.	Expt.	Sim.
1	y=1.5; z=5	385	369	369	379	371	400
2	y=1.5; z=6	364	353	356	363	340	383
3	y=1.5; z=7	329	335	329	344	346	364

The Figures 5.3(a), 5.3(b) and 5.3(c) below show the temperature histories for processed samples at different rotational speeds, but constant transverse speeds. The results are consistent and in good agreement with experimental results. Figure 5.3(a) and 5.3(b) shows a comparison of the calculated and the measured temperature–time history at the location 5 mm to the weld centerline and 1.5 mm below the top surface of the plate. The rotational speeds of the tool are 355 rpm, 710 rpm and traverse speed of 40 mm/min respectively. As the coefficient of friction and radius of shoulder and pin are constant for the present simulation the increase in rotational speed has to be compensated by decreasing the applied load. Similarly, as the traverse speed increases, the contact time per unit area of tool-workpiece interface is reduced and thus reducing the peak temperatures.

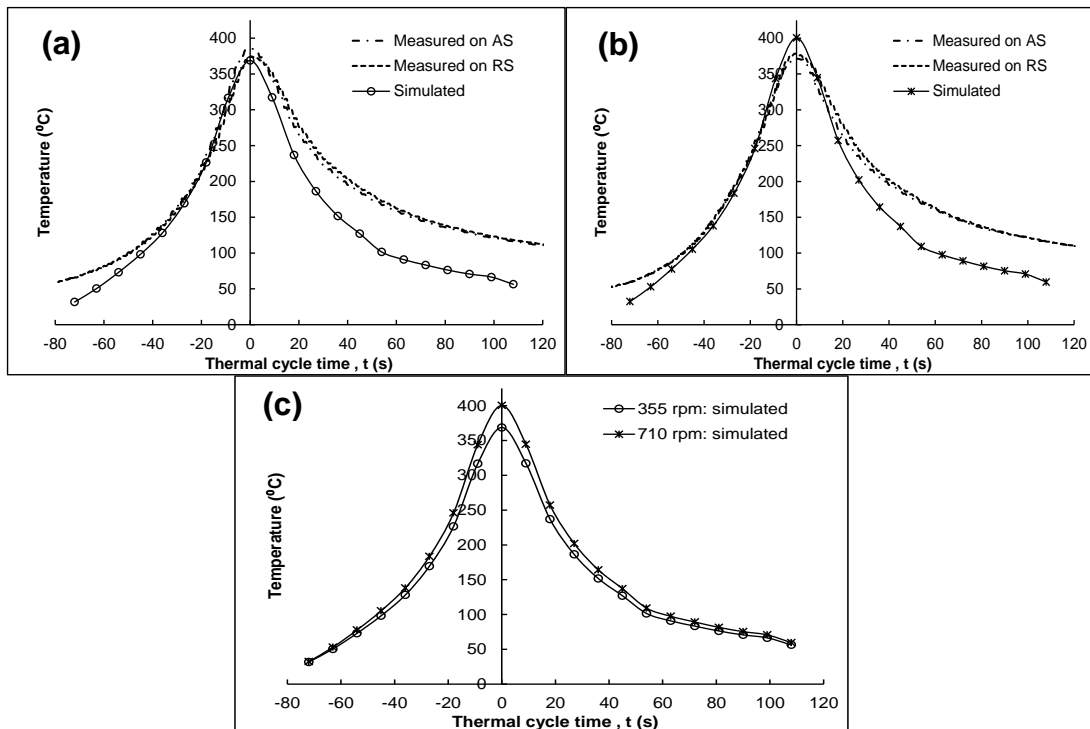


Figure (5.3) Thermal cycles at a point (depth,  $z=1.5$  mm and width,  $y=5$  mm) within the 4 mm thick plates; (a) 355 rpm, (b) 710 rpm, (c) both RS values.

Figure (5.3 (c) shows a temperature distribution along the lateral direction (for nodes 1.5 mm below the top surface of the plate) at the instant when the shoulder's center is passing over this location for the two rotational speeds of 355 rpm and 710 rpm and constant traverse speed of 40 mm/min. It is obvious that the increase in the traverse speed of the tool will significantly decrease the temperature of the welded plate, especially in the weld zone. A good agreement between the measured and calculated temperature indicates that the developed model for the prediction of temperature history is providing satisfactory results.

The simulated temperature history of FSW for AA5052-H32 at different process parameters are presented in Figures 5(b) and 5(c). At constant transverse speed of 28 mm/min, the heat generation and the peak temperature were increased when increasing the rotational speed due to the increased strain rate and plastic dissipation in the stir zone. Increasing speed from 355 rpm to 710 rpm causes significant changes in the thermal history where a maximum temperature of 400°C is observed at 710 rpm. At a constant rotational speed of 500 rpm, it was observed that higher transverse speeds lead to lower temperatures in the stir zone and also increasing the transverse speed from 28 mm/min to 56 mm/min leads to significant variation in the thermal history as shown in Table 5(temp-time), Where the maximum temperature is observed at 28 mm/min and 500 rpm. These observations were consistent with other studies (Nikhil et al., 2015). It was clear that softening degree of the stir zone was affected by the peak temperature and the process duration at high temperature. The exposed duration at three process parameters (28, 40 and 56 mm/min – 500 rpm) were 245.29, 176 and 121 seconds respectively. It is clear that the cooling rate with 56 mm/min and 710 rpm is higher than other two transverse speeds (28 and 40 mm/min). Further, higher traverse speed will reduce the processing time and subsequently the work piece will be exposed to higher temperatures for a shorter duration.

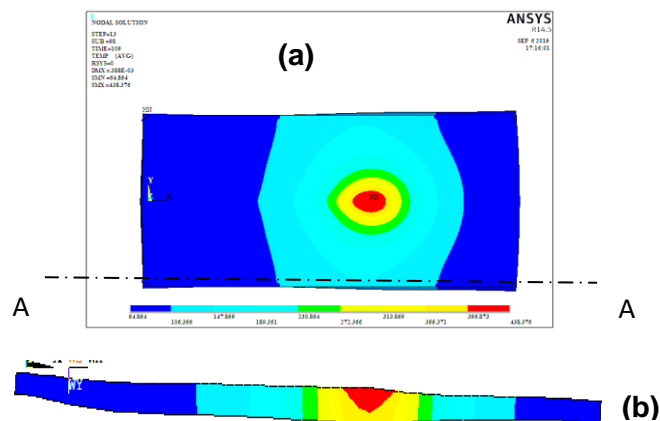


Figure (5.4) Predicted temperature distribution for RS=500 rpm and TS=40 mm/min; (a) top view (b) Cross-sectional view.

### 5.1.7 Thermal stresses in FSW

Thermal stresses are formed as a result of thermal processes, such as welding. These thermal processes cause non-uniform temperature changes in material. Effecting in local heating, expansion, and contraction occur around the heated zone of the material. However, the weld nugget zone is surrounded by material that has not undergone heating. This prevents the nugget from expanding or contracting freely and thus residual stresses are formed. The basic relation that expresses thermal stress is given in equation;

$$\sigma = E\alpha\Delta t \quad (5.5)$$

Where,  $\sigma$  is the thermal stress, E is the modulus of elasticity,  $\alpha_t$  is thermal expansion coefficient,  $\Delta t$  and is temperature change.

During friction stir welding, the compressive plastic deformation (equivalent plastic strain) of the plate starts when the thermal stresses (Von Mises stresses) become equal to the yield stress of the base material. The thermal stresses increase and yield stress of the material decreases as the temperature rises in the material. As long as thermal stresses are equal to the yield strength of the material, plastic strain accumulates in the welded region.

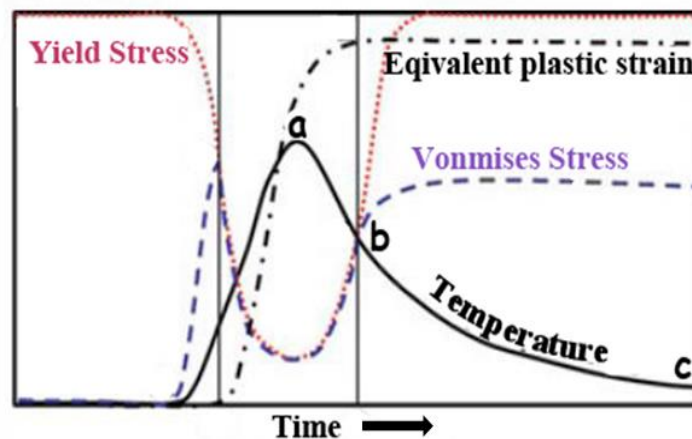


Figure (5.5): Temperature and stress-strain variations during FSW process (Mishra and Ma, 2005).

During cooling cycle, the yield strength of the material starts to rise and a point is reached where it is higher than the thermal stresses in the material. It eventually results in generation of tensile stresses in the welded region and compressive stresses away from the welded region. Furthermore, the rotational and the transverse movements of the tool will

cause additional stress in the weld due to the mechanical constraint of the plates by the fixture.

The longitudinal thermal stress contour Figure (5.6a) and lateral stress ( $S_1$ ) contour Figure (5.6b) show that the predicted maximum stress is located appropriately in the middle of the weld length. It is noticed that the start-portion and end-portion of the weld have different stress distributions as compared to the mid-portion of the plate, which may be caused by variance in the correlated thermo-mechanical process during the welding. The longitudinal stress Figure 5.6 (a), (b) reveals maximum value in the region extending down from the crown surface in a depth of 1.5 mm for 40 *mm/min*.

In the top-half of the weld region,  $S_x$  and  $S_z$  are in tensile stresses and taper significantly beyond the edge of the shoulder along the lateral direction. In FSW the misfit occurs mostly due to compressive plastic deformation of the welded region. The longitudinal stresses ( $S_x$ ) increase with the increase in rotational speed. The transverse stress ( $S_y$ ) variation with respect to rotational speed is more than the longitudinal stress variation. The stress increases with time for a decrease in TS. As the welding proceeds, the longitudinal stresses increase gradually because of the effect of mechanical constraint of the fixtures as well as higher thermal stresses produced at longer welding durations.

The maximum tensile longitudinal stress obtained is approximately 60 *MPa*, while 65 *MPa* is also observed for the maximum transverse stress. Longitudinal stresses are less compared to the transverse stresses. In the range between 5 and 10 *mm* from the centerline, the longitudinal stress reveals compressive values. Longitudinal compressive stresses are distributed around the rotating tool-pin while longitudinal tensile stresses are mainly produced in the edge of the sample in the regions far from the weld line.

In order to provide a quantitative framework for understanding the dynamics of the thermo-mechanical process of FSW, the predicted nodal stress evolution for the node located at the X position (10 *mm* from the centerline, as shown in Figure (5.2) is plotted in Figure (5.6). It is revealed that the compressive stresses are formed in both the longitudinal and lateral directions in front of the tool, and decrease with the tool moving near to the node position. It is interesting to note that  $S_x$  changes from compressive values to tensile values when the tool moves to an appropriate distance behind the node location, and then changes to compressive values again in front of the node location, as shown in Figure (5.7) when the tool moves to approximately 13 *mm* behind the node location. Similarly,  $S_z$  changes from compressive values to tensile values (maximum of 8 *MPa*) when the tool moves to approximately 6-11 *mm* behind the node location then changes again to compressive values.

The vertical stress-component  $S_z$  reveals tensile values until the tool moves near the node location, over which it shows compressive values, as shown in Figure (5.8) again appropriately 20 mm in front of the node location. Obviously, when the tool moves to a specific range of distance from the node location (approximately from 6 to 11mm in this case), all three stress-components reveal tensile values, and it is speculated that the most likely welding defects will occur in this region. Longitudinal stresses are quite low compared to transverse stresses, as expected, and its due to the geometry of the plate, welding direction and clamping boundary conditions.

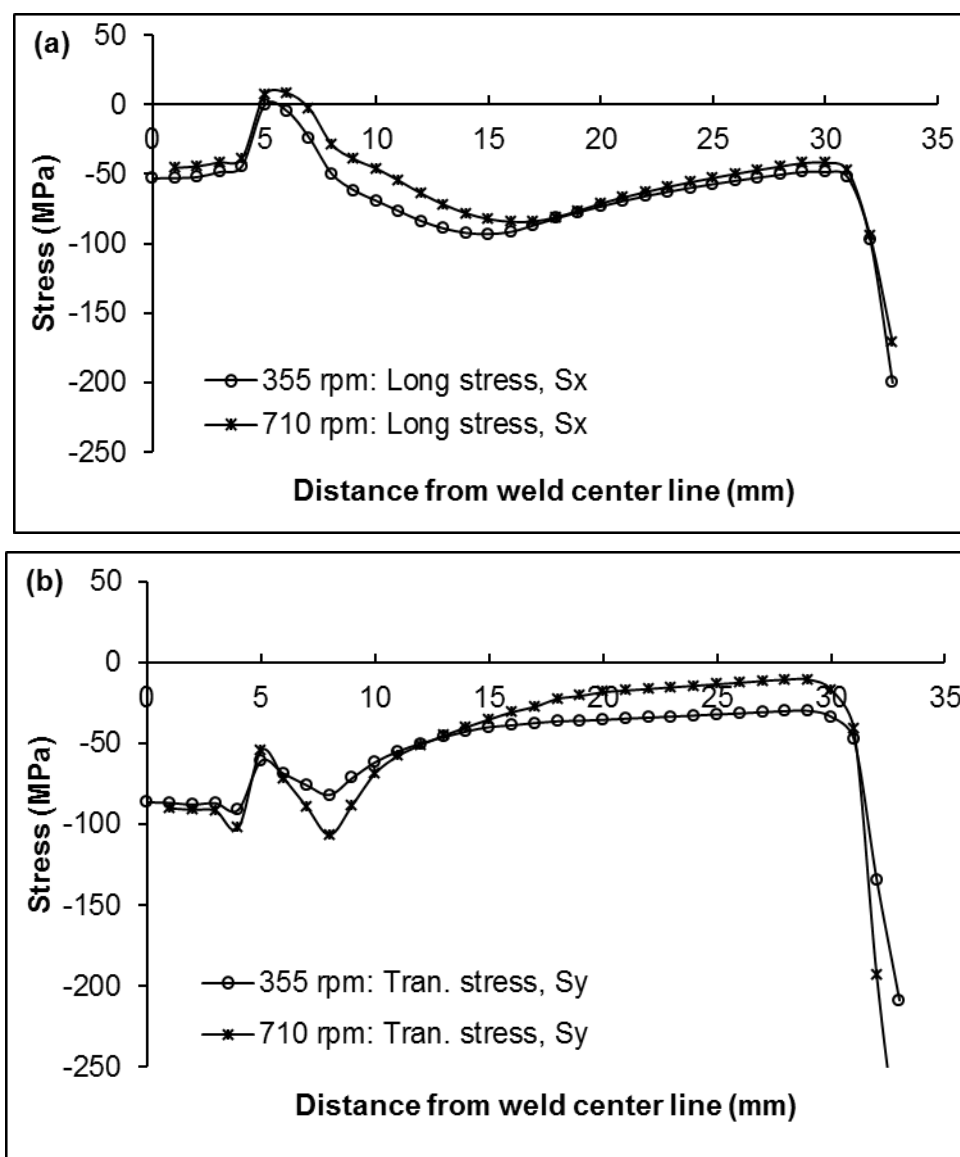


Figure (5.6) Stress variation at peak temperatures (start of heating period) on plate top surface for different RS, rpm; (a) longitudinal stress,  $S_x$  (b) transverse stress,  $S_y$ .

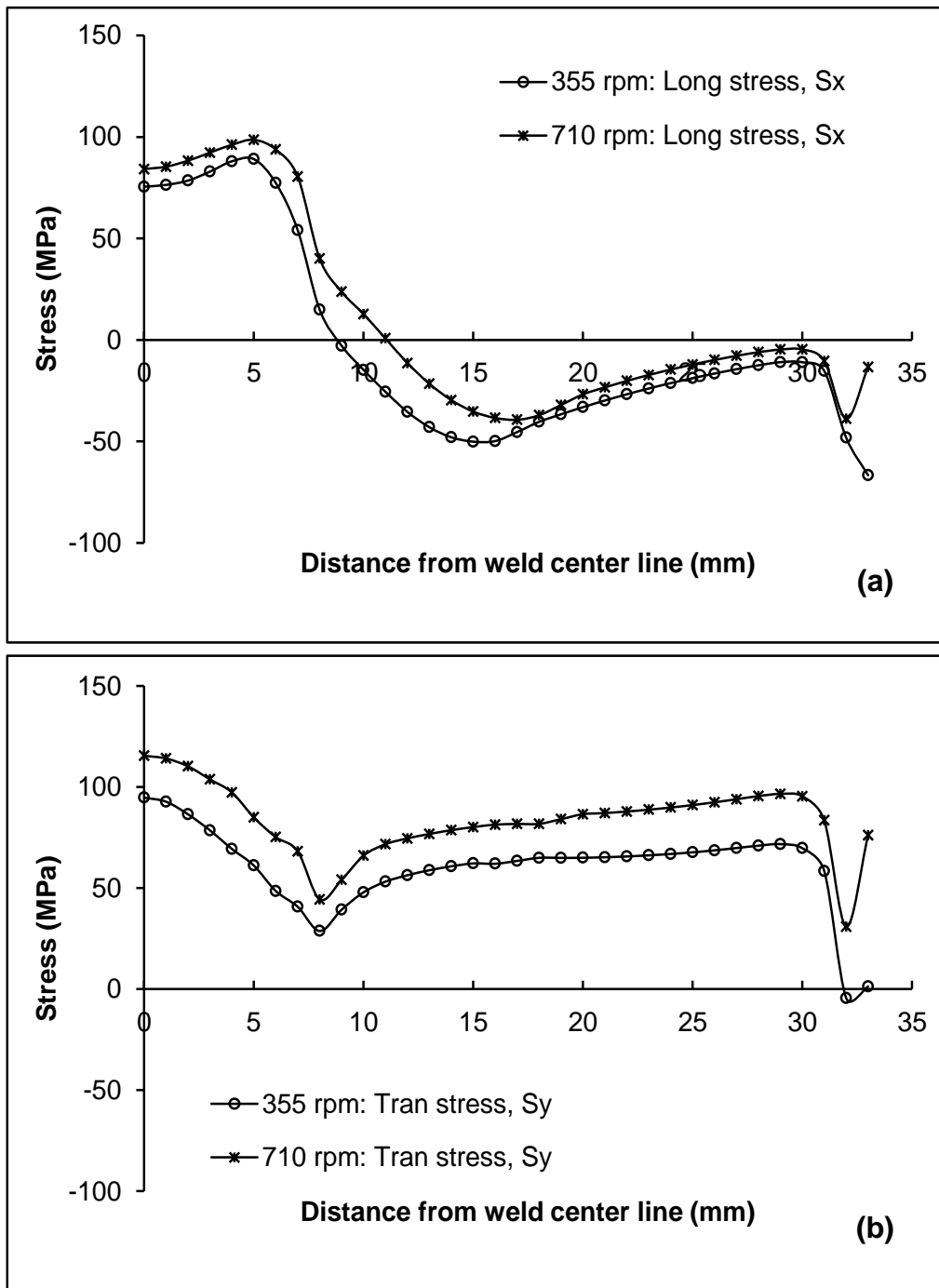


Figure (5.7) Stress variation at transition point (during cooling period) on plate top surface for different RS,  $rpm$ ; (a) longitudinal stress,  $S_x$  (b) transverse stress,  $S_y$ .



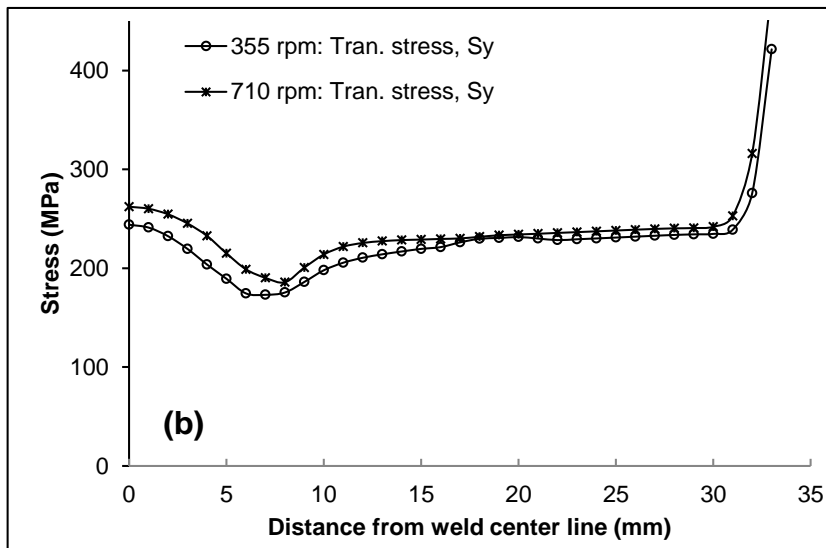
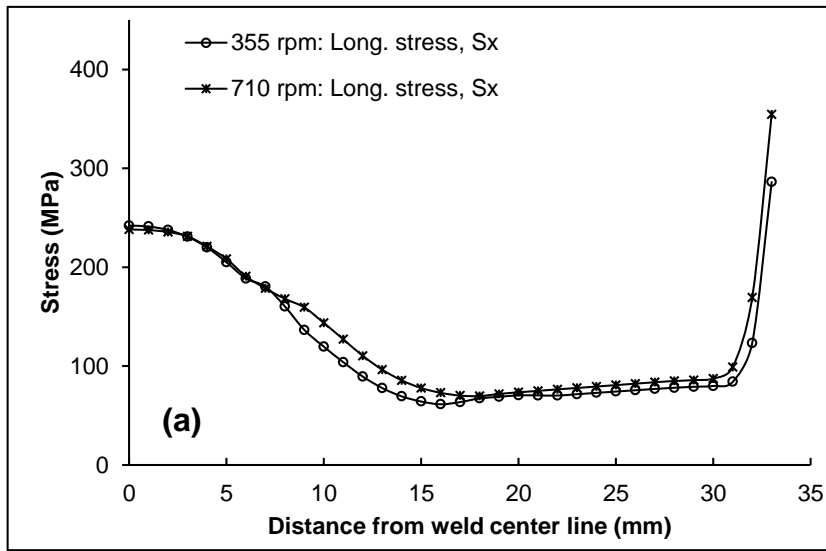


Figure (5.8) Stress variation at transition point (end of cooling period) on plate top surface for different RS,  $rpm$ ; (a) longitudinal stress,  $S_x$  (b) transverse stress,  $S_y$ .

Thermo-mechanical simulation of friction stir welding can predict the transient temperature field, active stresses developed in all the three dimensions, and residual stresses. The thermal stresses constitute a major portion of the total stress developed during the process. Boundary conditions in the thermal modeling of process play a vital role in the final temperature profile. The heating and cooling rates with the peak temperature attained by the workpiece determine the thermal stress. Also, predicting realistic peak temperature becomes important as the operating temperature at the interface of tool-workpiece is very close to the solidus temperature of the aluminum workpiece. The convection heat-transfer coefficients of the surfaces exposed to air can be theoretically determined using Newton's law of cooling. Contact conductance depends on the pressure at the interface and has a non-uniform

variation. The actual pressure distribution along the interface is dependent on the thermal stress from local temperature and non-linear stress–strain state. Therefore, applying an adaptive contact conductance can make the model more robust for process parameter variations. A finite element thermo-mechanical model with mechanical tool loading was developed considering a uniform value for contact conductance and used for predicting the stress at the workpiece and backplate interface. This pressure distribution contours are used for defining the non-uniform adaptive contact conductance used in the thermal model for predicting the thermal history in the workpiece. The thermo-mechanical model was then used to predict stress development in friction stir welding. As the coefficient of friction and radius of shoulder and pin are constant for the present simulation the increase in rotational speed has to be compensated by decreasing the applied load. Similarly as the traverse speed increases, the contact time per unit area of tool-workpiece interface is reduced, thus reducing the peak temperatures.

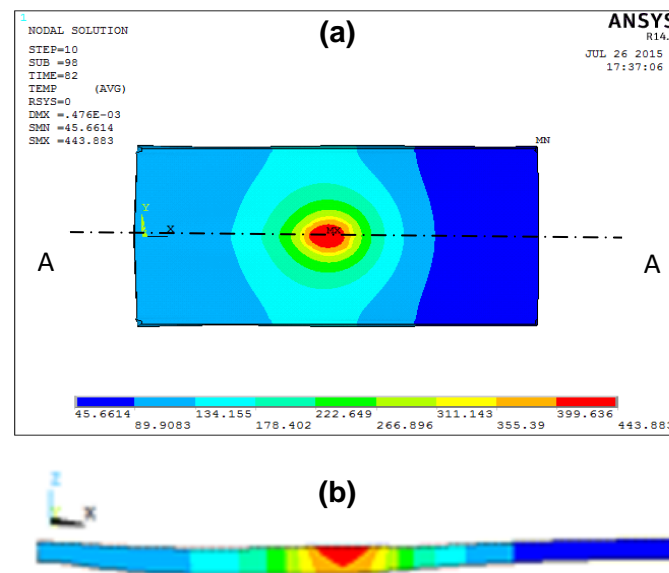


Figure 5.9. Predicted temperature distribution for RS=355 rpm and TS=40 mm/min;  
(a) top view (b) cross-sectional view.

### 5.1.8 Conclusions

A three dimensional thermal model is developed for simulating the heat transfer process for friction stir welding of AA5052-H32 alloy by using APDL programming code in ANSYS 14.0. At constant traverse speed, the temperature decreases with distance in the perpendicular direction of the tool on the surface ( $y=1.5\text{ mm}$  and  $2.5\text{ mm}$ ), for varying rotational speeds. The temperature decreases with distance away from the weld center line ( $z=5,6$  and  $7\text{ mm}$ ) for

varying welding speeds, at constant rotational speed. The moving heat source technique is reliable to simulate the friction stir welding process. Moreover the peak temperature variation is more dependent on the RS. The comparison of temperature profile developed between the simulated results and experimental values are in good agreement.

## **5.2 Residual Stresses**

Residual stresses can be developed in materials and engineering components during manufacturing by different processes. Some of these processes are plastic deformation, forging, welding, brazing, and machining. Compressive residual stress has a beneficial effect on the fatigue life, crack propagation and stress corrosion of materials; whereas tensile residual stress can reduce their performance capacity.

In the joining process, one is generally keen on observing both the overall quality of the weld (as manifested by the absence of voids, incomplete joints, highly-pronounced surface texture and other flaws) as well as the microstructure and the properties of the material in different zones of the weld (primarily in the HAZ and the stir zone). The computational analysis employed in the present work showed that if the FSW process parameters are properly selected, flaw-free FSW joints can be produced. The thermal stresses constitute a major portion of the total stress developed during the process. Therefore, applying an adaptive contact conductance can make the model more robust for process parameter variations.

### **5.2.1 Residual Stresses in FSW**

As it is seen during passing the welding heat source both of the base metals experience the compressive stresses. However, tensile stresses occur in the cooling stage. The magnitudes of these stresses are somehow constant during holding in the fixture. After removing the fixture a part of stress will be released and accordingly the amount of stress is decreased. The state of stress at the final point shows the welding residual stresses. In general, welds undergo yielding in the process of cooling after welding, then tensile residual stresses which are generated by the resistance of the material against contraction by cooling after welding, remain there.

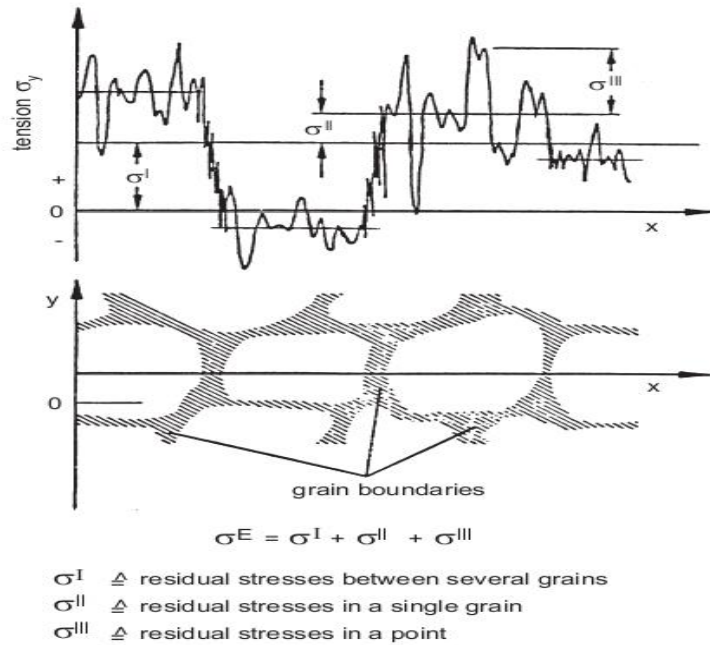


Figure (5.10) Types of Stresses (Mishra and Ma, 2005).

### 5.2.2 Methods to Measure Residual Stresses

Many technological processes introduce residual stresses in mechanical components. These residual stresses can have negative effects on the performance of structures by influencing fatigue life and fatigue crack propagation significantly. Some of these processes, however, are executed intentionally in order to introduce a favourable state of residual stress. Shot peening, hole expansion, and rolling, for example, introduce residual stress states that can have a positive influence on the nucleation and the propagation of fatigue defects, as well as fracture and stress corrosion resistance.

Among the non-destructive techniques, X-ray diffraction and neutron diffraction are most commonly used for detecting residual stresses. However, in addition to the fact that these methods require expensive equipment and are not easily applicable, there is a limitation in the maximum dimensions of the test sample. X-ray diffraction can measure residual stress in crystalline materials to a maximum depth of about 0.05 mm. Here we used X-ray diffraction method to measure the stresses on the top surface of the welded plates. Neutron diffraction can measure residual stresses to depths up to 10 cm, where measurements are made typically in volume elements of the order of 1 mm<sup>3</sup>. Other non-destructive techniques commonly used are the ultrasonic method, based on the variations in the velocity of ultrasonic waves that can be related to the residual stress state.

Among destructive methods for measurement of residual stresses, most commonly used are the hole drilling, ring core, crack compliance, and sectioning methods. These methods are sensitive to the macroscopic residual stresses only. The hole drilling method is considered to be a semi-destructive technique for the measurement of residual stresses. It is executed by introducing a hole at the center of a strain gauge rosette, which is connected to the test specimen. The measurements are performed at various depths, recording the residual stress values along the thickness of the specimen. The ring core method for the measurement of residual stresses is a variation of the hole drilling method. It is a mechanical strain gauge technique used to determine the principal residual stresses as a function of depth in materials, where linear elastic theory can be assumed (metal, ceramics, polymers).

### 5.2.3 Measurement of Residual Stresses in Welded Plates

Welding is one of the most common processes that introduce detrimental residual stresses in structures. A residual stress field is formed in a welded structure as a consequence of high thermal gradients developed during the welding process. These residual stresses are only partially relaxed during the phase of cooling, causing undesired deformations of the welded structure. Therefore, it is essential to evaluate accurately the state of residual stress before placing the welded component in operational conditions, in order to minimize the residual stress-related failures. A welding process generates a significant residual stress in the longitudinal (welding) direction ( $\sigma_y$ ), that generally has a peak tensile stress in the center of the weld bead and a peak compressive stress in lateral zones. At the same time, stress in the transversal direction is present ( $\sigma_x$ ), this reaches lower values with respect to the stresses acting in the longitudinal direction. Obviously, the residual stress field, in the absence of external loads, is in an auto-equilibrated state.

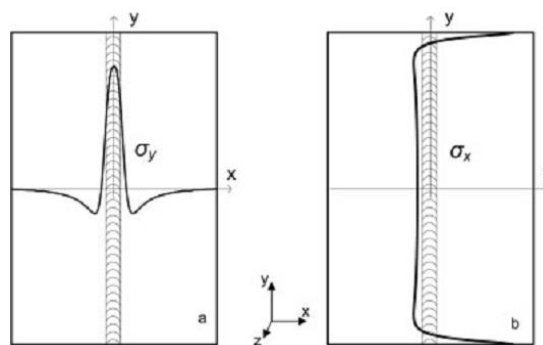


Figure (5.11) (a) Longitudinal and (b) transversal residual stress (a) Longitudinal  $\sigma_y$  and (b) transversal  $\sigma_x$  residual stress in a welded panel.

The distribution of the residual stress along the thickness of the panel, experimental results show that, it is possible to assume a constant distribution of the stress along the z axis, where thicknesses are up to 1 inch. For conveniently measuring the residual stress a double symmetric geometry is assumed (xz and yz symmetry planes). Double symmetry implies the absence of tangential stresses ( $\tau_{xy}$ ), on the axes, making the values ( $\sigma_y$ ) and ( $\sigma_x$ ), measured along the axes x and y, principal stresses.

It is well known that the transversal stress ( $\sigma_x$ ), in the center of the weld bead is about 10–20 per cent of the maximum value of the longitudinal stress ( $\sigma_y$ ), so strain gauges oriented in the direction of the y axis only can be used. In addition, the distribution of longitudinal stress ( $\sigma_y$ ) along the longitudinal y axis, is practically constant and decreases to zero at the edges of the panel, so it is not necessary to perform measurement along the entire weld bead. Therefore, a simplified analysis can be performed using y-axis-oriented strain gauges, positioned along the x axis only - the transversal direction of the panel. Strain gauges oriented in the longitudinal direction only are enough to characterize the residual stress correctly.

When using the results of strain gauges oriented in the y direction only, it is possible to evaluate  $\varepsilon_y$  in the first approximation, the longitudinal residual stress present in the examined panel by using the equation for the uniaxial stress state.

$$\sigma_y = E \varepsilon_y \quad (5.6)$$

where, E is Young's modulus.

Otherwise, when using the results of all strain gauges, oriented in both x and y directions, ( $\varepsilon_y$ ) and ( $\varepsilon_x$ ), together with the biaxial stress–strain equation a more accurate stress field can be obtained.

$$\sigma_y = \frac{E}{1-\nu^2} (\varepsilon_x + \nu \varepsilon_y) \quad (5.7)$$

where,  $\nu$  is Poisson's ratio.

#### **5.2.4 Residual Stress Distribution in Nugget**

Residual stresses arising after welding exert a considerable influence on the service characteristics of welded equipment and their control allows avoiding failure of welded joint. Distribution of residual stresses arising after welding is quite complex and inhomogeneous. Many factors have influence on the magnitude and the profile of the stress distribution curve. In this study, the residual stress distribution in Al alloys joined by FSW process is discussed.

Due to the intense concentration of heat in the welding, the regions near the weld line undergo severe thermal cycles. The thermal cycles cause non-uniform heating and cooling in the material, thus generating inhomogeneous plastic deformation and residual stresses in the welded structures. The distribution of welding residual stress depends on several main factors such as structural dimensions, material properties, restraint conditions, heat input, number of weld pass and welding sequence. Hence, for multi-pass welding the welding residual stresses may be very complex, and it is very difficult to predict the distribution of welding residual stress due to the multi-pass welding operation.

During experiments, the thermal cycles at several locations on inside and outer surfaces are to be measured using the thermo-couples. After completion of welding, using XRD technique the welding residual stresses are measured in this study.

A numerical simulation based on the finite element method can be used to determine residual stresses in welded plates. A conventional means to calculate residual stress distribution in engineering structures is the finite element method. The simulation consists of sequentially coupled, uncoupled thermal and structural analyses. In the thermal analysis, the heat source is introduced, using simplified heat flux. The temperature field, calculated in the thermal analysis, is used as the loading for the mechanical analysis.

Performing the thermal and the mechanical analysis separately is more computationally efficient. After the thermal analysis, the determined temperature fields are used as input loads for the mechanical analysis.

Good results of residual stress can be obtained using a uniform distribution of the volume heat flux at the weld bead. The consequence of taking a uniform heat flux is a different time dependent temperature field compared to that when the heat flux is entered as a volumetric heat flux. This difference is significantly expressed in the root of the weld, and with distance from the weld zone it disappears quickly. The magnitude of residual stresses in

the case of modeling with a uniform heat flux as the load, is slightly different from that in which the thermal analysis is performed with a volumetric heat flux. In a sequential thermal stress analysis, temperatures predicted by the heat transfer analysis are used as load.

### **5.2.5 Uncoupled formulation**

The temperature fields and the evolution of the residual stresses are investigated by means of finite element method. In order to accurately capture the temperature fields and the residual stresses in the welded structure, a 3-D finite element model is developed. The thermo-mechanical behavior of the weldment during welding is simulated using uncoupled formulation, because the dimensional changes in welding are negligible and mechanical work done is insignificant compared to the thermal energy from the welding.

The heat conduction problem is solved independently from the stress problem to obtain temperature history. However, the formulation considers the contributions of the transient temperature field to the stress analysis through thermal expansion, as well as temperature-dependent thermo-physical and mechanical properties. The solution procedure consists of two steps. First, the temperature distribution and its history in the welding model are computed by the heat conduction analysis.

The same finite element model used in the thermal analysis should be employed here, except for the element type and the boundary conditions. The temperature history generated by the thermal model is then sequentially coupled to a mechanical model that predicts the residual thermal stresses.

### **5.2.6 Predicted residual stresses in FSW process**

A sequentially coupled finite element model (stated above) of the friction stir welding process is utilized to study the residual stresses caused by the thermal cycles during friction stir welding of metals. This is a two-step simulation process. In the first step, the thermal history is predicted from an input torque based thermal model.

The second step of the analysis involves the use of the thermal histories predicted by the thermal model as an input for a mechanical model that ignores all other forces apart from those arising out of thermal expansion. Weld-induced residual stresses are typical macro residual stresses and can be estimated using continuum mechanics model without regard to the polycrystalline nature of the material. Additionally, friction stir welds are free of phase changes because of their solid-state nature.



$$\int_s t dS + \int_v f dV = 0 \quad (5.8)$$

$$t = n \cdot \sigma \quad (5.9)$$

$$\left(\frac{d}{dx}\right) \cdot \sigma + f = 0 \quad (5.10)$$

where,  $V$  is volume of space occupied by the material at the specific point in time,  $S$  is the surface bounding this volume,  $t$  is surface traction per unit area and  $f$  is the body force per unit volume,  $\sigma$  is the true or Cauchy stress matrix and  $n$  is the unit outward normal to the surface  $S$ .

The work-piece is assumed to be elastic–plastic isotropic material. Additive strain decomposition can be used to decompose the differential form of the total strain into three components:

$$d\varepsilon_{ij} = d\varepsilon_{ij}^E + d\varepsilon_{ij}^P + d\varepsilon_{ij}^T \quad (5.11)$$

where,  $d\varepsilon_{ij}^E$  is the elastic strain increment,  $d\varepsilon_{ij}^P$  is the plastic strain increment, and  $d\varepsilon_{ij}^T$  is the thermal strain increment.

The sum of the first two terms in the above Eq. represents the total mechanical strain. In the model, however, if no mechanical forces are considered and if only the forces arising out of the volumetric thermal expansion are taken into account, then it is only the thermal strain increment that contributes to the residual stresses. This thermal stress, however, can constitute both elastic and plastic components. The constitutive equation of the thermal elastic–plastic continuum, arrived through the principle of virtual work, can be expressed as:

$$\int_{\Omega} d\sigma_{ij} \delta d\varepsilon_{ij} d\Omega - \int_{\Omega} db_i \delta du_i d\Omega - \int_{\Gamma_t} dt_i \delta du_i d\Gamma = 0 \quad (5.12)$$

where,  $dt_i$  is the boundary traction,  $db_i$  is the body force,  $du_i$  is displacement,  $\Omega$  is the domain of interest and  $\Gamma_t$  is the boundary on which boundary tractions are prescribed (Bower, 2006).

Since the current FE mechanical model deals only with residual thermal stresses, the only forces considered were those caused by the thermal expansion of the work-piece material plus the downward force exerted by the tool shoulder. Constrained thermal expansion can cause significant stress. For typical structural metals, temperature changes of about 150 °C can lead to yielding if the thermal expansion is fully constrained. Therefore, particular care must be exercised in defining boundary conditions to avoid over constraining the thermal expansion. In the present study, the work-piece is considered to be constrained of vertical motion at the bottom surface with totally rigid boundary conditions applied at the

clamping locations. The motion constraints are gradually released 3–5 min after the completion of the welding process.

Temperature dependent thermo-physical and thermo-mechanical properties are needed to appropriately compute the residual thermal stresses. The thermo-physical properties required for the current models are specific heat, thermal conductivity and density while the thermo-mechanical properties required for successful simulation of the material model are elastic moduli, Poisson's ratio and thermal expansion coefficients as well as the true stress versus plastic strain correlations. Plastic strain values are required to define the strain hardening behavior in classical metal plasticity.

*(a) Thermo-mechanical analysis in FSW*

In the thermo-mechanical analysis, the incremental theory of plasticity is employed. The plastic deformation of the materials is assumed to obey the von Mises yield criterion and the associated flow rule. The relationship of the rate components between thermal stresses,  $\sigma_{ij}$ , and strains,  $\varepsilon_{ij}$ , is described by;

$$\varepsilon_{ij} = \frac{1+\nu}{E} \sigma_{ij} - \frac{\nu}{E} \sigma_{kk} \delta_{ij} + \lambda s_{ij} + \left[ \alpha + \frac{\partial \alpha}{\partial T} (T - T_o) \right] \quad (5.13)$$

where, E is the Young's modulus,  $\nu$  is the Poisson's ratio,  $\alpha$  is the thermal expansion coefficient,  $s_{ij} = (\sigma_{ij} - 1/3\sigma_{kk}\delta_{ij})$  are the components of deviatoric stresses and  $\lambda$  is the plastic flow factor.  $\lambda = 0$  for elastic deformation or  $\sigma_e < \sigma_s$ , and  $\lambda > 0$  for plastic deformation or  $\sigma_e \geq \sigma_s$ , here  $\sigma_s$  is the yield stress and  $\sigma_e = (3/2s_{ij}s_{ij})^{1/2}$  is the von Mises effective stress.

*(b) Effect of heat input on residual stresses in FSW welds*

Because of the lower heat input and grain refinements, friction stir welds in general have better mechanical properties such as the tensile strength and fatigue life than the corresponding fusion welds for both heat treatable and non-heat treatable aluminum alloys. Nevertheless, the microstructural changes caused by the thermo-mechanical processing of the material in FSW result in heterogeneous distribution of microstructure and mechanical properties in the weld region. Studies by Madhavi et al., (2014) have shown that the mechanical properties of friction stir welds of heat treatable Al alloys (such as 5052-H32) strongly depend on the resulting microstructure distribution of the joint. In a tensile test, the tensile strength of the joint is related to the minimum hardness, and the location of fracture is in the minimum hardness region. Changes in the welding process conditions significantly

influence the welding thermal cycle and thus the mechanical properties of the friction stir weld. It has been well established that the residual stress field in the weld region has a strong influence on the integrity and performance of a welded structure. So far, only limited information has been available about the residual stress distribution in friction stir welds. The resultant microstructure and mechanical property in the weld region are highly heterogeneous, and highly dependent on the welding process conditions. In order to accurately simulate the residual stress field in these alloys, the analysis included adequate constraints on the residual stresses.

The thermo-mechanical finite element modeling approach was used to simulate heat flow and residual stress formation during the friction stir welding process. In this approach, the analysis procedure is divided into two major steps. First, a transient nonlinear heat flow analysis is performed to determine the temperature distribution in the weldment for the entire heating and cooling cycle of the process. In the second step, the thermal history from the heat flow model, the composition of the Al alloy, and the temperature dependent material properties are used as inputs. The weld plate was modeled as a three-dimensional half model – the symmetry with respect to the weld centerline was utilized to reduce the model to the symmetric half of the plate for computational efficiency. The symmetry assumption was considered to be reasonable, as indicated by the neutron diffraction residual stress measurement data as well as other experimental data available in the literature.

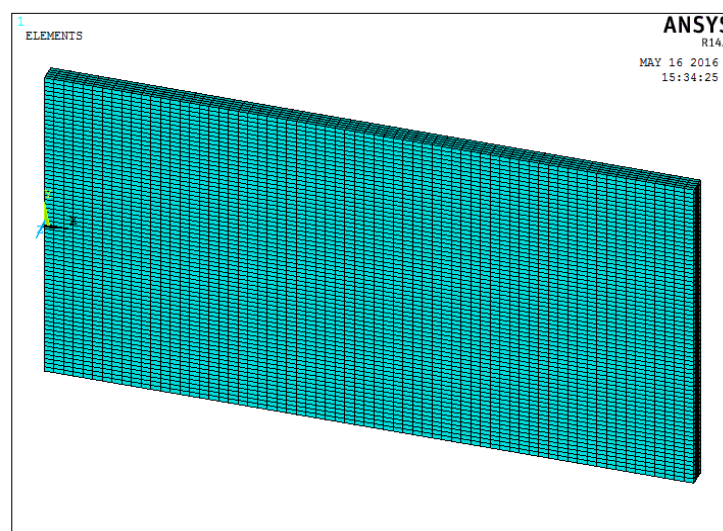


Figure (5.12) Finite element mesh used in this study.

Eight-noded brick elements were used to discretize the Al plate. The boundary conditions for the heat flow analysis included the surface heat loss due to natural convection and the heat generation between the tool shoulder and the work piece. The surface temperature involved was low – the radiation heat loss would be negligible compared to the conventional heat loss. For this reason, the radiation heat loss was not included in the model. For the mechanical analysis, reduced integration scheme was used. The moving tool shoulder and the backing anvil were treated as rigid contact surfaces that interface with the Al plate under the applied forge load. The rigid tool was prescribed to move along the weld joint line at the welding travel speed. The two sides of the plate are fixed during welding.

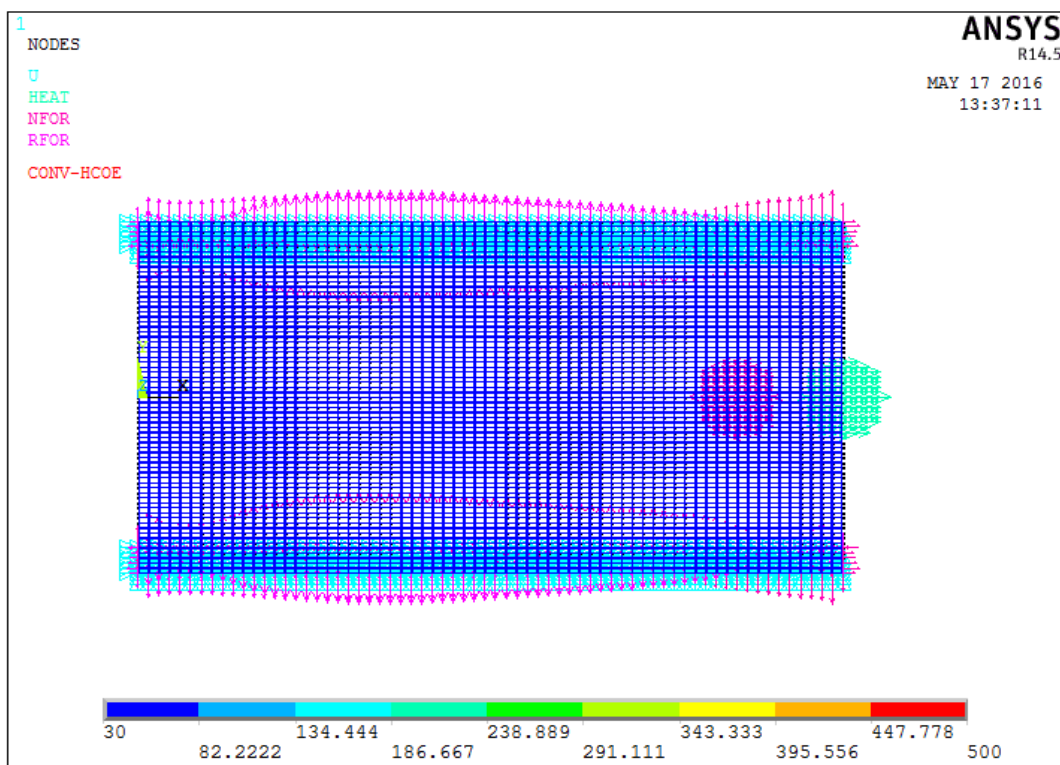


Figure (5.13) Finite element mesh constrained.

In addition, as shown in Figure (5.13), part of the top surface to the Al plate was also constrained vertically during welding to simulate the clamping effects. Both the end constraint and the top-surface clamping are released after the weld was cooled down to the ambient temperature, to obtain the as-welded residual stress field. The contacts between the tool and plate and between the anvil and the plate were also removed after the weld is cooled. The final step in the mechanical analysis was to simulate the natural aging process.

The material flow in the stir zone was ignored in the model. Thus, the heat flow was treated as a heat conduction problem. The heat flow model considered the heat generation between the tool shoulder and the workpiece to be the primary heat input mechanism of the FSW process. Such treatment is consistent with other heat flow analyses and experimental temperature measurements have shown to be adequate under typical process conditions similar to the ones studied here. The net heat generated per tool rotation in the heat region is uniformly distributed in cells located at a radial distance equal to pin radius ( $R_p$ ) and is expressed by the following equation;

$$Q_s = \frac{2}{3} \mu P P (R_s^3 - R_p^3) (1 + \tan \alpha) \omega \quad (5.14)$$

$$Q_p = \omega * R_p * F_v \quad (5.15)$$

where,

$$F_v = \mu * d_{pin} * h_{pin} * \sigma_{y80} \quad (5.16)$$

Total Heat

$$Q = Q_s + Q_p \quad (5.17)$$

But only 95% of total heat is given to workpiece, remaining 5% was dissipated into tool, where  $R_s$  = radius of shoulder,  $R_p$ = radius of pin,  $\alpha$ = tool tilt angle,  $\mu$ = coefficient of friction between the tool pin and work piece, where  $q$  is the surface heat flux ( $W/mm^2$ ),  $F$  the downward force ( $N$ ),  $\omega$  the rotation ( $rpm$ ), respectively, and  $\mu$  the interpretive coefficient of friction. The interpretive friction coefficient was assumed, based on the torque measurement study. The interpretive friction coefficient was difficult to determine. It was adjusted in the model, based on the peak temperature measurement data (Nikhil et al., 2015).

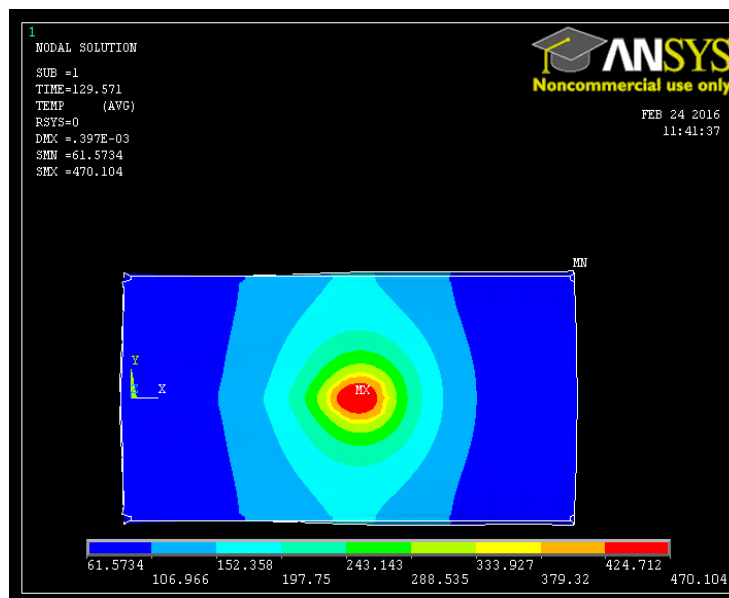


Figure (5.14) Heat generation model of friction stir welding.

Heat flow in Figure (5.14) shows the predicted temperature distribution in the Al plate when the welding was half-way done, for the lower welding speed case (28 mm/min). As the moving tool and the stationary back anvil were treated as rigid surfaces in the analysis, they were excluded from the heat flow calculations.

As shown in the Figure (5.14), the maximum temperature in the plate was near the top surface, reaching approximately 405 °C that is about 20 degrees below the solidus temperature of Al 5052. The predicted peak temperature is within the generally accepted temperature range in the stir zone of the weld. Comparisons between the calculated residual stresses and the XRD measurement results are given in Table (5.3) and Table (5.4). The comparisons are made on the top surface of the plate. The estimated standard deviation of XRD measurement uncertainties was approximately 15 MPa. Due to the softening of the weld region, the peak tensile stresses are located outside the stir zone. The reduction of the tensile residual stress in the weld center region is quite noticeable. These features were well captured by the finite element model

Table (5.3) Comparison of longitudinal residual stress results from FE simulations.

Longitudinal Peak Residual Stresses, $\sigma_{xx}$ (MPa)							
S. No	Distance(mm)	355 RPM					
		28 mm/min		40 mm/min		56 mm/min	
1	Z=1.5; y=5	-99	198	-102	201	-107	204
2	Z=1.5; y=6	-101	189	-103	191	-107	194
3	Z=1.5; y=7	-103	172	-106	174	-107	176
Longitudinal Peak Residual Stresses, $\sigma_{xx}$ (MPa)							
S. No	Distance(mm)	28 mm/min		40 mm/min		56 mm/min	
1	Z=2.5; y=5	-100	157	-103	160	-106	165
2	Z=2.5; y=6	-101	147	-103	151	-124	154
3	Z=2.5; y=7	-111	128	-102	131	-101	133

Table (5.4) Comparison of transverse residual stress results from FE simulations.

Transverse Peak Residual Stresses, $\sigma_{yy}(MPa)$							
S. No	Distance(mm)	355 RPM					
1	Z=1.5; y=5	28 mm/min		40 mm/min		56 mm/min	
		-177	177	-174	176	-178	173
2	Z=1.5; y=6	-171	171	-174	170	-173	168
3	Z=1.5; y=7	-170	168	-173	167	-173	165
Transverse Peak Residual Stresses, $\sigma_{yy} (MPa)$							
S. No	Distance(mm)	28 mm/min		40 mm/min		56 mm/min	
1	Z=2.5; y=5	-165	96.3	-173	96.2	-145	95.5
2	Z=2.5; y=6	-160	93.01	-172	93.1	-144	92.8
3	Z=2.5; y=7	-154	90.6	-182	90.7	-144	90

The overall as-welded residual stress distributions in the entire plate are shown in Figure (5.16) and Figure (5.17). Figure 5.15 presents the close-up cross-sectional views of the same residual stress field in x y and z directions. Tables (5.2) and (5.3) shows clearly the difference in the longitudinal and transverse stresses at 355 rpm and TPH of 3 mm for different TS from the FE simulations. Similarly, the residual stresses are observed for the other RS at all TS for a constant TPH of 3 mm. Here we can find small difference when the stresses are compared at different TPH both in longitudinal and transverse directions because the temperature difference found is also very less. When compared between RS of 355 rpm and 710 rpm we can find major difference in temperature as well as in the residual stresses. In the depth direction, for same RS the difference in both longitudinal and transverse residual stresses is significant.

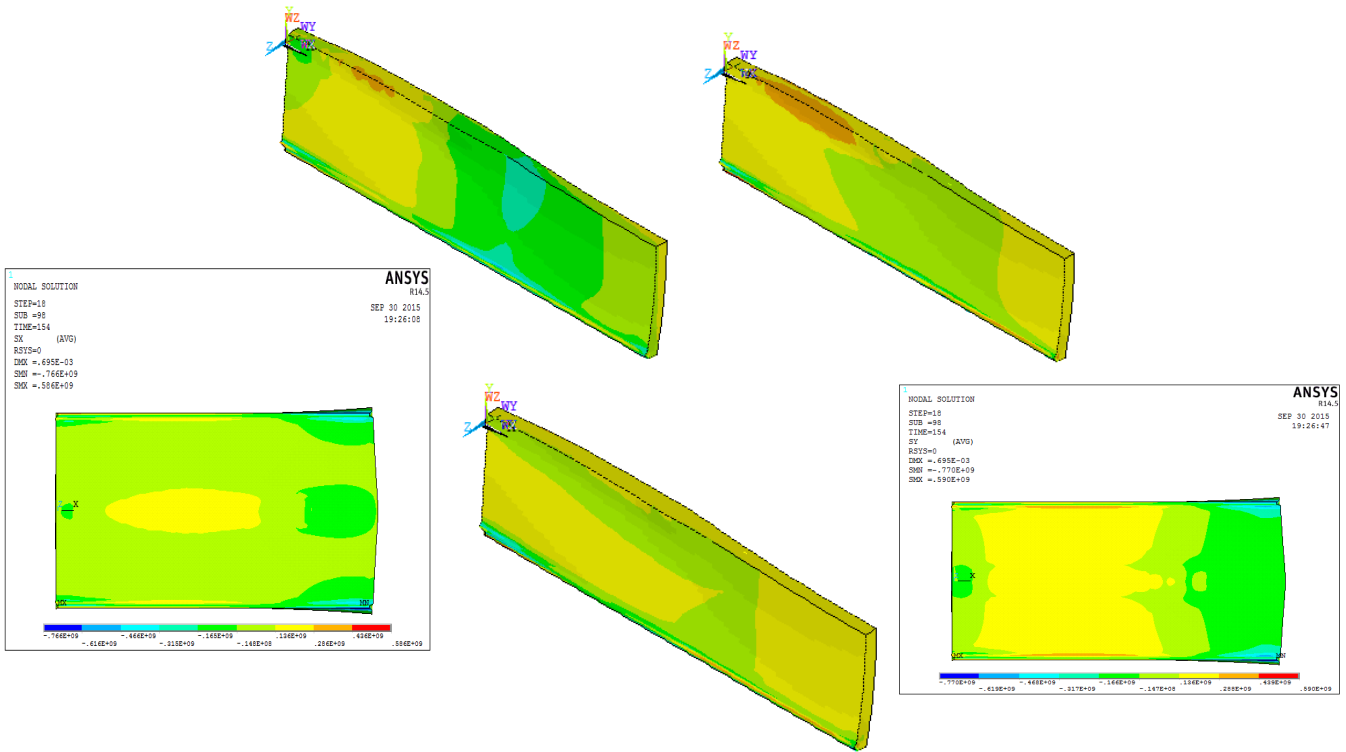


Figure (5.15) Stress distribution and close-up cross-sectional views of the residual stress field in x y and z directions.

Consistent with the XRD measurement results, the finite element modeling results reveal that the longitudinal residual stress is the predominant residual stress component in the weld. The transverse residual stress is considerably smaller in magnitude in the entire welded region, although relatively high compressive residual stress develops outside both ends of the weld. The residual stress in the through-thickness direction is nearly negligible when compared with the other two stress components.

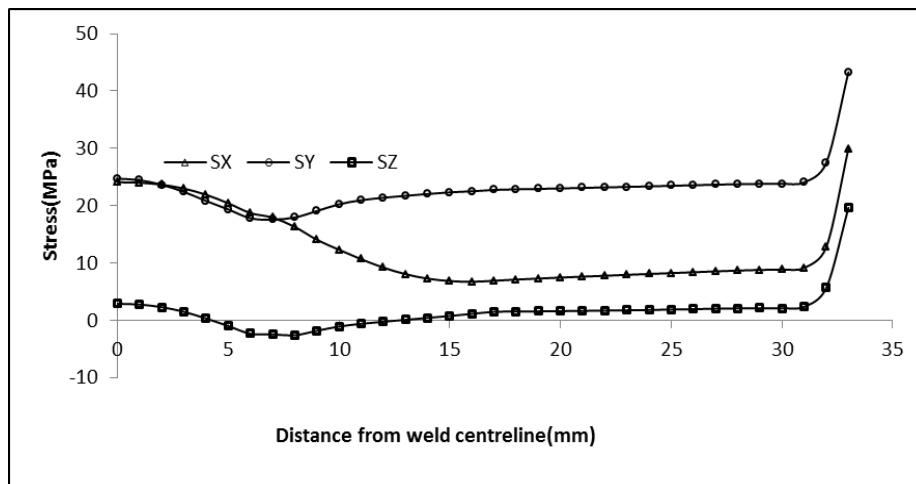


Figure (5.16) Longitudinal residual stress at RS=355 rpm, TS=28 mm/min and TPH=3.0 mm.



Figure (5.17) shows the longitudinal stress of the low welding speed case. A comparison with the high welding speed case in Figure (5.18) clearly revealed the effect of welding speed on the residual stress. Overall, the low heat input associated with the high welding speed results in higher tensile residual stresses in the weld region. On the other hand, the position of peak tensile residual stress is closer to the weld centerline.

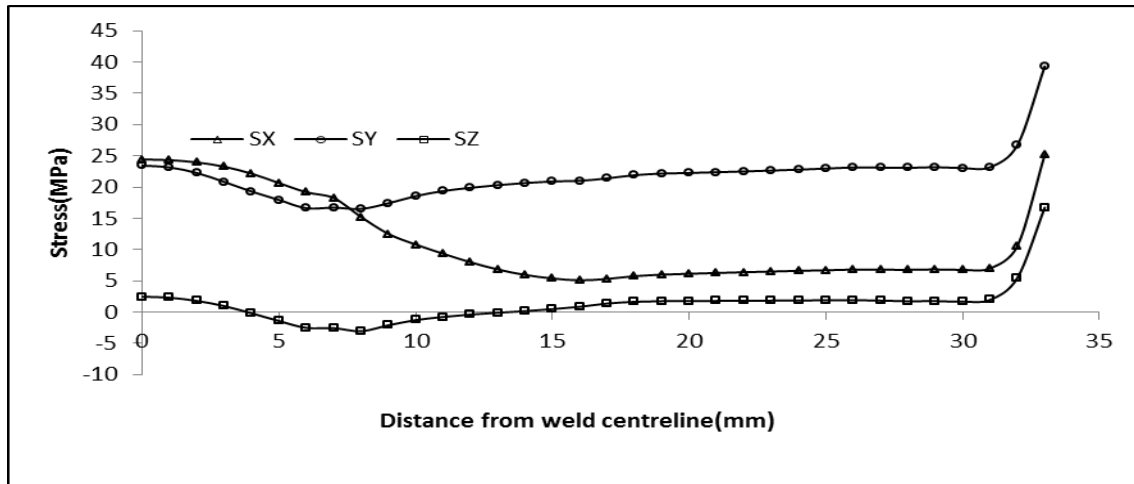


Figure (5.17) Longitudinal residual stress at RS=355 rpm, TS=56 mm/min and TPH=3.0 mm.

Although performance simulation of weld joint is still a subject requiring considerable development, recent attempts have shown the influence of RS, TS and constraints. Experimental data of the residual stresses taken from XRD technique on the top surface of the plate are shown in Table (5.5) and represented as graph in Figure (5.16). From the table (5.5), experimental residual stress values and from tables (5.3) and (5.4) simulations residuals values at same RS and at different TS can be compared and the difference can be noted. The experimental and simulated residual stresses follow the same wavy natured ‘W’ graph as shown in chapter 3.

Table (5.5) Residual stresses at RS=500 rpm; TS= 40 mm/min; TPH=3 mm

Measured Residual Stress in XRD (MPa)						
S.N	0 Deg (Longitudinal)		45 Deg		90 Deg (Transverse)	
	Stress	Error Reported	Stress	Error Reported	Stress	Error Reported
1	-117.9	± 4.4	-110.8	± 28.2	-167.4	± 66.0
2	-85.2	± 23.5	-88.9	± 17.5	-269.4	± 123.3
3	-93.9	± 20.3	-135.1	± 13	-188.5	± 29.8
4	-129.2	± 15.6	-94.3	± 45	-185.7	± 46.7
5	-129.1	± 43.5	-126.7	± 23.8	-104.2	± 4.5
6	-138.7	± 22.7	-191.6	± 21.3	-52.7	± 12.1
7	-143.2	± 39.1	-144.5	± 15.3	-61	± 13.5
8	-154.3	± 31.9	-129.4	± 30	-58.8	± 21.7

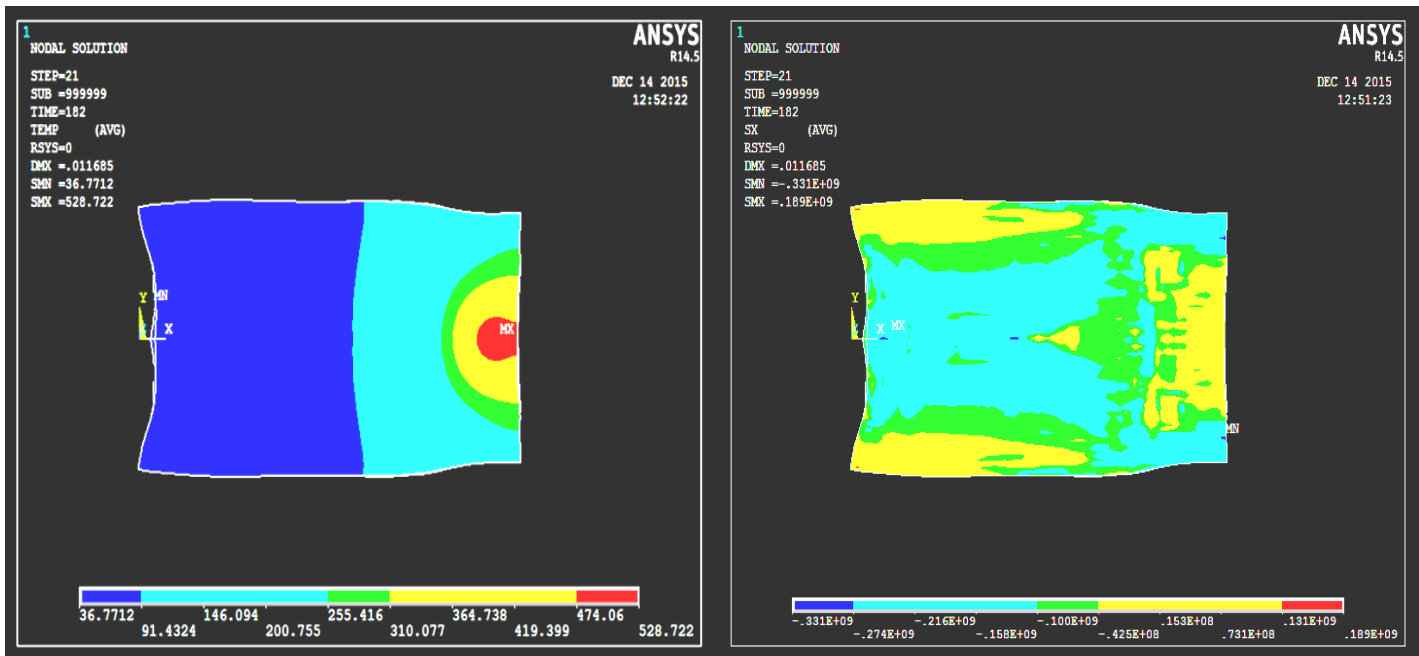


Figure (5.18) Temperature and residual stress distribution at RS=500 rpm; TS=40, mm/min; TPH=3 mm.

Residual stresses combined with distortion influence the buckling strength and fatigue life of weld structure. Larger residual stress and distortions are expected parallel to weld direction and closer to weld zone. The distortion of plates and temperature in perpendicular direction to weld is as shown in figure (5.18).

### 5.3 Conclusions

An integrated thermo-mechanical finite element modeling approach was applied to investigate the effects of welding process conditions and the formation of residual stresses in friction stir welded AA5052-H32 plate. Experimental data from previous studies confirmed the validity of the model. The finite element modeling results revealed tensile residual stresses in both the transverse and longitudinal directions in the weld region. However, the longitudinal stress was the predominant residual stress component in the weld. The peak tensile longitudinal residual stress is located in the HAZ, approximately corresponding to tool shoulder impact on the plate surface. It is lower than the yield strength of the base metal. The residual stress distribution is strongly dependent on the welding speed. The high heat input associated with low welding speed leads to more profound softening in the weld region. This in turn results in overall reduction in magnitude of the longitudinal residual stress, but a wider tensile stress zone. The integrated model can be further used to effectively predict the performance of the welded structures under various situations.

## CHAPTER 6

### Conclusions and Future Work

This chapter describes the conclusions of the research, and describes the summary of the thesis. There are many applications of aluminum and copper in today's manufacturing industries with faster travel speeds and improved post weld properties. Process parameters affect the weld, and they can be optimized to obtain better mechanical properties. We need to understand the fundamental phenomena like nature of material deformation, heat generation, and physics of the tool-weld metal interface. Relationships between process inputs (tool design, RS, TS, and TPH) and measured outputs (forces, tool temperatures, and residual stresses) are studied in this work.

The experimental data shows that the increased rotational speed/decreased traverse speed relationship exists for rotational speeds ranging from 355 *rpm* to 710 *rpm*, and for traverse speeds from 28 *mm/min* to 56 *mm/min*. Reducing the traverse speed was observed to be a more effective method for reducing weld defects. Increasing rotational speed was observed to be a viable option for reducing axial force as well. The graphs /plots of the mechanical properties like tensile strength, hardness, % elongation in the chapter 3 showed that the general parametric relationship of increased rotational speed / decreased traverse speed is followed.

#### 6.1 Nugget Mechanical Properties of AA5052-H32

This paragraph briefly explains about the summary and conclusions obtained from the experimental study to optimize the process parameters for joining the AA5052-H32 plates. First, defect free joints are selected and then examined for hardness variation across the nugget. Also, based on the better tensile properties, further experiments are carried out by varying RS and TS keeping TPH constant (=3 *mm*) with the objective of optimizing RS and TS. In general, heat input to the workpieces plays an important role in the final mechanical properties of the welded joints. In FSW process, due to material flow, more heat is diffused in advancing side than retreating side causing asymmetry in the nugget geometry. Nugget geometry (size and shape) is significantly influenced by RS and TS. Increasing TS lowers the net heat input to the plates and hence decreases the plasticized material flow around the tool-

pin. Thus the heat diffusion around the tool-pin increases the weld penetration beyond the tool-pin tip causing the weld geometry to become narrow and deep (at all rotational speeds). Due to this, hardness on advancing side is significantly higher than those values in the retreating side. Hardness variation is more in retreating side than in advancing side. Further, hardness values on the retreating side are lower than the base material at low rpm. Mean hardness increases with increase in RS and decreases with TS both on advancing side and retreating sides. Also, at same RS the variation in mean hardness with TS is very low. Therefore, it can be concluded that tool rotational speed significantly influences the mean hardness of FSW joints of AA5052-H32 as compared to the weld traverse speeds.

It is observed that % elongation decreased with increasing RS and also at constant RS, tensile strength decreased with increasing TS. However, tensile strength and mean hardness of FSW joint are closer to the base metal values.

## **6.2 Heat and Material Flow in FSW joints**

In general, the temperature at any given location within the workpiece rises as the heat source approaches it and decreases once moves away from it. Therefore, the thermal cycle consists of heating and cooling periods. The maximum temperature (peak temperature, *TP*) attained at any given location depends on its location from the weld center line, i.e., depth (*y*-value) and width (*z*-value) away from the weld axis in cross-sectional view. In FSW process, due to material flow, more heat would be transported and diffused in the direction of tool rotation making the weld joint asymmetry with respect to weld axis.

The net heat input to the workpieces has been varied by changing the weld traverse speed (TS). The overall observations from this study are, at same location in AS and RS, the peak temperatures are higher in AS than RS at all TS values and the cooling rates in AS and RS are very much comparable. However, the heating rates increased at higher TS, and at lower TS, the temperature difference in AS and RS is less at locations near the surface and increases in the direction of depth.

## **6.3 Grain size and Hardness in FSW joints**

The experimental work carried out to study the heat and material flow effects on average grain size and hardness variation in Friction-stir welded joint of AA5052-H32 is presented. In

order to quantify the heat input effects on the resulting microstructures and hardness, temperatures are measured at selected locations within the workpieces. Further, the thermo-mechanical effects due to tool's rotation are studied by examining the grain size variation across the weld geometry for different weld traverse speeds. Finally, the peak temperatures and average grain sizes are correlated qualitatively to the resulting hardness of the friction-stir welded joint. The net heat input to the workpieces has been varied by changing the weld traverse speed (TS). The overall observations from this study are as follows; (i) at same location in AS and RS, the peak temperatures are higher in AS than RS at all TS values (ii) the cooling rates in AS and RS are very much comparable. However, the heating rates increased at higher TS (iii) at higher TS, the increased peak temperatures in HAZ increased the average grain size and decreased the hardness both in AS and RS.

#### **6.4 Taguchi's Orthogonal Array**

The L27 Taguchi orthogonal designed experiments of FSW on aluminium alloy AA 5052 are successfully conducted. The FSW process parameters are optimized to maximize the tensile strength of joint. The optimum levels of the rotational speed, welding speed and tool-pin height are found to be 500 *RPM*, 40 *mm/min* and 3.0 *mm* respectively. The rotational speed plays an important role and contribution 48% of the overall response; welding speed and tool-pin height contribute 13% and 39 % respectively of the overall response for the tensile strength.

#### **6.5 Thermal and Residual Stresses**

A thermo-mechanical model was developed to predict the material deformations and temperature histories in the FSW process. During welding, every point in the material experiences different peak temperatures, and heating and cooling periods. The comparisons of simulated and measured thermal cycles at two different rotational speeds and at constant TS are verified. We clearly notice the increase in temperature with increase in RS. Similarly we observed the trend of decrease in temperature with increase in TS. The maximum temperatures obtained from the numerical analyses near the weld are higher than recrystallizing temperature of the aluminium. It can be observed that the predicted

temperature variation is in good agreement with the measured data. Further, simulations are carried out with different RS values, keeping the above TS constant and the results are compared. It should be noted that significant variations in peak temperature, and heating and cooling periods will result in variation in final weld mechanical properties, such as hardness, strength and residual stresses. Besides the physical constraints by the fixtures, the tool rotational and traverse speeds affect the thermal residual stresses as these parameters directly contribute to the total heat per unit length. It can be observed from top view that the thermal stresses are nearly same on either side of the weld axis, which is a clear indication of the absence of material flow effects due to tool's rotation. The variation of thermal residual stress components (longitudinal,  $S_x$  and transverse,  $S_y$ ) on the workpiece surface across the width from the weld axis, are observed. The longitudinal thermal stresses are in tension (tensile stress) near the weld nugget and compression (compressive stress) away from it. Also, increasing RS lowered the tensile stresses very significantly and is a desirable effect. The effect of TS on the thermal stress components at the workpiece top surface are noted that the longitudinal stresses are tensile near the weld nugget and decreased with increasing TS. However, the transverse stresses increased with increasing TS. In overall, the effect of TS is more pronounced on the resulting thermal residual stresses than that of with RS.

From the above observations, it can be qualitatively concluded that the thermal and hence residual stresses are more sensitive to TS than the RS. It should be noted here that increasing TS directly affects the net heat input per unit length, which may result in weld defects such as tunnel defect due to insufficient heating and material flow around the rotating tool pin. This problem can be arrested by increasing RS. Therefore, both TS and RS plays significant role in achieving the defect free welds with acceptable tensile stresses near the weld nugget and compressive away from it.

A transient 3-D, non-linear, thermo-mechanical model has been built using APDL in ANSYS software and studied the effects of FSW process parameters on thermal history and resulting residual stresses. Predicted peak temperatures and heating and cooling rates are in close agreement with the measured data, which indicates that the tedious experiments can be minimized by the use of numerical modelling and simulation of FSW process. Predicted thermal data is further used to analyze the thermal residual stresses across the FSW joints. Based on the overall observations, it is concluded that TS has strong influence on the longitudinal stresses and increasing its values lowers the tensile stresses near the weld nugget and increases compressive stresses away from it. However, increasing TS also increases the

transverse stresses. Also, increasing RS increases the tensile and compressive stresses across the weld nugget and its surrounding region. Finally, it is concluded that the thermally induced tensile stresses can be minimized either by increasing TS or decreasing RS, or both. These observations and conclusions can be extended to the prediction of final residual stresses (at ambient conditions), except that the magnitudes would be different. This is because the exact stress values depend on the cooling rates. Slow cooling rates aids to minimize the tensile stresses near the weld nugget and maximize compressive stresses away from it.

## 6.6 Future Works

The present work has provided a fundamental understanding of the influence of process parameters in the FSW process, microstructure development in Al-based alloy welds, and thermo-mechanical modelling for thermal and residual stresses. For future work, experimental investigations need to be carried out to verify the numerical simulations and optimal solutions obtained in this thesis. The process variables used in this study were limited to responses, maximum temperature and residual stress and the following input variables: RS, TS, and TPH. The optimization can be performed on a process model that includes more input process variables and output responses. The materials to be welded are considered identical in this study. Similar studies can be extended to other variants of friction stir welding processes such as laser-assisted friction stir welding process, or the welding of dissimilar materials that will be technically more challenging due to the differences in material properties.

More comprehensive thermo-metallurgical-mechanical models could also be considered for optimization..

- To develop model for fatigue crack growth propagation in FS welded joints.
- To develop model for the formability of FS welded joints for dissimilar joints.
- Additive manufacturing of FSW process.
- To find the weldability in Lap and T-joints for different thickness of similar and dissimilar materials using FSW

## REFERENCES

- [1] Adamowski, J., C. Gambaro, E. Lertora, M. Ponte, and M. Szkodo. "Analysis of FSW welds made of aluminium alloy AW6082-T6", *Archives of Materials Science and Engineering*, 28, no. 8 (2007): 453-460.
- [2] Afrin, N., D. L. Chen, X. Cao, and Jahazi M.. "Strain hardening behavior of a friction stir welded magnesium alloy." *Scripta Materialia*, 57, no. 11 (2007): 1004-1007.
- [3] Ahmed, *Journal of Materials Science and Engineering*, 2 (2014).
- [4] Ananthakrishna.G, "Current theoretical approaches to collective behavior of dislocations", *Physics reports*, 440 (2007): 113-259.
- [5] Armentani, E., Esposito R., and Sepe R. "The effect of thermal properties and weld efficiency on residual stresses in welding." *Journal of Achievements in materials and Manufacturing Engineering* 20, no. 1-2 (2007): 319-322.
- [6] Assis, J. T., Monin V., Teodosio J. R., and Gurova T.. "X-ray analysis of residual stress distribution in weld region." *Adv X-ray Anal* 45 (2002): 225-31.
- [7] Babu, B., Jambulingam, S., Jhonbritto, P. (2014). *Experimental and Analysis of Process Parameters of Aluminium Alloys using CNC and VMC*, *Int. J. of latest trends in engineering and technology*, no. 4 (2014): 37–47.
- [8] Bahemmat P., Rahbari A., Haghpanahi M. and Besharati M.K., "Experimental study on the effect of rotational speed and tool pin profile on AA2024 aluminium friction stir welded butt joints", *proceedings of ECTC,2008*.
- [9] Bahemmat, P., M. K. Besharati, M. Haghpanahi, A. Rahbari, and R. Salekrostam. "Mechanical, micro-, and macrostructural analysis of AA7075-T6 fabricated by friction stir butt welding with different rotational speeds and tool pin profiles." *Proceedings of the Institution of Mechanical Engineers, Part B: Journal of Engineering Manufacture* 224, no. 3 (2010): 419-433.
- [10] Barnes, T. A., and Pashby I. R.. "Joining techniques for aluminium spaceframes used in automobiles: Part I—solid and liquid phase welding." *Journal of materials processing technology* 99, no. 1 (2000): 62-71.
- [11] Barnik Saha Roy, Subhash Chandra Saha and John Deb Barma, "3-D Modeling & Numerical Simulation of Friction Stir Welding Process", *Advanced Materials Research*, 488-489 (2012): 1189-1193.
- [12] Basil M. Darras, "Experimental and analytical study of friction stir processing",



University of Kentucky, Master's Thesis Paper 353.

- [13] Benyounis, K. Y., and Abdul-Ghani Olabi. "Optimization of different welding processes using statistical and numerical approaches—A reference guide." *Advances in engineering software* 39, no. 6 (2008): 483-496.
- [14] Bjorn Carlsson, Joachim Larsson and Tony Nilson, SSAB Tunnplat AB, Borlange, Sweden "Dual phase steels for Autobody: Design, Forming and Welding aspects".
- [15] Bower, Allan F. *Applied mechanics of solids*. CRC press, 2009.
- [16] Bozkurt, Yahya, and Serdal duman. "The effect of welding parameters on the mechanical and microstructural properties of friction stir welded dissimilar AA 3003-H24 and 2124/SiC/25p-T4 alloy joints." *Scientific Research and Essays* 6, no. 17 (2011): 3702-3716.
- [17] Bozkurt, Yahya. "The optimization of friction stir welding process parameters to achieve maximum tensile strength in polyethylene sheets." *Materials & Design* 35 (2012): 440-445.
- [18] Cam, Gürel, and Selcuk Mistikoglu. "Recent developments in friction stir welding of Al-alloys." *Journal of Materials Engineering and Performance* 23, no. 6 (2014): 1936-1953.
- [19] Cartigueyen, S., Sukesh O. P., and Mahadevan K. "Numerical and experimental investigations of heat generation during friction stir processing of copper." *Procedia Engineering* 97 (2014): 1069-1078.
- [20] Cerri, E., and Leo P. "Mechanical properties evolution during post-welding-heat treatments of double-lap friction stir welded joints." *Materials & Design* 32, no. 6 (2011): 3465-3475.
- [21] Chao, Yuh J., Qi X., and Tang W.. "Heat transfer in friction stir welding-experimental and numerical studies." *Transactions-American Society of Mechanical Engineers, Journal of Manufacturing Science and Engineering*, 125, no. 1 (2003): 138-145.
- [22] Chen XU, 11th OAPS Working Paper Series, School of Materials Science and Engineering
- [23] Chen, C. M., and Kovacevic R. "Finite element modeling of friction stir welding—thermal and thermomechanical analysis." *International Journal of Machine Tools and Manufacture* 43, no. 13 (2003): 1319-1326.
- [24] Chi-Sung, J. E. O. N., H. O. N. G. Sung-Tae, K. W. O. N. Yong-Jai, C. H. O. Hoon-Hwe, and Heung Nam Han. "Material properties of friction stir spot welded joints of

- dissimilar aluminum alloys." Transactions of Nonferrous Metals Society of China 22 (2012): 605-613.
- [25] Colegrove P, 3 Dimensional flow and thermal modeling of the Friction Stir Welding process, in: the Second FSW Symposium, Gothenburg, Sweden, 2000
- [26] Davies. A. C., "A text book on Welding",10th edition, Cambridge University press, Cambridge CB2 2RU, United Kingdom, 2005.
- [27] Dean, Edwin B. "Modeling personnel turnover in the parametric organization." (1991).
- [28] DebRoy, T., and Bhadeshia H. K. D. H.. "Friction stir welding of dissimilar alloys—a perspective." Science and Technology of Welding and Joining 15, no. 4 (2010): 266-270.
- [29] Deng, Dean, and Hidekazu Murakawa. "Numerical simulation of temperature field and residual stress in multi-pass welds in stainless steel pipe and comparison with experimental measurements." Computational materials science 37, no. 3 (2006): 269-277.
- [30] Dieter, George Ellwood, and David J. Bacon. Mechanical metallurgy. Vol. 3. New York: McGraw-hill, 1986.
- [31] Dorbane, Abdelhakim, Bilal Mansoor, Georges Ayoub, Vasanth Chakravarthy Shunmugasamy, and Abdellatif Imad. "Mechanical, microstructural and fracture properties of dissimilar welds produced by friction stir welding of AZ31B and Al6061." Materials Science and Engineering: A 651 (2016): 720-733.
- [32] Elangovan, K., Balasubramanian V., and Babu S. "Developing an empirical relationship to predict tensile strength of friction stir welded AA2219 aluminum alloy." Journal of materials engineering and performance 17, no. 6 (2008): 820-830.
- [33] Elangovan, K and Balasubramanian, V., and Valliappan, M., "Influences of tool pin profile and axial force on the formation of friction stir processing zone in AA6061 aluminium alloy", International Journal of advanced manufacturing technology, 38, (2008): 285-295.
- [34] Feng, A. H., Chen D. L., and Ma Z. Y.. "Microstructure and low-cycle fatigue of a friction-stir-welded 6061 aluminum alloy." Metallurgical and Materials Transactions A 41, no. 10 (2010): 2626-2641.
- [35] Feng, A.H., Chen D. L., Ma. Z. Y., Ma W. Y., and Song R. J.. "Microstructure and Strain Hardening of a Friction Stir Welded High-Strength Al–Zn–Mg Alloy." Acta

- Metallurgica Sinica (English Letters) 27, no. 4 (2014): 723-729.
- [36] Feulvarch, Eric, Roux J.C., and Bergheau J.M.. "A simple and robust moving mesh technique for the finite element simulation of Friction Stir Welding." *Journal of Computational and Applied Mathematics* 246 (2013): 269-277.
- [37] Fujii, Hidetoshi, Ling Cui, Masakatsu Maeda, and Kiyoshi Nogi. "Effect of tool shape on mechanical properties and microstructure of friction stir welded aluminum alloys." *Materials Science and Engineering: A* 419, no. 1 (2006): 25-31.
- [38] Fujimoto M., Koga S., Abe N., Sato Y. S. and Kokawa H., "Microstructural analysis of stir zone of Al alloy produced by friction stir spot welding", *Science and Technology of Welding and Joining*, no. 13(2008): 663-670.
- [39] Ghosh, M., Kumar. K., Kailas. S. V., and Ajoy K. Ray. "Optimization of friction stir welding parameters for dissimilar aluminum alloys." *Materials & Design* 31, no. 6 (2010): 3033-3037.
- [40] Govind. N, Nageswararao.D and Ramanaihah. N, "Effect of microstructural changes on mechanical properties of friction stir welded Nano Sic reinforced AA6061 composite", *Int. Journal of Engg Sci and Tech*, no2(11),(2010): 6491- 6499.
- [41] Gupta, S. K., and Pandey, K. N., Application of Taguchi method for optimization of Friction Stir Welding process parameters to joining of aluminium-alloy, *Int. J. of Advanced Materials Manufacturing and Characterization*, no.3(1),(2013):253-258.
- [42] Hamilton, C., S. Dymek, I. Kalemba, and M. Blicharski. "Friction stir welding of aluminium 7136-T76511 extrusions." *Science and Technology of Welding and Joining* 13, no. 8 (2008): 714-720.
- [43] Hasan I. Dawood, S. Mohammed, and Mumtaz Y. Rajab, *Advances in Mater. Sci. Engg.*, 2014, Article ID 105713, (<http://dx.doi.org/10.1155/2014/105713>)
- [44] Hassan, Kh AA, Prangnell P. B., Norman A. F., Price D. A., and Williams S. W.. "Effect of welding parameters on nugget zone microstructure and properties in high strength aluminium alloy friction stir welds." *Science and Technology of Welding and joining* 8, no. 4 (2003): 257-268.
- [45] Hattel, Jesper Henri, Kim Lau Nielsen, and Cem Celal Tutum. "The effect of post-welding conditions in friction stir welds: from weld simulation to ductile failure." *European Journal of Mechanics-A/Solids* 33 (2012): 67-74.
- [46] He, Xiaocong, Fengshou Gu, and Andrew Ball. "A review of numerical analysis of friction stir welding." *Progress in Materials Science* 65 (2014): 1-66.

- [47] Hosford, William F., and Robert M. Caddell. *Metal forming: mechanics and metallurgy*. Cambridge University Press, 2011.
- [48] Ivetic, G., A. Lanciotti, and Polese C. "Electric strain gauge measurement of residual stress in welded panels." *The Journal of Strain Analysis for Engineering Design* 44, no. 1 (2009): 117-126.
- [49] Jacquin, Dimitri, B. De Meester, Aude Simar, Dominique Deloison, Frank Montheillet, and Christophe Desrayaud. "A simple Eulerian thermomechanical modeling of friction stir welding." *Journal of Materials Processing Technology* 211, no. 1 (2011): 57-65.
- [50] Jamshidi Aval, H., Serajzadeh S., Kokabi A. H., and Loureiro A. "Effect of tool geometry on mechanical and microstructural behaviours in dissimilar friction stir welding of AA 5086–AA 6061." *Science and Technology of Welding and Joining* 16, no. 7 (2011): 597-604.
- [51] Jayaraman M., Sivasubramanian R. and Balasubramanian V., "Effect of Process Parameters on Tensile Strength of Friction Stir Welded Cast LM6 Aluminium Alloy Joints", *J. Mater. Sci. Technol*, no. 25 (2009): 655-664.
- [52] Jayaraman, M., Sivasubramanian, R., Balasubramanian, V., and Lakshminarayanan, A. K. (2009), Optimization of process parameters for friction stir welding of cast aluminium-alloy A319 by Taguchi method, *Journal of scientific and Industrial research*, no. 68 (2009): 36-43.
- [53] Jeyabalakrishnan S., ArunSenthil Kumar A., Vivek Prabhu M., "Temperature Distribution Analysis of Friction Stir Welding of Al-Sic-Gr Hybrid Composites", *Int. journal of innovative research in science, engineering and technology*, no. 4 (2015):77-81.
- [54] Jeyakumar, M., T. Christopher, R. Narayanan, and B. Nageswara Rao. "Residual stress evaluation in butt-welded steel plates." *Indian journal of engineering and materials sciences*,18 (2011):425-434
- [55] Jiju Antony , "Design of Experiments for Engineers and Scientists", School of Management and Languages, Heriot-Watt University, Edinburgh, Scotland, UK, Second edition, 2014.
- [56] Joseph, V. Roshan, and CF Jeff Wu. "Performance measures in dynamic parameter design." *Journal of Japanese Quality Engineering Society* 10 (2002): 82-86.
- [57] Kadian, A. K., Puri, G., Biswas, P., " Prediction of Thermal History of Friction Stir

- Welding by Considering Combined Stick & Slip Condition of AA1100”, (AIMTDR), (2014):1–7.
- [58] Khandkar, Mir Zahedul H., Jamil A. Khan, Anthony P. Reynolds, and Michael A. Sutton. "Predicting residual thermal stresses in friction stir welded metals." *Journal of Materials Processing Technology* 174, no. 1 (2006): 195-203.
- [59] Khodaverdizadeh, H., Mahmoudi A., Heidarzadeh A., and Nazari E. "Effect of friction stir welding (FSW) parameters on strain hardening behavior of pure copper joints." *Materials & Design* 35 (2012): 330-334.
- [60] Khodir, Saad Ahmed, Toshiya Shibayanagi, and Masaaki Naka. "Control of hardness distribution in friction stir welded AA2024-T3 aluminum alloy." *Materials transactions* 47, no. 6 (2006): 1560-1567.
- [61] Khumbhar N T, and Bhanumurthy K, “Friction stir welding of Al 6061 alloy”, *Asian J. Expt. Sci*, no. 22(2008):63-74.
- [62] Kiral, Binnur Gören, Mustafa Tabanoğlu, and H. Tarık Serindağ. "Finite element modeling of friction stir welding in aluminum alloys joint." *Mathematical and Computational applications* 18, no. 2 (2013): 122-131.
- [63] Koilraj, M., Sundareswaran V., Vijayan S., and Koteswara Rao S.R. "Friction stir welding of dissimilar aluminum alloys AA2219 to AA5083–Optimization of process parameters using Taguchi technique." *Materials & Design* 42 (2012): 1-7.
- [64] Kumar, K. S. V. K., and Satish V. Kailas. "The role of friction stir welding tool on material flow and weld formation." *Materials Science and Engineering: A* 485, no. 1 (2008): 367-374.
- [65] Lakshmi Narayanan A K., Balasubramanian. V., “Process parameters optimization for friction stir welding of RDE-40 aluminium alloy using Taguchi technique”, *Trans. Nonferrous Met. Soc, Elsevier*, no. 18 (2008):548-554.
- [66] Lakshminarayanan, A. K., and Balasubramanian V. "An assessment of microstructure, hardness, tensile and impact strength of friction stir welded ferritic stainless steel joints." *Materials & Design* 31, no. 10 (2010): 4592-4600.
- [67] Lakshminarayanan, A. K., and Balasubramanian V.. "Comparison of RSM with ANN in predicting tensile strength of friction stir welded AA7039 aluminium alloy joints." *Transactions of Nonferrous Metals Society of China* 19, no. 1 (2009): 9-18.
- [68] Li, Hongjun, and Di Liu. "Simplified Thermo-Mechanical Modeling of Friction Stir Welding with a Sequential FE Method." *International Journal of Modeling and*

- Optimization 4, no. 5 (2014): 410.
- [69] Mansoor M., Salam I., and Tauqir A., 14th Int. Symposium on Advanced Materials, Materials Science and Engineering, no. 146 (2016).
- [70] Madhavi .B, Jeevan .J. , “Influence of Strain Hardening Behaviour in Friction Stir Welded Joints of Aluminium-alloy Plates”, Materials today proceedings, ICMPC-2017.
- [71] Madhavi, B., Anvesh Krishna, and Jeevan Jaidi. "Finite Element Modelling of Friction Stir Welding Process to Study the Thermal Impact and Evolution of Stresses in Aluminium-alloy Plates."(2016).www.coep.org.in/AIMTDR-016/main/pdf/1828.pdf
- [72] Madhavi.B., Jeevan .J, and karthik.M.Teja, “Optimization Study of Friction Stir Welding Process Parameters and Nugget Properties of Aluminium-alloy”, ICONS-2014,IGCAR, Kalpakkam.India, (2014), 129.
- [73] Madhusudhan. R., Sarcar.M.M.M., Ramanaiah. N., “An experimental study on mechanical and microstructural properties of dissimilar aluminium alloy friction stir welds”, Int. J.of Mechanical and Production Engineering, no 1(2013): 2320-2092.
- [74] MadhusudhanReddy G., Suresh D. Meshram, “Study on the effect of tool rotational speed and tool pin profile on AA2014 aluminium alloy friction stir welds”, IIW international conference on global trends in joining , cutting, and surfacing technology, (2011): 117-124.
- [75] Manual on the Use of Thermocouples in Temperature Measurement (4th Ed.). ASTM. 1993. pp. 48–51. ISBN 978-0-8031-1466-1
- [76] Mendes, N., Loureiro A., Martins C., Neto P., and Pires J. N. "Effect of friction stir welding parameters on morphology and strength of acrylonitrile butadiene styrene plate welds." Materials & Design 58 (2014): 457-464.
- [77] Meng, Z., Chen, H., and Yue, X., International Federation for Information Processing (IFIP), in Knowledge Enterprise: Intelligent Strategies In Product Design, Manufacturing, and Management. Wang K., et al. Editors, Springer. (2006): 483-491.
- [78] Metals-Mechanical Testing Standards, Vol. 3.01: American Society of Testing and Materials (ASTM), 2010.
- [79] Miller, W. S., Zhuang L., Bottema J., Wittebrood A.J, De Smet P., Haszler A., and Vieregge. A. "Recent development in aluminium alloys for the automotive industry." Materials Science and Engineering: A 280, no. 1 (2000): 37-49.
- [80] Mishra, Rajiv S., and Ma Z. Y.. "Friction stir welding and processing." Materials

- Science and Engineering: R: Reports 50, no. 1 (2005): 1-78.
- [81] Miroslav Mijajlovi, Dragan Milcic, and Miodrag Milcic, "Numerical simulation of friction stir welding", *Thermal science*, 18, (2014): 967-978.
- [82] Morris.J.G. , "Luder bands in Al-Mg alloys", *Journal of material science and engineering*, 5, (1970): 299-302.
- [83] Nandan, R., Roy G. G., Lienert T. J., and DebRoy T. "Numerical modelling of 3D plastic flow and heat transfer during friction stir welding of stainless steel." *Science and Technology of Welding and Joining* 11, no. 5 (2006): 526-537.
- [84] Nandan, R., Roy G. G., Lienert T. J., and DebRoy T. "Welding Research", *Improving Reliability of Heat Transfer and Materials Flow Calculations during Friction Stir Welding of Dissimilar Aluminum Alloys*, 86, (2007): 313-322.
- [85] Nandan, R., Roy G. G., Lienert T. J., and DebRoy T. "Three-dimensional heat and material flow during friction stir welding of mild steel", *Acta Materialia*, 55, no. 3 (2006): 883 – 895.
- [86] Nikhil T, Shreyas M, Jeevan J, Karthik Teja M, "Predicted and Measured Thermal Profiles During Friction Stir Welding Process of Aluminium-alloy", *Int. J. of Appl. Engg. Research*, 10, (2015): 607-612.
- [87] Nourani, Mohamadreza, Abbas S. Milani, and Spiro Yannacopoulos. "Taguchi optimization of process parameters in friction stir welding of 6061 aluminum alloy: A review and case study." *Engineering* 3, no. 02 (2011): 144.
- [88] Okuyucu, Hasan, Adem Kurt, and Erol Arcaklioglu. "Artificial neural network application to the friction stir welding of aluminum plates." *Materials & Design* 28, no. 1 (2007): 78-84.
- [89] Palanivel, R., Koshy Mathews P., and Murugan N. "Development of mathematical model to predict the mechanical properties of friction stir welded AA6351 aluminum alloy." *Journal of engineering science and technology review* 4, no. 1 (2011): 25-31.
- [90] Pawar, Satish P., and Shete M. T.. "Optimization of friction stir welding process parameter using Taguchi method and response surface methodology: A Review." (2013).
- [91] Pierpaolo Carlone, Gaetano Palazzo S., "Influence of Process Parameters on Microstructure and Mechanical Properties in AA2024-T3 Friction Stir Welding", *Journal of Metallurgical and microstructural analysis*, no. 2 (2013): 213-222.
- [92] Prasanna, P., Subba Rao B., Krishna Mohana Rao G., and Prasad A. "Experimental

- and numerical evaluation of friction stir welds of AA6061-T6 aluminium alloy." *J. Eng. Appl. Sci* 5 (2010): 1-18.
- [93] Prasanna, P., Penchalayya, Ch., Anandamohana Rao, D., Optimization and Validation of Process Parameters in Friction Stir Welding on AA 6061 Aluminum Alloy Using Grey Relational Analysis, *Int. J. of Engineering Research and Applications* no. 3(1)(2013):1471–1481.
- [94] Qasim M. Doos., and Samer J. Mahmood., “The influence of tool geometry of friction stir welds on mechanical properties and microstructure of AA2218-T72 aluminium alloy”, no. 17, *Journal of Engineering*, (2014).
- [95] Raghu Babu G., Murti K. G. K. and Ranga Janardhana G., “An experimental study on the effect of welding parameters on mechanical and microstructural properties of AA6082-T6 friction stir welded butt joints”, *ARPN Journal of Engineering and Applied Sciences*, no. 3, (2008):68-74.
- [96] Rahul jain, Surjya k. Pal and Shiv B.Singh, “Finite element simulation of pin shape influence on material flow,forces in friction stir welding”, *International journal of advanced manufacturing technology*, 94 (2017): 1781-1797.
- [97] Rahul jain, Surjya k. Pal and Shiv B.Singh, “ A study on the variation of forces and temperature in a friction stir welding process: a finite element approach”, *Journal of manufacturing process*, 23(2016) :278–286.
- [98] Rajakumar, S., and Balasubramanian V. "Establishing relationships between mechanical properties of aluminium alloys and optimised friction stir welding process parameters." *Materials & Design* 40 (2012): 17-35.
- [99] Rajamanickam, N., and Balusamy V.. "Effects of process parameters on mechanical properties of friction stir welds using design of experiments." *Indian journal of engineering materials sciences*, no.15 (2008): 293-299.
- [100] Rajamanickam, N., Balusamy V., Thyla P. R., and Hari Vignesh G.. "Numerical simulation of thermal history and residual stresses in friction stir welding of Al 2014-T6." (2009).
- [101] Ranjibarnodeh, Eslam, and Mehdi Farajpour. "Evolution of plastic strains in dissimilar weld of stainless steel to carbon steel." *Metallurgical and Materials Engineering* 18, no. 1 (2012): 19-27.
- [102] Reynolds, Anthony P., Tang W., Khandkar Z., Jamil A. Khan, and Lindner K. "Relationships between weld parameters, hardness distribution and temperature



- history in alloy 7050 friction stir welds." *Science and Technology of Welding and Joining* 10, no. 2 (2005): 190-199.
- [103] Rodrigues, D. M., Leitao C., Louro R., Gouveia H., and Loureiro A. "High speed friction stir welding of aluminium alloys." *Science and Technology of Welding and Joining* 15, no. 8 (2010): 676-681.
- [104] Rose, A. Razal, Manisekar K., and Balasubramania V.. "Influences of tool rotational speed on tensile properties of friction stir welded AZ61A magnesium alloy." *Proceedings of the Institution of Mechanical Engineers, Part B: Journal of Engineering Manufacture* 226, no. 4 (2012): 649-663.
- [105] Roxana Hutana, Lynann Claphama, and R.B. Rogge, "Intergranular strain and texture in steel Luders bands", *Acta Materialia*, 53, (2005): 3517-3524.
- [106] Roy, Ajit K., Anand Venkatesh, Vikram Marthandam, Dronavalli S. B., Douglas Wells, and Ronald Rogge. "Residual stress characterization in structural materials by destructive and nondestructive techniques." *Journal of materials engineering and performance* 14, no. 2 (2005): 203-211.
- [107] Kalpakjian.S, and Schmidt.R, *Manufacturing Engineering and Technology*, Pearson, 5th Edition, 2006
- [108] Liang S. X., Yin L. X., Zheng L. Y., Ma M. Z. and Liu R. P., *J. of Mater. Engg. and Performance*, no.25 (2016): 530-535.
- [109] Chowdhurya S.M., Chena D.L., Bholea S.D., Caob X, Powidajkoc E., Weckmanc D.C., and Zhouc Y., *Materials Science and Engineering*, A 527 ( 2010), 2951-2961.
- [110] Sahu, Prakash Kumar, and Sukhomay Pal. "Multi-response optimization of process parameters in friction stir welded AM20 magnesium alloy by Taguchi grey relational analysis." *Journal of Magnesium and Alloys* 3, no. 1 (2015): 36-46.
- [111] Selvamani S.T, Umanath K and Palani kumar K, "Heat Transfer Analysis during Friction Stir Welding of Al6061-T6 alloy", *International Journal of Engineering Research and Applications (IJERA)* no. 1 (2014): 1453-1460.
- [112] Simões, F., and Rodrigues D. M. "Material flow and thermo-mechanical conditions during friction stir welding of polymers: literature review, experimental results and empirical analysis." *Materials & Design* 59 (2014): 344-351.
- [113] Squillace, A., Segreto T., Prisco U., Teti R., and Campanile G. "Optimization of friction stir welds of aluminium alloys." In *Intelligent Production Machines and Systems-2nd I\* PROMS Virtual International Conference 3-14 July 2006*, p. 247.

Elsevier, 2011.

- [114] Stamenković, Dragi, and Mato Perić. "Determination of Residual Stresses in Welded Pipes Using a Simplified Heat Source." *Scientific Technical Review* 61, no. 1 (2011): 12-16.
- [115] Su, Hao, Chuan Song Wu, Marcel Bachmann, and Michael Rethmeier. "Numerical modeling for the effect of pin profiles on thermal and material flow characteristics in friction stir welding." *Materials & Design* 77 (2015): 114-125.
- [116] Svensson, L-E., Karlsson L., Larsson H., B. Karlsson, Fazzini M., and Karlsson J. "Microstructure and mechanical properties of friction stir welded aluminium alloys with special reference to AA 5083 and AA 6082." *Science and technology of welding and joining* 5, no. 5 (2000): 285-296.
- [117] Thomas, W. M., Nicholas E. D, Needham J. C., Murch M. G., Templesmith P., and Dawes C. J.. International patent application no. No. 9125978.8. PCT/GB92/02203 and GB patent application, 1991.
- [118] Threadgill, P. L., Leonard A. J., Shercliff H. R., and Withers P. J.. "Friction stir welding of aluminium alloys." *International Materials Reviews* 54, no. 2 (2009): 49-93.
- [119] Ulysse, Patrick. "Three-dimensional modeling of the friction stir-welding process." *International Journal of Machine Tools and Manufacture* 42, no. 14 (2002): 1549-1557.
- [120] Uzun, Fatih, and Ali Nezihi Bilge. "Investigation of total welding residual stress by using ultrasonic wave velocity variations." *G U Fen Bilimleri Dergisi(G. U. Journal of Science)* 24, no. 1 (2011).
- [121] Varma, R. R., and Ibrahim, A. B.(2014), Mechanical properties of the friction stir welded, *Int. J. of Mechanical and production engineering*, no. 2 (2014): 3-7.
- [122] Varun Kumar, A., and Balachandar K. "Effect of welding parameters on metallurgical properties of friction stir welded aluminium alloy 6063-O." *Journal of Applied Sciences* 12 (2012): 1255-1264.
- [123] Venkateswarlu, D., Mandal N. R., Mahapatra M. M, and Harsh S. P.. "Tool design effects for FSW of AA7039." *Weld J* 92 (2013): 41-47.
- [124] Vidala C., Infante V. , Peças P., Vilaça P., "Application of taguchi method in the optimization of friction stir welding parameters of an aeronautic aluminium alloy", *International Journal of Hybrid Information Technology*, no.7 (2014):153-162.

- [125] Vijayan, S., Raju R., Subbaiah K., Sridhar N., and Rao S. R. K. "Friction stir welding of Al–Mg alloy optimization of process parameters using Taguchi method." *Experimental Techniques* 34, no. 5 (2010): 37-44.
- [126] Vijayan, Sundaravel, Raju R., and Rao S.R K. "Multiobjective optimization of friction stir welding process parameters on aluminum alloy AA 5083 using Taguchi-based grey relation analysis." *Materials and Manufacturing Processes* 25, no. 11 (2010): 1206-1212.
- [127] Vilaca, P., Quintino, L., and dos Santos, J.F., iSTIR - Analytical thermal model for friction stir welding. *Journal of Materials Processing Technology*, no.169 (2005):.452-465.
- [128] Vision for Welding Industry, American Welding Society,550 N.W. Lejeeune Road, Miami, FL 33126.
- [129] Wade, M., and Anthony P. Reynolds. "Friction stir weld nugget temperature asymmetry." *Science and Technology of Welding and Joining* 15, no. 1 (2010): 64-69.
- [130] Xu, Weifeng, Jinhe Liu, Guohong Luan, and Chunlin Dong. "Microstructure and mechanical properties of friction stir welded joints in 2219-T6 aluminum alloy." *Materials & Design* 30, no. 9 (2009): 3460-3467.
- [131] Yong-Jai, K. W. O. N., Shim Seong-Beom, and P. A. R. K. Dong-Hwan. "Friction stir welding of 5052 aluminum alloy plates." *Transactions of Nonferrous Metals Society of China* 19 (2009): 23-27.
- [132] Zhu, Li-na, Bin-shi Xu, Hai-dou Wang, and Cheng-biao Wang. "Measurement of residual stress in quenched 1045 steel by the nanoindentation method." *Materials Characterization* 61, no. 12 (2010): 1359-1362.
- [133] Zhu, X. K., and Chao Y. J. "Numerical simulation of transient temperature and residual stresses in friction stir welding of 304L stainless steel." *Journal of materials processing technology* 146, no. 2 (2004): 263-272.

## LIST OF PUBLICATIONS

### List of journal publications

1. **Madhavi, B.**, Jeevan. J., and Karthik Teja M., "Heat and Material Flow Effects on Microstructures and Hardness in Friction-Stir Welded Joints." *Procedia Engineering*, vol. 86, pp. 209-214. (DOI: 10.1016/j.proeng.2014.11.030; *Citations=1*)
2. **Madhavi B.**, Jeevan J., "Influence of Strain Hardening Behaviour in Friction Stir Welded Joints of Aluminium-alloy Plates", *Materials Today: Proceedings*, vol. 5, Issue 2P1 (2018), pp. 3851-3860.
3. **Madhavi, B.**, and Jeevan .J. "Experimental and Numerical Studies of Tool Geometry Effects on Mechanical Properties and Stresses in Friction Stir Welded Joints", (to be submitted).
4. **Madhavi, B.**, and Jeevan. J. "Optimization of Friction Stir Welding process of AA5052-H32 using Taguchi OA", (to be submitted).

### List of conference publications

1. **Madhavi B.**, Jeevan J, and karthik.Teja M, "Optimization Study of Friction Stir Welding Process Parameters and Nugget Properties of Aluminium-alloy", *International Conference on Structural Integrity (ICONS-2014)*, IGCAR, Kalpakkam, INDIA, February 4-7, 2014, pp. 129. (*Citations=2*)
2. **Madhavi B.**, Anvesh Krishna S. and Jeevan J., "Finite Element Modelling of Friction Stir Welding Process to Study the Thermal Impact and Evolution of Stresses in Aluminium-alloy Plates", *AIMTDR-2016*, College of Engineering , Pune, December 16-18, 2016, pp. 243.

## BRIEF BIOGRAPHY OF THE SUPERVISOR

Name of the supervisor	Prof. Jeevan Jaidi
Qualifications	Ph.D (IISc, Bangalore)
Designation and Address	Associate Professor, Mech. Engg. Dept. BITS-Pilani, Hyderabad Campus
Experience (years)	14
Journals	05
Conferences	25
No. of Ph.D. students supervised	Nil

### Research areas

- Thermal-mechanical-metallurgical studies in joining (fusion and FSW) processes.
- CFD studies of heat and mass transfer in phase change materials and processes.
- CFD studies in microfluidics - including biological systems for DNA synthesis, process optimization and scale-up for commercialization.
- Nanoparticle synthesis using aerosol flame reactor - coupled (CFD+PBM) approach.
- Wind turbine process modelling and simulations.

### Sponsored Projects

- Process Modeling and Validation of Flotation Cell: Development of 3-D Multiphase Turbulent Model, Tenova -Delkor (June-Sept 2014), .
- CFD based Process Optimization of Flotation Cell and Scale-up for Larger Cells, Tenova –Delkor, (Dec 2014-May 2015).

## BRIEF BIOGRAPHY OF THE STUDENT

Name of the student	Barla Madhavi
ID No	2010PHXF0028H
Qualifications	M.E (CAD/CAM), Andhra University.
Designation and Address	Research Scholar, Mech. Engg. Dept. BITS-Pilani, Hyderabad Campus
Journals	02
Conferences	02